THE DEVELOPMENT AND IMPLEMENTATION OF HIGH-THROUGHPUT TOOLS FOR DISCOVERY AND CHARACTERIZATION OF PROTON EXCHANGE MEMBRANES

A Dissertation
Presented to
The Academic Faculty

by

Keith Gregory Reed

In Partial Fulfillment
of the Requirements for the Degree
Doctor of Philosophy in the
School of Chemical and Biomolecular Engineering

Georgia Institute of Technology
December 2009

THE DEVELOPMENT AND IMPLEMENTATION OF HIGH-THROUGHPUT TOOLS FOR DISCOVERY AND CHARACTERIZATION OF PROTON EXCHANGE MEMBRANES

Approved by:

Dr. J. Carson Meredith, Advisor
School of Chemical and Biomolecular Engineering
Georgia Institute of Technology

Dr. David Bucknall
School of School of Polymer, Textile & Fiber Engineering
Georgia Institute of Technology

Dr. Tom Fuller
School of Chemical and Biomolecular Engineering
Georgia Institute of Technology

Dr. Anselm Griffin
School of Polymer, Textile & Fiber Engineering
Georgia Institute of Technology

Dr. William Koros
School of Chemical and Biomolecular Engineering
Georgia Institute of Technology

Date Approved: October 9, 2009

I dedicate this work to my mother, whose wisdom and love have kept me pushing forward, and to my father, who I know is smiling down on me from heaven.

Acknowledgements

First and foremost, I must thank God for blessing me with the opportunity to have this experience. Through His love and favor, I have discovered the strength, the wisdom, and the confidence to make it this far. To my mom, for the morals and values that you have instilled upon me from a young age, I am truly grateful. To my little brother and sister, Kevin and Krisitn, I hope that my life's journey thus far has encouraged you both to discover your passions in life, and that you remain focused in pursuing your dreams. To my Nana, you have always supported and encouraged my academic pursuits; and to Grandma, you have imparted so much wisdom upon me. I love you both so much and I am truly blessed to have you both in my life. I am especially grateful to my advisor, Dr. Carson Meredith, who gave me the opportunity to pursue my research interests and discover new ones. You have challenged my way of thinking while encouraging my progress. You pushed me to be creative yet critical in my work, and allowed me to really take ownership of this project. Your continuous support and guidance throughout my tenure at Georgia Tech has been invaluable. I am also extremely grateful to my research committee, who has shown genuine interest in my work and has given me valuable feedback throughout the years to improve my research. Your questions, your concerns, and your words of encouragement have motivated my development into a well-rounded, critical thinker.

I'd like express my sincerest gratitude to Dr. Sue Ann Bidstrup-Allen, who gave me the opportunity to be more than just a graduate student, but a leader and role-model for other students. The opportunities that you have provided for me have made my Georgia Tech experience so unique. I'd also like to thank Dr. Lakeisha Taite, Dr. Keith Oden, and Dr. Comas Haynes, for showing interest in my academic progress and

professional development. I look forward to passing along the knowledge and insight that you have bestowed upon me. I am truly grateful to the administrative staff in the ChBE Department , especially Ms. Brenda Maddox, Ms. Janice Whatley, Ms. Juanita Freeman, Ms. Phyllis Jones, Ms. Claudia Clarkson, Ms. Rochelle Moses and Ms. Josie Giles – with all of your assistance and encouragement, there was no issue that could not be easily resolved – thank you for taking care of me. I'd like to thank Dr. John Walsh, Dr. Chris Wieble, Dr. Valarie Thomas, and other faculty associated with the Ivan Allen School of Public Policy that I have had the pleasure of interacting with. You all have given me a great deal perspective on my work and allowed me to really grasp "the bigger picture" of my research.

To those esteemed ChBE graduate alumni who have come before me: Dr. Akua Asa-Awuku, Dr. Joe Lahai-Sormana, Dr. Charlene Rincon, Dr. Pedro Zapata, Dr. Jing Su – for sharing your knowledge and experience with me, I am ever so grateful. Whether it was lab training, academic or non-academic guidance, or just a few laughs, you all have added much wisdom and enjoyment to my Georgia Tech experience. I can only hope that I have impacted others as you all have impacted me.

I want to thank my incoming class of 2004 who has taken the journey with me, especially JR Johnson and Shara McClendon – you have both been great colleagues and amazing friends. To my Exxon Mobil mentees, both past and present: Tracie, Mallerie, Arlyne, Mayisha, Katrina, Namory, Charmaine, and Channel – encouraging your professional and academic development has also helped me to develop as person and I wish you all much success in your future endeavors. I'd like to acknowledge those students who aided me in my research efforts, especially Ryan Hart, Tori Blasucci, Hillary Huttenhower, Pamela Pollet, Ven Rajarathinam, and Cheng Chen, as well as the members of the Koros research group for generously allowing me to use their commercial resins. To Jung-Hyun Lee, for your amazing TGA and SEM work, for putting

in the extra late hours, and for offering your insight to my research, I am very grateful. Also to Ismael Gomez, I'm glad that I you decided to come to Tech and work with our group – the past two years have been a lot of fun. I know that you will accomplish great things both in and out of the lab, and I wish you much success as you continue through Tech.

I also have to thank the Black Graduate Student Association and the crazy fast members of the Georgia Tech Runnin' Wreck Running Club – you have encouraged me strive for the best in all facets of life and helped me to maintain the work-life balance that I so desperately needed throughout my time at Georgia Tech.

Last but not least, I have to acknowledge the organizations that funded my research: the Department of Energy, Arkema, Inc., Honda, and Applied Materials. Also, I must thank the FACES organization, who not only provided financial support but also provided me with a wealth of insight into the world of academia. And to the rest of my family, friends, and colleagues, I am very grateful to have established fulfilling relationships with you all.

Table of Contents

List of Tables

List of Figures

Summary

The need for sustainable energy use has motivated the exploration of renewable alternative fuels and fuel conversion technology on a global scale. Fuel cells, which convert chemical energy directly into electrical energy with high efficiency and low emissions, provide a promising strategy for achieving energy sustainability. The current progress in fuel cell commercialization is mainly in portable and stationary applications, but fuel cell technology for transportation applications, which make up a substantial portion of the global energy market, have seen little commercial success. Proton exchange membrane fuel cells (PEMFCs) have high potential for addressing the future energy needs of the transportation energy sector. However, one of the prevailing limitations of the PEMFC is the availability of high-performance, cost-effective electrolyte materials. These materials may be realized in the near future by developing multi-functional polymer blends targeted at specific performance capabilities. Since the number of available polymer combinations and numerous processing variations provide an almost infinite source of PEMFC membrane candidates, efficient methods of discovering high-performance PEM materials are necessary. Combinatorial methods meet these needs using gradient or discrete techniques to capture process variations such as annealing temperature, thickness, and chemical composition into a single polymer sample that serves as a library of materials. To characterize these heterogeneous samples for fuel cell performance, specific high-throughput measurement techniques are necessary. In this work, a high-throughput mass transport assay (HT-MTA) has been developed to characterize water flux and permeability at multiple sample locations in parallel. The functionality of HT-MTA was evaluated using standard Nafion® films and a model semi-interpenetrated polymer network with commercial polyvinylidine

fluoride as the host matrix for a proprietary polyelectrolyte supplied by Arkema, Inc. Although mass transport values were generally lower than reported literature values, pervaporation experiments showed that HT-MTA could be used to effectively screen and optimize relative water transport characteristics in PEMs. To further demonstrate the utility of HT-MTA, the instrument was incorporated into the lab's current high-throughput characterization toolset and used to investigate the mechanisms and effects of rapid free radical degradation of Nafion® membranes based on various concentrations of H_2O_2 and Fe^{2+}. The results showed that changes in Nafion's® mechanical, conductive, and water transport properties were strong functions of H_2O_2, and that maximal degradation could be achieved around 50 ppm Fe^{2+}. Furthermore, by including chemical composition analysis techniques in the characterization toolset, the dominating free radical degradation pathways could be deduced. These results are promising for later correlating rapidly aged degradation experiments to *in situ* fuel cell lifetime testing which is both time-intensive and costly.

The high-throughput toolset was also used to develop a novel optimized blend consisting of polyetherimide (PEI), a low-cost high performance resin, and sulfonated PEI (S-PEI) made using a relatively mild post sulfonation reaction with trimethylsilyl chlorosulfonate. The effects of blend composition and thermal annealing on film performance were evaluated and the polymer system was shown to have optimal mechanical and ion-conducting properties between 20 – 30 wt% S-PEI in the unannealed state. Although the properties of the proposed PEI-based polymer system were below PEMFC performance standards, a PEI film with superior mechanical properties was discovered and should prove to be useful in other applications. In general, this work shows promising results for efficiently developing advanced polymer materials using high-throughput screening techniques.

Chapter 1
Introduction

The engineering discipline is defined by its use of basic science and fundamental understanding to solve practical problems and generate socially aware innovation. The work described in this dissertation remains true to this concept, and so it is essential for the reader to grasp the context of the problems being addressed. Chapter 1 highlights the driving forces that motivate the development of high-performance polymer membranes for utilization in fuel cells. Starting with the broadest global challenges, this chapter discusses the growing energy demands and the diminishing supply of conventional fossil fuels which intensify the effects of global warming. To achieve energy sustainability and mitigate anthropogenic climate change, a shift from fossil fuels to renewable alternative energy resources with reduced emissions is critical. However, the most abundant natural alternatives have had very limited application and have yet to make significant impacts in the global energy market. To efficiently harness alternative energy for broader applications with significantly reduced environmental impacts, a broad range of fuel cell technologies can be implemented. Each type of fuel cell possesses specific advantages and limitations which make it a suitable power source for certain energy sectors. This chapter reviews the common types of fuel cells and their operating principles, but will focus specifically on the proton exchange membrane fuel cell (PEMFC), which has high potential to address the future energy needs of the transportation energy sector. One of the prevailing limitations of the PEMFC is the availability of high-performance, cost-effective electrolyte materials. These materials may be realized in the near future by developing multi-functional polymer blends

targeted at specific performance capabilities. However, the number of available polymer combinations and numerous processing variations provide an almost infinite source of PEMFC membrane candidates, such that efficient methods of discovering high-performance polymer systems are necessary. This chapter will explain how such needs can be supported using combinatorial synthesis and high-throughput screening, for which a high-throughput water transport characterization tool has been developed in this work. The importance of water management in PEMFCs will be discussed, and the functionality of the new measurement method will be presented in subsequent chapters.

1.1. ENERGY SUSTAINABILITY

Sustainable living and development is necessary to meeting the needs of today without comprising the ability of future generations to do the same. Energy sustainability in particular can be achieved by balancing the availability of energy resources with energy consumption. However, a stabilized energy supply alone is not enough for sustainable growth and must be complemented with environmentally sound energy acquisition and usage to assure future socioeconomic stability. This section identifies prospects of achieving global sustainability by examining each of these key components. As will be shown, the current and projected trends in energy consumption, conventional resource availability, and climate shifts demand urgent implantation of low-emitting, renewable alternatives to fossil fuels. While the focus here is on worldwide sustainability, much attention is directed at the US, whose substantial energy use has led to dilemmas whose solutions can serve as a model for current developing countries.

1.1.1. Energy Consumption

The Industrial Revolution of the 18th century marked the transition to machine-based economies and the emergence of factories for mass production, which in turn

ignited a growth in global energy consumption that persists today. As the world's currently developing nations carry forth this industrial movement with expanding economies and growing populations, the global demand for energy will continue its upward trend well into the future. The Energy Information Administration (EIA) has used historical energy trends and anticipated industrial activity in forecasting a 50 % increase in energy usage between 2005 and 2030, as shown in Figure 1-1 [1]. Industrialization remains to be a key component to this projection, with an 80 % projected increase within developing countries alone, while the high-income countries which form the Organization for Economic Co-operation and Development (OECD) are only projected to grow in energy use by 20 % (see Figure 1-2). Still, the US historically and currently accounts for approximately 25 % of the total energy consumed in the world, but only has less than 5 % of the world population. Therefore, while it is necessary to address the stabilization of global energy consumption among developing countries, it is just as important to reduce usage in the world's industrialized nations.

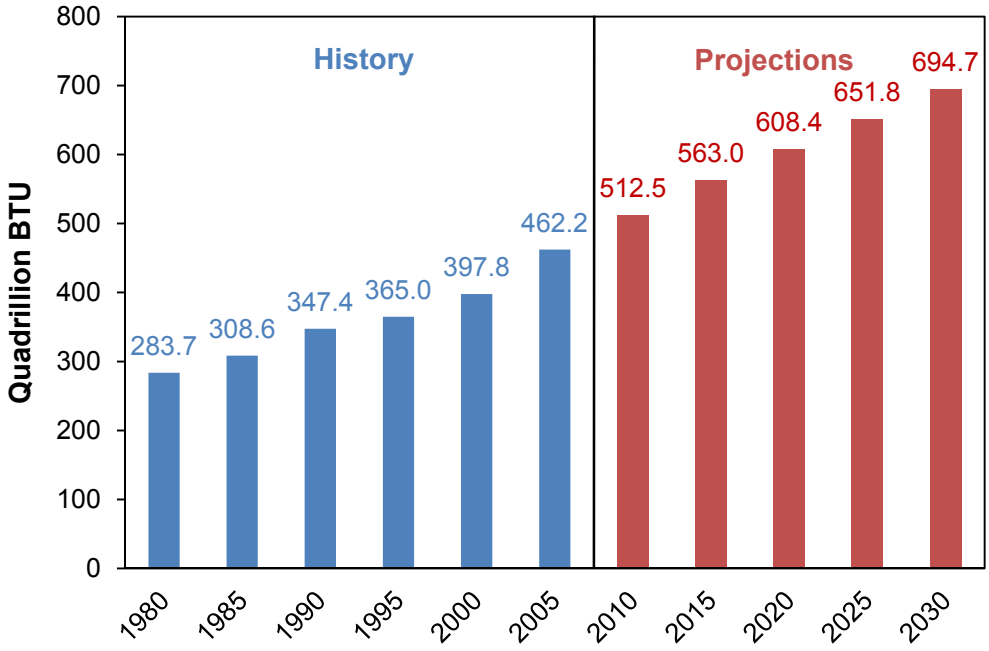

Figure 1-1: Historical and projected total world energy consumption, 1980-2030 (adapted from the EIA, Annual Energy Review 2007)

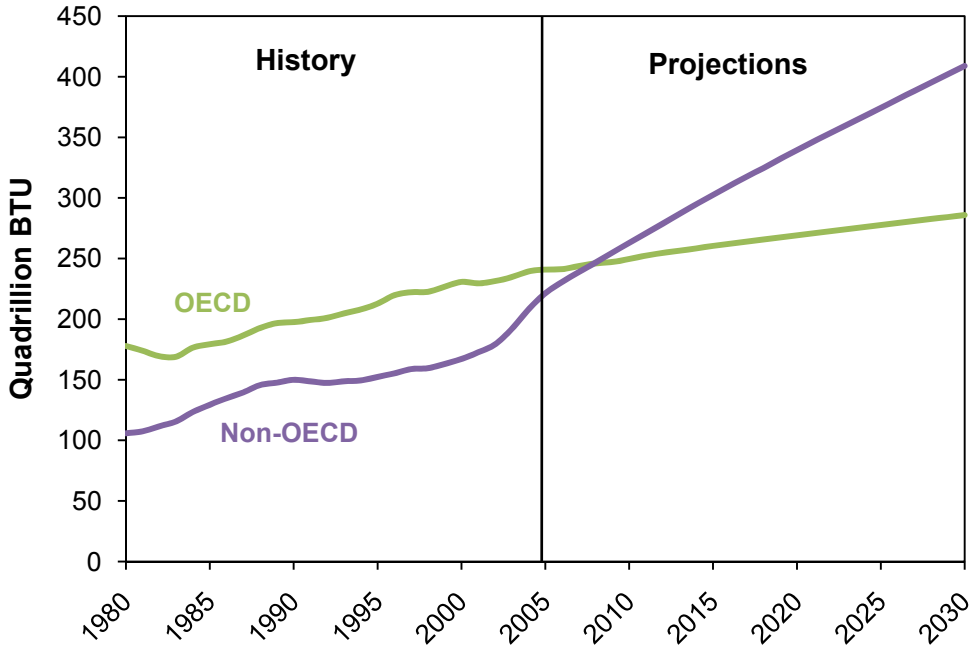

Figure 1-2: Historical and projected world energy consumption by membership to the OECD, 1980-2030 (adapted from the EIA, Annual Energy Review 2007)

Energy consumption takes place within four economic sectors: commercial, residential, industrial, and transportation. Both commercial and residential energy are used for heating, cooling, lighting, and the operation of appliances. The industrial sector includes energy required to operate any industrial process, which is dominated by the refining of petroleum and the manufacturing steel, aluminum, paper, chemicals, and cement. Transportation energy is used to power automobiles, commercial trucks, planes, railroads, and mass transit. In the US, industrial energy consumption consistently dominates all other sectors, followed by transportation, residential, and then commercial energy consumption, as shown in Figure 1-3.

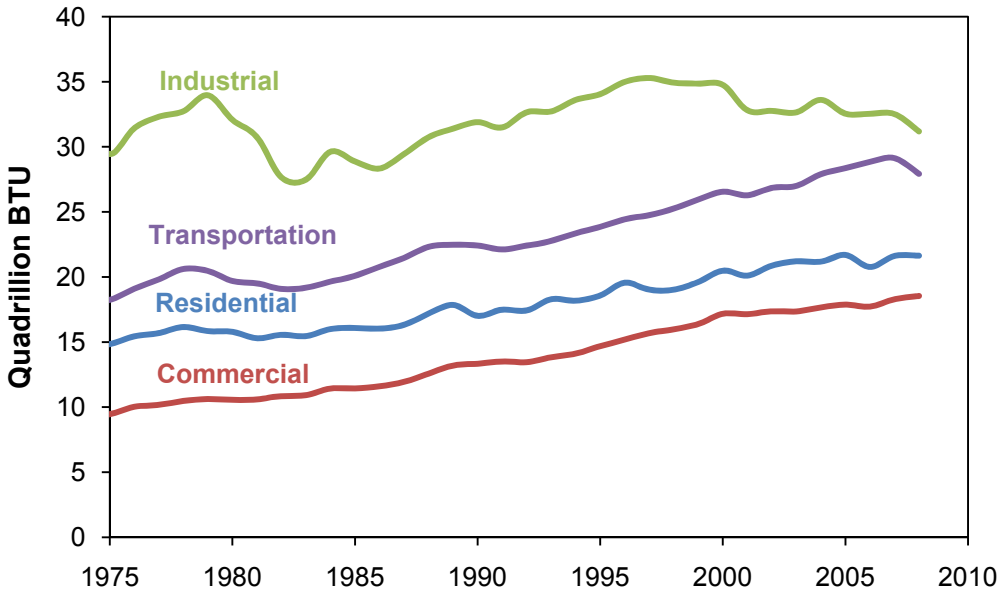

Figure 1-3: US energy consumption by sector, 1975-2008 (source: EIA, Monthly Energy Review May 2009)

1.1.2. Fossil Fuels

Each economic sector requires a combination of fuel sources to meet its energy needs. These resources come from fossil fuels, nuclear fission, and renewables which consist of wind, biomass, water flow, geothermal energy, and solar radiation. The most widely tapped energy source by far is fossil fuel in the form of petroleum, coal, and natural gas. Fossil fuels are refined for direct use as primary energy, and also used indirectly as secondary energy through the generation of electricity. In the US, approximately 70 % of electricity comes from fossil fuels, of which approximately 70 % is coal [2]. However fossil fuels have numerous drawbacks that require an urgent transition to alternative energy sources.

1.1.2.1. Foreign Dependence

Dating as far back as the 1980's, fossil fuels have been used to meet approximately 85 % of the total energy needs both globally and within the US [1, 3]. However, as shown in Figure 1-4, the US consumption of fossil fuel energy exceeds its production capacity, resulting in a growing dependence on foreign fossil fuel imports, especially petroleum. The impact of such foreign dependence was felt both nationally and globally in the mid-1970's as a result of the Oil Embargo imposed by the Organization of Petroleum Exporting Countries (OPEC). When OPEC significantly cut back on its exportation of oil to numerous nations, the price of oil experienced a dramatic increase of 330 %. The national effects were devastating, marked by a major trade deficit, high inflation, and a 240 % increase in gas prices by 1980 [4], while in many other nations, mass economic recessions arose. With the current US production of petroleum making up only less than 40 % of petroleum needed for its transportation sector [2], it is clear that there is an urgent need for energy independence to prevent the repetition of past fossil fuel crises.

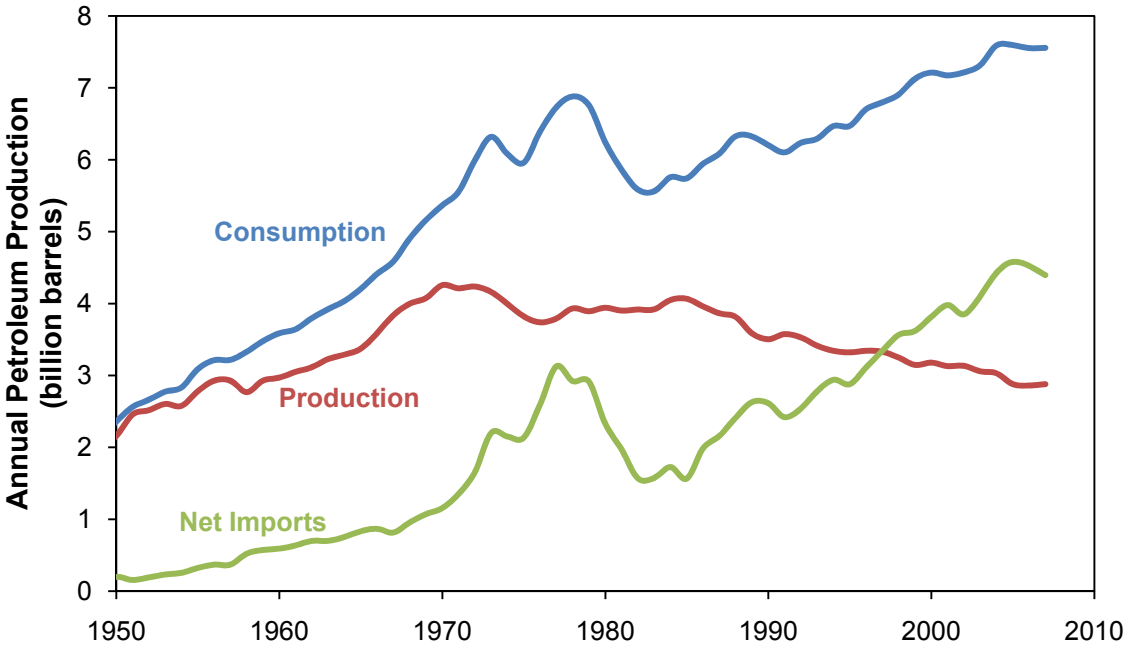

Figure 1-4: US production, consumption, and net imports of petroleum, 1950-2007 (source: Annual Energy Review 2007)

1.1.2.2. Natural Abundance

Foreign control of fossil fuel is just one of many limitations that restrict its sustainable use. Fossil fuels are also naturally limited in capacity since they are derived from millions of years of heat and compression. The finite supply of fossil fuels implies that at some point in time, reserves will be depleted beyond feasible recovery, and there is much dispute as to when this will occur. In 1956, Marion K. Hubert, American geophysicist, proposed that for a given geographical oil-producing area, the rate of petroleum production is determined by the rate of new well recovery. Therefore, according to Hubert, the production rate follows a bell-shaped trend that peaks at maximum extraction and then enters a terminal decline when new wells no longer being recovered. Hubert used his Peak Theory to accurately predict that the US would reach maximum oil production in 1970, as shown in Figure 1-4. The world as a whole, however, has yet to reach a peak production rates as Hubert's Theory might suggest. According to the predictions made by the EIA, global fossil fuel production will continuously increase at a rate of 235 million barrels per year through 2030 [3]. Other institutions have made predictions that more directly diverge from the Peak Theory, claiming it to be over simplistic when applied at the global scale. The Cambridge Energy Research Association (CERA), a global energy consulting company, suggests that the theory fails to account for resource growth, advances in technology, geopolitics, and basic commercial factors [5]. They propose an undulating plateau in petroleum production after 2030, followed by a slow decline, as shown in Figure 1-5. However, the increasing petroleum projections from CERA include significant growth in non-conventional crude oil usage, which are extracted using techniques other than the traditional oil well method. The use of these supplemental fossil fuels is less efficient than that of convention oil, with a much lower ratio of energy output to input. When also considering the environmental drawbacks of non-conventional oil, which will be

presented in the next section, long-term and widespread exploitation of these fuels are highly likely to have significantly adverse affects on humanity. Overall, continuing with “business as usual” fossil fuel practices, from both conventional and non-conventional sources, will hinder the world’s capability to live sustainably, and will ultimately lead to unmanageable levels of global economic and ecological instability.

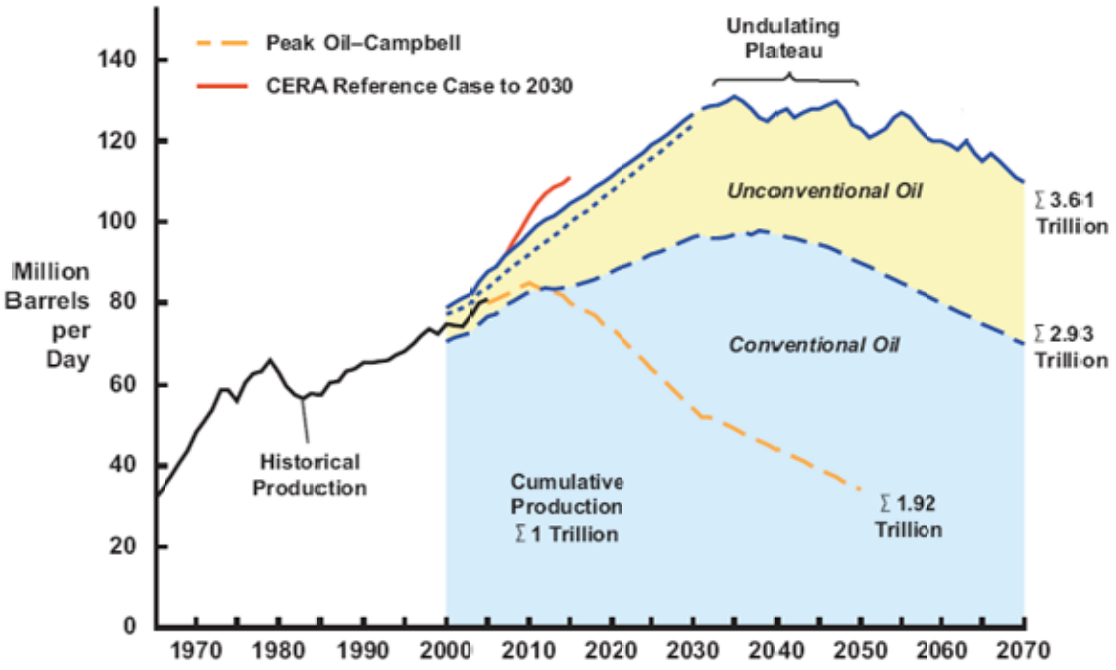

Figure 1-5: Predictions of World Oil Production – Peak Oil vs. Undulating Plateau (source: CERA, [5])

1.1.2.3. Emissions

Fossil fuels must be burned to obtain useable energy. The combustion process, however, also generates a host of side products: carbon dioxide, nitrogen oxides, sulfur dioxide, volatile organic compounds, particulate matter, and heavy metals. Each of these chemicals, once released into atmosphere, can severely impact human health, wildlife, and even global climate stability. Nitrogen and sulfur oxides, upon mixing with water vapor in air, form acidic compounds that create acid rain, causing structural damage, contaminating soil, and harming aquatic wildlife. The release of particulate matter, which consists of unburned hydrocarbons and hazardous metals, has adverse effects on the human respiratory system and has been cited for aggravating asthma, chronic bronchitis, airway obstruction, and blood-gas exchange [6]. In addition, volatile organics as well as nitrogen oxides released during combustion react with air to form ground level ozone, also known as smog, that along with human respiratory complications, has been associated with reduced agricultural yields through photosynthesis inhibition [7].

While not as toxic as many of the other fossil fuels emissions, carbon dioxide also receives worldwide attention for its impact on the environment. Along with ozone, methane, water vapor, and nitrous oxide, CO_2 is classified as a greenhouse gas (GHG). Through the greenhouse effect, GHGs absorb the sun's infrared radiation reflected from the earth's surface and trap it as heat in the atmosphere. While the long term effects may still be under heavy debate, it is generally acknowledged that human activity, especially the growing usage of fossil fuels, has enhanced global warming through the greenhouse effect. Over the past century, this additional heat has increased the earth's average near-surface air temperature by approximately 1 °C, and is expected to increase the surface temperature by an additional 1-6 °C within the next century [8]. Although this temperature change may seem minute, it has already been attributed to observed glacial retreat and rising sea levels around the world. The effects are expected

to propagate in the long term, leading to changed precipitation patterns and possibly more frequent and intense weather events. Other plausible effects include the expansion of subtropical deserts, forest shrinkage, and species extinctions. While some countries may be able to adapt to these warming-induced changes, others will be at high risk of severe devastation that will ultimately affect the global economy. As a part of the world's strategies to mitigate the impacts from excessive global warming, fossil fuels usage must be reduced.

1.1.2.4. Extraction and Transportation

The harmful environmental impacts of from fossil fuels are not only from their use, but also from their extraction. Since fossil fuels are found deep in the ground, they must be drilled and mined from the earth, and then transported for end use. Such practices have caused a variety of environmental problems in the form of landscape subsidence, surface and ground water contamination, habitat damage, and the release of gaseous residues [9]. One of the more visible fossil fuel hazards, however, is the potential for transportation spills and production site explosions. The extent of the possible damage has been demonstrated by the Exxon Valdez spill of 1989, but even more recently by spills off the coasts of Louisiana, Beirut, and the Philippines in 2006; South Korea and Russia in 2007; Louisiana again in 2008; and most recently, Australia in March 2009. The resulting pollution from these accidents can last up to decades, and cleanup is often very costly. It is clear the world's massive addiction to fossil fuels, while convenient for today's generations, will serve as a substantial burden for future generations to endure. As a part of the world's strategies to reduce the potential disastrous effects of fossil fuel extraction and transportation, their consumption will need to be significantly reduced, while policy and technology allow energy alternatives to become mainstream.

1.1.3. Alternative Energy Resources

Nuclear and renewable resources provide an alternative means to meeting global energy needs with the potential of avoiding the issues related to fossil fuels. Figure 1-6 illustrates how these alternatives compare with fossil fuel usage in the US. Global percentages follow a similar relationship, with non-fossil alternatives making up 15 % of the total usage. Each of these alternative resources has the benefit of infinite or near-infinite abundance with significantly reduced emissions, but has yet to be used to its full commercial potential due to combination of technical, environmental, and political obstacles.

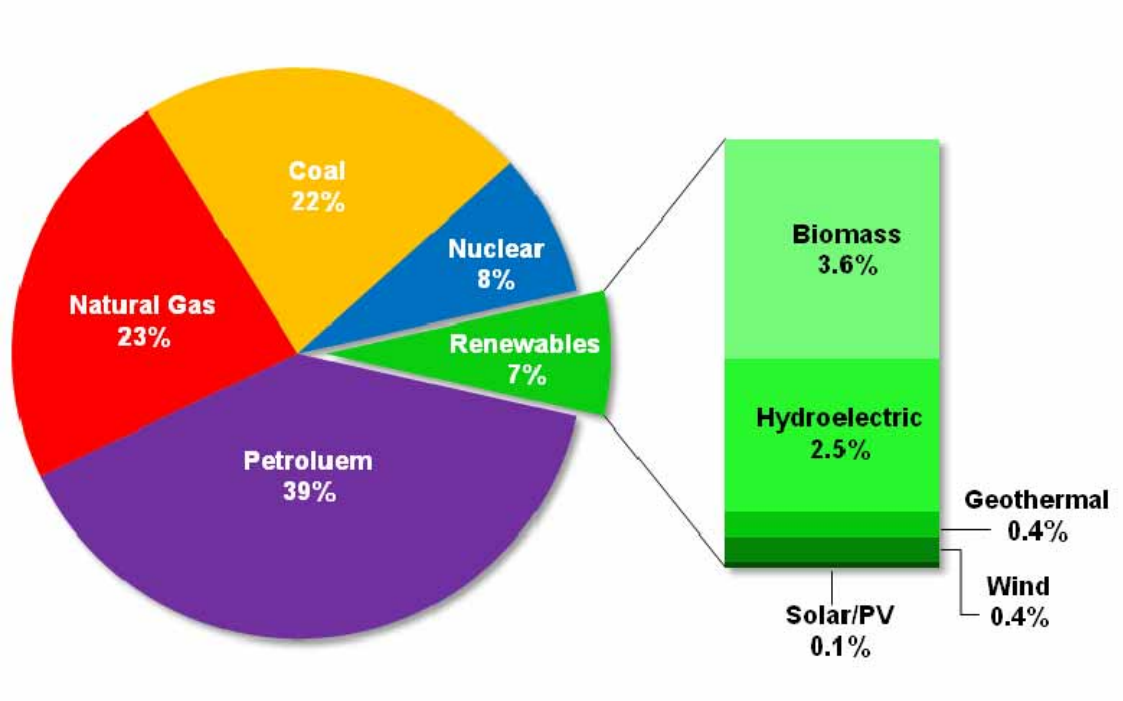

Figure 1-6: US energy consumption by fuel type, 2007 (source: EIA, Renewable Energy Review 2007[10])

1.1.3.1. Energy Storage, Transmission, and Conversion

The storage and transmission capabilities of any energy resource, whether renewable or non-renewable, are vital to its utility in any of the four energy sectors. Such capabilities are necessary to addressing fluctuations in energy demand, intermittent resource availability, wasted energy recovery, and geographical distribution limitations [11]. The mainstream success of fossil fuels and biomass energy has been attributed to their ability to satisfy these criteria. As primary energy sources, fossil fuels and biomass can be transported via pipeline or freight. For energy conversion, these fuels can be combusted at multiple scales, making fossil fuels and biomass suitable for mobile, commercial, residential, and industrial applications.

As an alternative to combustion, biomass and fossil fuels, as well as every other energy resource can be converted to electricity, a widely used energy carrier. While its generation is less efficient than direct combustion and applications are presently limited in the transportation sector, electricity can be dispatched over relatively long distances at costs that are much lower than freight transportation. Electricity is also much easier to use than the resources from which it is derived. However electrical energy cannot easily be stored in quantities large enough to meet energy demands on a global or national scale, and must be produced as needed at all times. Conventional fossil fuel and nuclear power plants overcome this obstacle by continuously delivering baseload power with additional turbine technology that operates according to daily and seasonal peaks and disturbances [16]. For the storage of renewable resources, geothermal energy is naturally held beneath the earth's crust until needed, while hydroelectric plants meter the conversion of flowing water accumulated in dams to address fluctuating electricity demands. Unfortunately, other emerging and infinitely abundant renewable sources, i.e. wind and solar electricity can not be delivered in the same capacity due their frequent, often unpredictable variations in availability.

To better utilize intermittent renewable sources such as wind and solar radiation for a much broader range of applications, they can be used indirectly to produce synthetic, yet environmentally benign fuels that are storable, transportable, and efficiently converted to end-use power. These synthetic fuels can then serve as alternative energy carriers to fossil fuels and electricity. Hydrogen is an ideal synthetic fuel because it is the most abundant element on the planet, has potential to produce zero emissions during energy conversion, and has the highest energy content of any common fuel by weight. Hydrogen can be produced by steam reforming of hydrocarbons or electrolysis of water. Steam reforming is currently used to for 95% of the hydrogen produced in the US, most of which is used for petroleum refining and ammonia production for fertilizer. In addition to hydrocarbons, reforming requires water and energy to convert organic compounds into hydrogen and carbon dioxide. If the energy input is derived from fossil fuels or biomass, the overall synthesis of hydrogen from reforming can be highly emissions-intensive. Water electrolysis, on the other hand, produces no carbon dioxide in the dissociation of water into hydrogen and oxygen gas. Therefore, if the energy input into a water hydrolysis reactor is provided by from non-emitting resources such as wind and solar-derived electricity, then the indirect conversion of these renewable resources into hydrogen fuel is essentially emissions-free. This method for fuel synthesis is essential to realizing a sustainable hydrogen economy in the long-term future while making better use of infinitely abundant natural energy resources.

To convert hydrogen into useable energy, it can be combusted in same fashion as fossil fuels or biomass. However, the energy generated through hydrogen combustion makes the fuel extremely inefficient when compared to energy input used to produce it. Therefore, in order to efficiently use alternative fuels made from renewable resources, alternatives methods for combustion are necessary. Fuel cell technology, as described

in the following section, offers a highly promising alternative to conventional fuel combustion.

1.2. FUEL CELLS

The prospects of producing hydrogen and other energy carrying alternatives from renewable energy are large. However specific technology is required to efficiently convert these fuels into energy. Combustion is feasible but highly inefficient when considering the energy requirements for producing synthetic fuels from renewable resources. An alternative strategy is to generate electrical energy from the chemical energy stored within these fuels using fuel cells to is to carry out an “electrochemical combustion” [11]. In a typical combustion, the fuel and oxidant mix and react directly. In a fuel cell, however, the fuel and oxidant are reacted in separate regions connected by two conduits for charged particles to exchange. One of these conduits is the electrode located in fuel and oxidant regions of the fuel cell. At the fuel side, where oxidation takes place and electrons are released, this electrode is called the anode. The electrode on the oxidant side, where reduction takes place and electrons are accepted is called the cathode. Both electrochemical reactions are catalytically driven at temperatures which determine the overall fuel cell operating conditions. During operation, electrons flow from the anode to the cathode through an external circuit to deliver electricity. The second conduit for charged particle transport is the electrolyte, which physically separates the fuel from the oxidant. The electrolyte can be a solution, solid polymer, or ceramic which permits the transfer of charged particles that are much larger than electrons, such as H^+, OH^-, or O^{2-}. A fuel cell is characterized by the type of electrolyte it employs, which also dictates the oxidation and reduction mechanisms taking place at the electrodes. A

general fuel cell assembly is illustrated in Figure 1-7, and the five common types of fuel cells are summarized in Table 1-1.

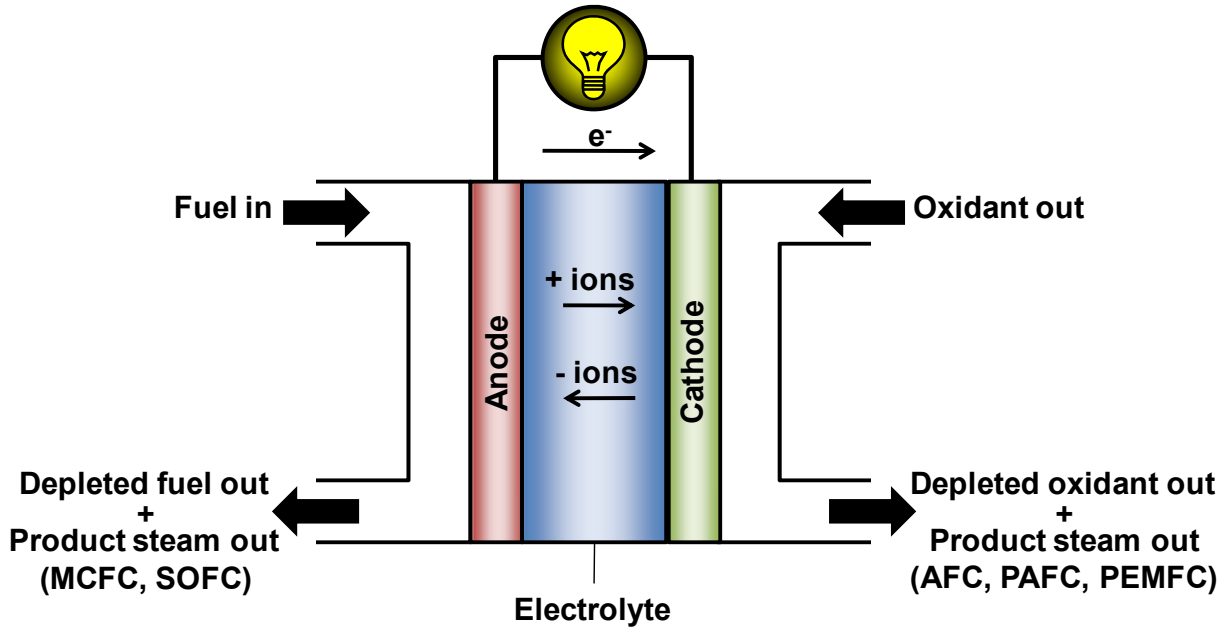

Figure 1-7: Schematic of basic fuel cell operation

Table 1-1: Summary of Common Fuel Cell Technologies

Fuel Cell Type	Electrolyte	Anode Reaction	Mobile Ion	Cathode Reaction	Operation Temp. (°C)	H_2-to-Electricity Efficiency
PAFC	Phosphoric acid	$H_2 \rightarrow 2H^+ + 2e^-$	H^+	$½O_2 + 2H^+ + 2e- \rightarrow H_2O$	150–200 °C	37–42 %
AFC	Aqueous base	$H_2 + 2OH^- \rightarrow 2H_2O + 2e^-$	OH^-	$½O_2 + H_2O + 2e^- \rightarrow 2OH^-$	80–200 °C	>60 %
MCFC	Molten metal carbonate	$H_2 + CO_3^{2-} \rightarrow H_2O + CO_2 + 2e^-$	CO_3^{2-}	$½O_2 + CO_2 + 2e^- \rightarrow CO_3^{2-}$	600–700 °C	50–60 %
SOFC	Solid ceramic oxide	$H_2 + O^{2-} \rightarrow H_2O + 2e^-$	O^{2-}	$½O_2 + 2e^- \rightarrow O^{2-}$	600–1000 °C	50–60 %
PEMFC	Solid polymer	$H_2 \rightarrow 2H^+ + 2e^-$	H+	$½O_2 + 2H^+ + 2e- \rightarrow H_2O$	70–90 °C	30–50 %

1.2.1. Phosphoric Acid Fuel Cells (PAFCs)

Phosphoric acid fuel cells use liquid phosphoric acid retained in a silicon carbide matrix as the electrolyte, along with porous carbon electrodes containing a platinum catalyst. They were developed in the mid-1960s, field-tested since the 1970s, and are the first fuel cells to be commercialized [12]. PAFCs are typically used in stationary applications for distributed generation, with limited application in large ground transportation [13, 14]. The lower and upper limits of the operation temperature are necessary to maintain the ionic conductivity and stability of the electrolyte, respectively. Overall, the high operating temperatures give PAFCs significantly more catalytic tolerance to impurities that may accompany hydrogen or hydrocarbon fuel sources, such as carbon monoxide, carbon dioxide, or sulfur. When generating only electricity, PAFCs can operate at approximately 40 % efficiency. However, PAFC operating temperatures are also ideal for cogenerating electricity and heat for hot water or steam applications, in which case the efficiency is approximately 85 %. For a given weight and volume, PAFCs generate less power than other fuel cells. While the operating costs have been driven down over years of development, platinum catalyst costs have always been a significant disadvantage [15].

1.2.2. Alkaline Fuel Cells (AFCs)

The alkaline fuel cell is also a part of first generation of fuel cells, developed in the 1960s for use in the US space program. The electrolyte is a solution of aqueous potassium hydroxide within porous stabilized matrix. The base concentration can be varied, and in turn, allows for the very broad range of operating temperatures. While the electrical conversion efficiency is the highest of the common types of fuel cells, AFC efficiencies can be improved further with cogeneration depending on the operating temperature. The electrode chemistry also allows for a variety non-precious metals to be used as catalysts, making this type of fuel cell the cheapest to manufacture. With

potentially low operating temperatures and fast reaction kinetics, AFCs are ideal for quick starting applications. The major disadvantage to ACFs is their high susceptibility to contamination, especially trace carbon dioxide which can severely degrade fuel cell performance by rapidly reacting with the electrolyte. Therefore, AFCs have been limited to closed-environment applications, such as space and undersea vehicles, and must be run on pure hydrogen and oxygen [16]. If operated within atmospheric conditions, a purification system is required, which can add significant costs to operation. Also, the corrosive nature of the electrolyte significantly limits the lifetime of the fuel cell to approximately 8,000 h, whereas specifications for commercial, large-scale power generation AFCs are set at 40,000 h [21].

1.2.3. Molten Carbonate Fuel Cells (MCFC)

The electrolyte in a molten carbonate fuel cell is usually a combination of alkali carbonates, such as sodium carbonate and lithium carbonate, or potassium carbonate. These mixtures are retained in a ceramic matrix and require the high operating temperatures to remain in the molten phase where high ionic mobility can be achieved. High operating temperatures give the MCFC the ability to function with cheaper catalysts and stainless steel electrodes, as well as the flexibility to reform fossil fuel internally to for the indirect production of hydrogen. Along with hydrocarbons, MCFCs can also use carbon oxides, either atmospheric or diverted from internal reforming, as fuel at the cathode. Excess heat given off during MCFC operation can be used for cogeneration, potentially improving the fuel cell's efficiency to 85 %. High temperatures unfortunately have the disadvantage of accelerating component corrosion and reducing fuel cell durability. These temperatures also prevent quick startup and fast response to power demands, which is necessary for transportation applications [16]. Instead, MCFCs are most suitable for large-scale, stationary power generation applications. However, until

materials resistances can be resolved for better durability, the costs of replacing the MCFCs will limit global commercialization.

1.2.4. Solid Oxide Fuel Cells (SOFCs)

The solid oxide fuel cell uses a solid nonporous metal oxides as its electrolyte, typically composed of yttria or zirconia, which are excellent conductors of negatively charged ions at high temperatures. Operating at the highest temperatures of all the common fuel cells, the SOFC shares many properties with the MCFC. In addition to carbon monoxide and carbon dioxide tolerance, SOFCs are also more resistant to sulfur, making them better suited for fossil fuels that can be internally reformed into hydrogen. Also, corrosion-induced fuel cell degradation is reduced in SOFCs since the electrolyte is solid. However, material stability at such high temperatures significantly impacts the fuel cell's lifetime and operation costs. Still, since cheaper catalysts and electrodes can be used, and high efficiencies can be achieved through cogeneration, SOFCs, like MCFCs, are being considered for a variety of stationary heat and power applications in the residential, commercial, and industrial energy markets.

1.2.5. Proton Exchange Membrane Fuel Cells (PEMFCs)

The target applications for this research project are aimed at proton exchange membrane fuel cells, which incorporate an ion-conductive polymer electrolyte and have the most potential for bringing renewable hydrogen to the transportation sector. Among the collection of fuel cells, the PEMFC is considered most attractive for its low operating temperature, CO_2 tolerance, high power density, and potential for cost-effective performance [17]. These factors make the PEMFC a highly versatile power source, not only fit for transportation power, but also suitable for stationary and portable applications. As with the SOFC, the use of a solid electrolyte in the PEMFC allows for a rugged, simplistic design without the additional cost of special materials to handle high temperatures or corrosive liquid electrolytes. Operating at a low temperature allows for

quick startup, rapid changes in power output, and better fuel cell lifetimes, but it also has disadvantages. Since cogeneration is practically ineffective in PEMFCs, the efficiencies remain low relative to .most of the other fuel cells. These temperatures are also insufficient for internal reformation, so fossil fuel flexibility can only be achieved through expensive external conversion technology. In order to maintain the low-temperature reaction kinetics at each electrode, precious metal catalysts such as platinum are required. The additional cost of using platinum is accompanied by its extreme sensitivity to CO poisoning, requiring additional equipment to remove the impurity if hydrogen is indirectly derived from fossil fuels.

The cost concerns associated with PEMFC catalysts have been recently addressed by increasing catalyst efficiency using techniques such as sputtering, electrodeposition [18], and catalyst impregnation with polymer electrolyte solution to increase the active surface area [19-21]. With advances such as these, catalyst costs are predicted to become insignificant in the near future, accounting for less than 15 % of the total cost for a commercially available PEFC [22]. While carbon monoxide poisoning is not an issue for renewable hydrogen fuels generated through electrolysis, the transition to a hydrogen-dominated transportation system will require flexible automotive power sources capable of handling both renewable hydrogen and hydrogen derived from externally reformed fossil fuels. Recent research has investigated the use of ruthenium-platinum core-shell nanoparticles to selectively oxidize carbon monoxide to form carbon dioxide prior to entering the fuel cell. The additional fuel processing increases the cost PEMFC operation, but could potentially offset by increased fuel cell lifetime.

The more critical limitation of the PEMFC is the electrolyte material that is subjected to highly acidic conditions and frequent temperature cycling from operation and shut-off periods. Under such conditions, DuPont's Nafion®, a fluorinated sulfonic acid polymer which is considered one of the most successful commercial PEM products

currently available, displays significant degradation at less than 1,000 h and costs around $65 /kW. This performance, while superior to the other types of fuel cells, is far from sufficient in meeting transportation targets set by the Department of Energy, aiming to have commercial membrane durability greater than 5000 h and cost per unit power less than $10 /kW [23]. In order to close this critical gap in PEM technology and provide a market for renewable hydrogen in the transportation energy sector, low cost polymer systems with significantly improved performance must be developed for PEMFCs. The following section describes a rapid, low-cost approach to discovering these materials that could make the commercialization of PEMFC technology practical in the near future.

1.3. COMBINATORIAL METHODS FOR POLYMER DISCOVERY

The properties of any functional material are the result of many complex molecular interactions that are highly sensitive to chemical composition and processing. Unfortunately, many challenges still remain in predicting these interactions and the resulting material properties [24, 25]. Consequently, the discovery and optimization of many materials involves trial-and-error experiments, which can be extremely time-consuming and overwhelming when considering an essentially infinite combination of variables [25]. To accelerate this process in a systematic manner, the use of combinatorial libraries, i.e., samples with controlled arrays of chemical and/or processing variations can be fabricated and screened for structure-property relationships [25, 26]. Combinatorial methods have been very successful in the pharmaceutical industry for drug discovery, and have since been applied in discovering high performance catalysts, inorganic materials, and polymers [27, 28]. Each of these applications requires its own unique set of library synthesis techniques in addition to specific high-throughput screening methods based on properties of interest. Conventional instrumentation is

typically ill-suited for either of these tasks, and for that reason, a number of novel library fabrication and high-throughput screening techniques have been developed for discovering and optimizing materials. To address the limitations of the PEMFC, this section will focus primarily on combinatorial technology as it applies to developing high-performance polymer membranes.

1.3.1. Library Synthesis and Processing

Regardless of the type of material, combinatorial libraries can be broadly categorized as discrete or continuous. Discrete libraries involve spatially resolved synthesis variations that result in one-dimensional or two-dimensional arrays [29]. For efficiency and quality control, discrete libraries are often manipulated using special robotics for chemical deposition and treatment. Continuous libraries, on the other hand, often take make use of less complex fabrication equipment, since variations are captured with continuous chemical or processing gradients. Instead, gradient synthesis typically incorporates moving stages or variable exposure devices that are particularly well-suited for the field of polymer chemistry.

Continuous combinatorial polymer library fabrication has seen significant developments in recent years. Meredith, Smith, et al. have reported the use of a variable-velocity knife-edge coating instrument to produce polystyrene films with thickness gradients to study effects on dewetting [30]. In the same study, these researchers also reported thermomechanical effects on polystyrene dewetting by applying linear annealing temperature gradients over films mounted on an aluminum stage attached to a heat source and heat sink. Gradients in polymer blend composition have also been recently developed. By varying blend ratio of copolymer solution using two syringe pumps while simultaneously withdrawing the solution gradient into a third syringe, Meredith, Karim, et al. were able to produce linear variable composition films by depositing a stripe of the gradient solution onto a substrate to be casted orthogonally

using the knife-edge flow coater mentioned previously [28]. An alternative approach has been taken by Meredith, Zapata, and Basak [31], which makes use of a microchannel coating blade with an inlet for multiple polymer solutions to be pumped at variable rates through a small, high-shear mixing chamber. The microchannel outlets dispense the well-mixed polymer solution directly onto a substrate mounted on a moving stage to produce the composition gradient film. Figure 1-8 illustrates each these techniques, as they are currently used in our lab. There are also many other methods for producing continuous gradients, with controlled variations of properties such as polymer grafting density, cross-linking density, and surface chemistry through controlled exposure to ultra violet light, plasmas, chemical vapor chambers, and reactant solutions, among other chemical environments. These techniques have been recently and extensively reviewed by numerous authors [29, 32-34].

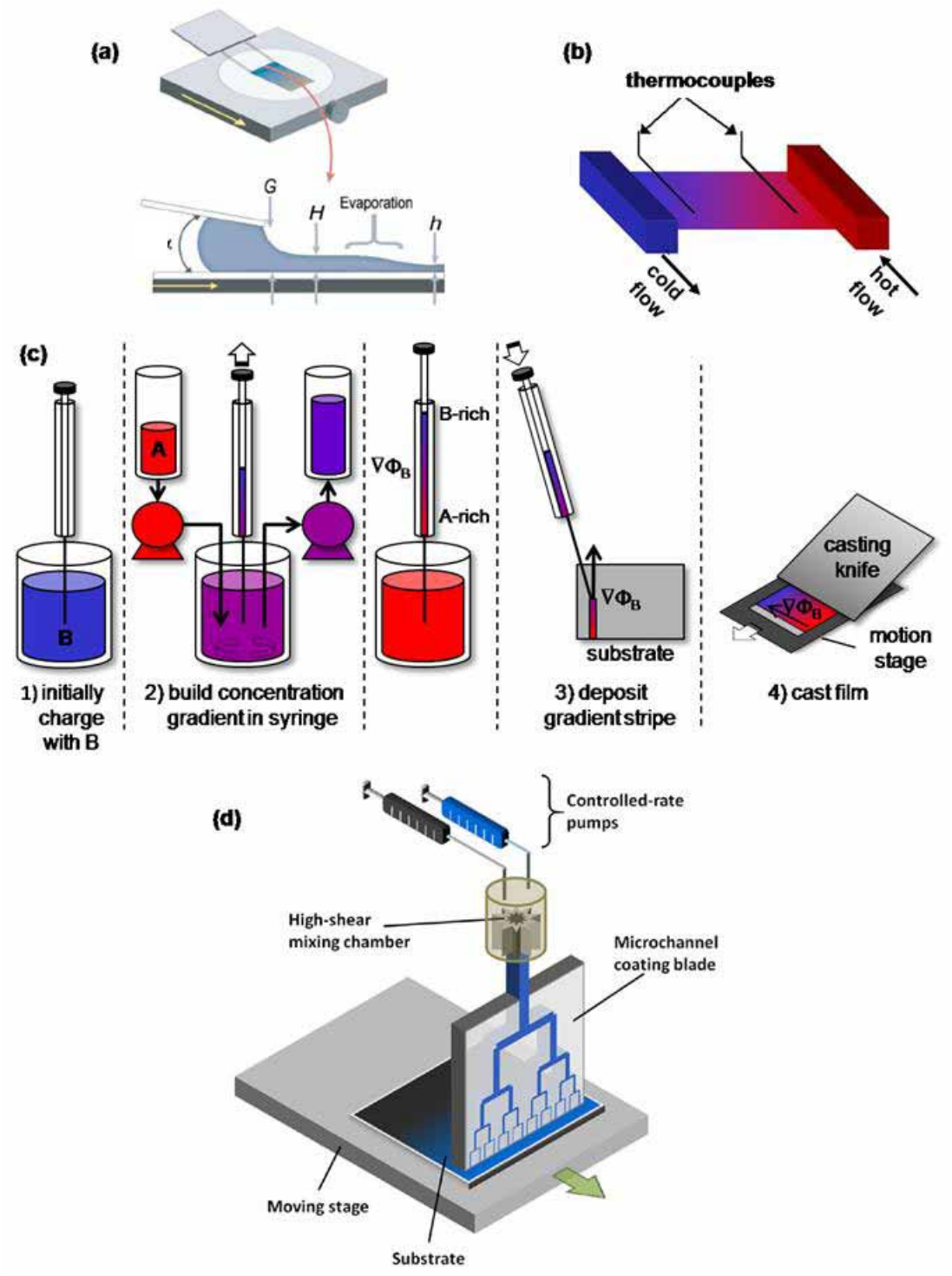

Figure 1-8: Continuous combinatorial library fabrication techniques. (a) Motion stage and knife-edge flow coater for thickness gradients, G is the height of the blade above the substrate, H is the thickness of the wet film, and h is the dry film thickness [35]. (b) Annealing stage with a heat source and heat sink for temperature gradients. (c) Syringe deposition and (d) microchannel extrusion for composition gradients [31].

1.3.2. High-Throughput Characterization

Once combinatorial libraries have been fabricated, it is then necessary to rapidly screen the heterogeneous samples for properties of interest. Although detailed characterization may require bulk samples, quick measurements of a few key properties within a combinatorial sample is crucial for discovering structure-property relationships that direct further study [25]. Since a single library can contain millions of different chemical and processing combinations, it is also necessary that quick screening techniques be capable of systematically measuring specific sample locations. Therefore, efficient combinatorial screening must be carried out with high-throughput techniques that provide for parallel or rapid sequential characterization of heterogeneous samples. Although high-throughput characterization technology is highly developed for combinatorial drug and catalysis screening, there are only a few examples where the concept has been applied to polymer libraries [27]. In order to use combinatorial methods for identifying novel fuel cell polymers, high-throughput characterization techniques need to be developed to measure those polymer properties that are key for high fuel cell performance.

1.3.2.1. Proton Conductivity and Mechanical Strength

In selecting high performing polymers for PEMFC applications, the properties most often investigated are proton conductivity and mechanical strength [36, 37]. Proton conductive membranes are required to maintain ion separation which provides efficient electron conduction and water formation at the cathode. Insufficient conductivity results in a drastic reduction of power density, requiring additional material to compensate the loss. The compensation, in turn, increases the cost per unit power. Currently, membrane proton conductivity should exceed 100 mS/cm to be competitive with Nafion [38].

Mechanical strength plays an import role in long-term fuel cell durability. The mechanical properties determine how well the membrane will withstand the stresses of

electrode processing and attachment, as well as startup and shutdown cycling involving swelling, heating, drying, and cooling. Under such conditions, Nafion undergoes a viscoelastic relaxation causing the membrane to develop pinholes that lead to a significant reduction in long-term performance. Polymers with higher glass transition temperatures, however, will display less rubber-like behavior and potentially limit mechanical degradation at higher temperatures [39]. In addition to glass transition temperature, tensile strength, percent elongation, and Young's modulus have also been used to characterize the mechanical behavior of PEMFC membranes [37]. These properties provide a broad array of parameters by which PEM performance can be predicted and screened.

1.3.2.2. Water Management

While both conductivity and mechanical strength play key roles in PEM performance, water transport heavily influences both of these properties and is therefore vital to the membrane's functionality. With respect to conductivity, the presence of moisture in the membrane is required to facilitate proton transport via electro-osmotic flow from the anode to the cathode [40, 41]. This mechanism of transport is severely hindered if the membrane is dehydrated, which is often the result of low humidity operating conditions typical in automotive applications [42-45]. In addition to the using moisture supplied via fuel and air streams, hydration can be maintained with water produced at the cathode. Hence, the membrane must allow back-diffusion to the anode. If back-diffusion is hindered, not only can dehydration occur, but water accumulation may lead to flooding at the cathode, limiting access of reactant gas to valuable active catalyst sites [40, 42, 44, 46]. As with dehydration, electrode flooding results in reduced current and decreased fuel cell performance, requiring proper water management to balance moisture between both electrodes [44]. Membrane water transport also affects fuel cell performance with respect to mechanical stability [47]. The presence of water in

the membrane causes plasticization, leading to a reduction in glass transition temperature that may affect membrane rigidity [48]. Therefore, in addition to mechanical and conductive high-throughput characterization, a tool for screening various combinatorial polymer effects on water transport is vital to discovering and optimizing proton exchange membranes for fuel cell applications.

1.4. OUTLINE

This chapter has described how specific high-throughput methods can be used to address global sustainability issues through improved transportation fuel cell technology that takes advantage of renewable energy resources. Chapter 2 describes how the current high-throughput toolset for PEMFC polymers has been expanded with the development of a mass transport assay that characterizes water uptake properties at multiple sample locations in parallel. Details on construction and theory for this apparatus are provided. In addition, the functionality of the high-throughput device is evaluated using standard Nafion® films and a model semi-interpenetrated polymer network with commercial polyvinylidine fluoride as the host matrix for a proprietary polyelectrolyte supplied by Arkema, Inc. In Chapter 3, the new instrument is used to evaluate the effects of rapid Fenton's degradation on water transport through Nafion®. Using the basic protocols for Fenton's reagents, aqueous solutions with different concentrations of hydrogen peroxide and ferric chloride were prepared for film exposure at a controlled temperature. The resulting discrete combinatorial library of samples representing various degradation conditions was then screened for trends in mass transport properties to determine if certain rapid degradation conditions could possibly be correlated to the real time degradation of Nafion® during fuel cell operation.

Moving away from commercially available and proprietary proton exchange membranes, Chapter 4 describes the first attempt at discovering novel polymer systems for PEMFC applications. Similar to the concept of semi-interpenetrating networks, the goal here was to create low-cost two-component systems with mechanically stable and proton conductive polymers. However, rather than generating a two phase blend, we attempted to minimize phase separation without the use of additives by using two structurally similar polymers. Polyetherimide was selected as the base polymer for its availability, low cost, thermochemical tolerance, and mechanical stability. To produce its ion-conductive counterpart, polyetherimide was sulfonated using a number of techniques obtained from literature. Each technique is evaluated based on degree of sulfonation and chain scission, as well as blend compatibility and film formation. The most effective sulfonation procedure from Chapter 4 was then used in Chapter 5 for the optimization of sulfonated polyetherimide blends with the high-throughput methods described previously. Various blend compositions and film formation conditions were evaluated for maximizing ion-conductivity and reducing phase separation. In addition to these optimized properties, thermal, mechanical and water uptake properties were characterized in selected blends to predict membrane performance during fuel cell operation. Chapter 6 concludes with a summary of the important findings and provides future recommendations based on this work.

1.5. REFERENCES

1. *Annual Energy Outlook*. 2009, Energy Information Administration, US Department of Energy: Washington, DC.

2. *Annual Energy Review*. 2007, Energy Information Administration, US Department of Energy: Washington, DC.

3. *International Energy Outlook*. 2008, Energy Information Administration, US Deparment of Energy: Washington, DC.

4. Newton, D.E. *The Oil Embrago*. 2005. BookRags. [cited 2009 1 May]; Available from: http://www.bookrags.com/research/oil-embargo-enve-02/.

5. Jackson, P.M., *Why the "Peak Oil" Theory Falls Down -- Myths, Legends, and the Future of Oil Resources*, in *Cambridge Energy Research Associates*. 2006.

6. Nel, A., *ATMOSPHERE: Enhanced: Air Pollution-Related Illness: Effects of Particles.* Science, 2005. **308**(5723): p. 804-806.

7. Mutters, R. and S. Soret, *Statewide Potential Crop Yield Losses From Ozone Exposure*. 1998, Division of Agricultural and Natural Resources, North Region, University of California: Davis, CA.

8. *IPCC, 2007: Summary for Policymakers.*, in *Climate Change 2007: The Physical Science Basis. Contribution of Working Group I to the Fourth Assessment Report of the Intergovernmental Panel on Climate Change*, S. Solomon, et al., Editors. 2007, Cambridge University Press: New York, NY.

9. Graedel, T.E. and J.A. Howard-Grenville, *Fossil Fuel Extraction and Processing*, in *Greening the Industrial Facility: Perspectives, Approaches, and Tools*. 2005, Springer. p. 129-146.

10. *Renewable Energy Annual*. 2009, Energy Information Administration, US Department of Energy: Washington, DC.

11. Tester, J.W., et al., *Sustainable energy : choosing among options*. 2005, Cambridge, Mass.: MIT Press. xxiii, 846 p.

12. *Types of Fuel Cells: Phosphoric Acid Fuel Cells (PAFC)*. Fuel Cell Basics 2009. U.S. Department of Defense Fuel Cell Test and Evaluation Center. [cited 2009 May 29]; Available from: http://www.fctec.com/fctec_types_pafc.asp.

13. Larkins, J.T., *Fuel cell powered transit bus development activities at Georgetown University.* Fuel Cells Bulletin, 1998. **1**(1): p. 6-8.

14. Carlson, E., et al., *Using Phosphoric-Acid Fuel Cells For Distributed Generation* ASHRAE Journal 2007. **49**: p. 50-51.

15. Smith, J.A., et al., *A broad look at the workings, types, and applications of fuel cells.* Power Engineering Society Summer Meeting, IEEE, 2002. **1**: p. 70-75.

16. *Types of Fuel Cells*. 2009. U.S. Department of Defense Fuel Cell Test and Evaluation Center. [cited 2009 2009]; 29 May]. Available from: http://www.fctec.com/fctec_types_afc.asp.

17. Prater, K.B., *Polymer electrolyte fuel cells: a review of recent developments* Journal of Power Sources, 1994. **51**(1): p. 129-144.

18. Litster, S. and G. McLean, *PEM fuel cell electrodes.* Journal of Power Sources, 2004. **130**(1): p. 61-76.

19. Parthasarathy, A., S. Srinivasan, and A.J. Appleby, *Electrode kinetics of oxygen reduction at carbon-supported and unsupported platinum microcrystallite/Nafion® interfaces.* Journal of the Electrochemical Society, 1992. **339**(1): p. 101-121.

20. Ticianelli, E.A., et al., *Methods to advance technology of proton exchange membrane fuel cells.* Journal of the Electrochemical Society, 1988. **135**(1): p. 2209-2214.

21. Murphy, O.J., G.D. Hitchens, and D.J. Manko, *High power density proton-exchange membrane fuel cells.* Journal of Power Sources, 1994. **47**(3): p. 353-368.

22. Zegers, P., *Fuel cell commercialization: The key to a hydrogen economy.* Journal of Power Sources, 2006. **154**(2): p. 497-502.

23. *DoE Decision Team Committee Report, On-Board Fuel Processing Go/No Decision, August 2004*. 2004. [cited 2005; Available from: http://www.eere.energy.gov/hydrogenandfuelcells/.

24. DiSalvo, F.J., *Solid State Chemistry: A A Rediscovered Chemical Fronteir.* Science, 1990. **247**(4943).

25. Xiang, X.-D., *Combinatorial Materials Synthesis and Screening: An Integrated Materials Chip Approach to Discovery and Optimization of Functional Materials.* Annual Review of Materials Science, 1999. **29**(1): p. 149-171.

26. Xiang, X.D., et al., *A Combinatorial Approach to Materials Discovery.* Science, 1995. **268**(5218): p. 1738-1740.

27. Richard Hoogenboom, M.A.R.M., Ulrich S. Schubert,, *Combinatorial Methods, Automated Synthesis and High-Throughput Screening in Polymer Research: Past and Present.* Macromolecular Rapid Communications, 2003. **24**(1): p. 15-32.

28. Meredith, J.C., A. Karim, and E.J. Amis, *High-Throughput Measurement of Polymer Blend Phase Behavior.* Macromolecules, 2000. **33**(16): p. 5760-5762.

29. Rajan, K., *Combinatorial Materials Sciences: Experimental Strategies for Accelerated Knowledge Discovery.* Annual Review of Materials Research, 2008. **38**(1): p. 299-322.

30. Meredith, J.C., et al., *Combinatorial Materials Science for Polymer Thin-Film Dewetting.* Macromolecules, 2000. **33**(26): p. 9747-9756.

31. Zapata, P.J., *High Throughput Study of Fuel Cell Proton Exchange Membranes: Poly(Vinylidene Fluoride)/Acrylic Polyelectrolyte Blends and Nanocomposites with Zirconium*, in *School of Chemical and Biomolocular Engineering*. 2009, Georgia Institute of Technology: Atlanta, GA. p. 269.

32. Webster, D.C., B.J. Chisholm, and S.J. Stafslien, *Mini-review: Combinatorial approaches for the design of novel coating systems*, in *Biofouling*. 2007, Taylor & Francis Ltd. p. 179-192.

33. Genzer, J. and R.R. Bhat, *Surface-Bound Soft Matter Gradients.* Langmuir, 2008. **24**(6): p. 2294-2317.

34. Meredith, J.C., *Advances in combinatorial and high-throughput screening of biofunctional polymers for gene delivery, tissue engineering and anti-fouling coatings.* Journal of Materials Chemistry, 2009. **19**: p. 34 - 45.

35. Stafford, C.M., et al., *Generating thickness gradients of thin polymer films via flow coating.* Review of Scientific Instruments, 2006. **77**(2): p. 023908.

36. Reyna-Valencia, A., S. Kaliaguine, and M. Bousmina, *Tensile mechanical properties of sulfonated poly(ether ether ketone) (SPEEK) and BPO4/SPEEK membranes.* Journal of Applied Polymer Science, 2005. **98**(6): p. 2380 - 2393.

37. Qiao, J., T. Hamaya, and T. Okada, *New highly proton conductive polymer membranes poly(vinyl alcohol)–2-acrylamido-2-methyl-1-propanesulfonic acid (PVA–PAMPS).* Journal of Materials Chemistry, 2005. **15**(41): p. 4414 - 4423.

38. Gao, Y., et al., *Sulfonated copoly(phthalazinone ether ketone nitrile)s as proton exchange membrane materials* Journal of Membrane Science, 2006. **278**(1): p. 26-34.

39. Hickner, M.A., et al., *Alternative Polymer Systems for Proton Exchange Membranes (PEMs).* Chemical Reviews, 2004. **104**(10): p. 4587-4612.

40. Zawodzinski, T.A.J., et al., *Characterization of polymer electrolytes for fuel cell applications.* Solid State Ionics, 1993. **60**(1): p. 199-211.

41. Cappadonia, M., et al., *Conductance of Nafion 117 membranes as a function of temperature and water content.* Solid State Ionics, 2000. **77**(1): p. 65-69.

42. Wang, Y. and C.-Y. Wang, *Transient analysis of polymer electrolyte fuel cells.* Electrochimica Acta 2005. **50**(6): p. 1307-1315.

43. Watari, T., et al., *Water vapor sorption and diffusion properties of solfonated polyimide membranes* Journal of Membrane Science, 2003. **219**: p. 137-147.

44. Lee, W.K., et al. *Effect of Humidty on PEM Fuel Cell Performance: Part I - Experiements PART I*. in *International Mechanical Engineering Congress & Exposition*. 1999. Nashville, TN.

45. Ge, S., et al., *Absorption, Desorption, and Transport of Water in Polymer Electrolyte Membranes for Fuel Cells.* Journal of the Electrochemical Society, 2005. **152**(6): p. A1149-A1157.

46. Yan, W.-M., et al., *Analysis of thermal and water management with temperature-dependent diffusion effects in membrane of proton exchange membrane fuel cells.* Journal of Power Sources, 2004. **129**(2): p. 127-137.

47. Yoshioka, S., et al., *Development of a PEFC under low humidified conditions.* Journal of Power Sources, 2005. **144**(1): p. 146-151.

48. Hickner, M.A., C.H. Fujimoto, and C.J. Cornelius, *Transport in sulfonated poly(phenylene)s: Proton conductivity, permeability, and the state of water* Polymer, In Press, Corrected Proof, 2006. **xx**(xx): p. 1-7.

Chapter 2
High-Throughput Mass Transport Characterization of Polymer Membranes

Reproduced with permission from Keith Reed and J.C. Meredith
Unpublished work (*submitted to the Journal of Combinatorial Chemistry*)

A parallel high-throughput mass transport analysis tool has been developed that uses downstream pressure detection to determine the flux and permeability of permeates through either multi-composition (combinatorial) or homogeneous polymer films in parallel. The functionality of this device was evaluated using water pervaporation experiments at various temperatures on standard perfluorosulfonic acid (PFSA) membranes (Nafion®), modified PFSA membranes with alkyl ammonium bromides, and degraded PFSA membranes from an accelerated durability test. In addition, polymer blends consisting of polyvinylidene difluoride (Kynar®) and an acrylic polyelectrolyte (PE), have been evaluated to determine the effect of composition on water transport. The results show that water flux and permeability values fall within the range of reported literature values for PFSA pervaporation experiments. Both transport properties varied with temperature according to an Arrhenius model, which allowed for the determination of characteristic water transport activation energies. As expected, the cationic substitution of PFSA films with alky ammonium bromides resulted in lower transport values, while exposure to Fenton's degradation reagent resulted in higher water flux and permeability. The HT-MTA also detected changes in transport properties due to

increasing the PE content in polymer blends. Both water flux and permeability were maximized in the range of 40 – 55 wt% PE, consistent with a previous study showing optimal proton conductivities for the same polymer system over the same concentration range.

2.1. INTRODUCTION

Tailoring the mass transport properties of polymer films and membranes has proven to be essential for a broad range of industrial separation applications, including CO_2 extraction, O_2 purification, and water desalination [1-5]. Transport characterization and optimization are also essential to achieving desired transport properties in ion-exchange membranes, such as proton exchange membranes for fuel cells (PEMFCs). These electrolyte materials facilitate proton mobility, provide electrical insulation to the anode and cathode, and serve as gas barriers against fuel and oxidant crossover – functions which are all impacted by the transport of water, fuel, and air. Structural stability and durability are also strongly affected by water transport, particularly due to the cycling between hydrated and non-hydrated states [6, 7]. Optimization of these properties is essential to the commercial success of PEMFCs.

Most current commercially available PEMs utilize perfluorinated, sulfonic acid containing ionomers such as DuPont's Nafion®, Asahi Glass's Flemion®, and Asahi Chemical's Aciplex® [8]. Additionally, recent reviews cite the investigation of polystyrenes, polybenzimidazoles, polyphenylene oxides, and poly(arylene ether)s, among others, for PEM applications [9-12]. While these materials may display high proton conductivity under proper hydration, opportunities for improving cost, high-temperature hydration, chemical and mechanical stability, and fuel permeability exist.

For this reason, there has been continued interest in developing optimized multi-component polymer membrane systems for PEMFCs.

Due to the abundance of material combinations, the numerous degrees of freedom in polymer processing, and time-intensive characterization of transport and mechanical properties, efficient methods are needed for screening new formulations [13]. Combinatorial methods meet these objectives using gradient or discrete techniques to capture process variations such as annealing temperature, thickness, and chemical composition into a single polymer sample that serves as a library of materials [14, 15]. However, a comprehensive toolset of high-throughput measurement techniques is needed to characterize the libraries. Previous work in our group has resulted in the development of high-throughput conductivity and mechanical characterization tools for proton exchange membranes [14, 16]. This chapter introduces a novel instrument for high-throughput measurement of transport properties as an addition to the characterization toolset. Water pervaporation measurements have been used to demonstrate the parallel screening of transport properties in multi-film libraries.

Many techniques are currently available for measuring water uptake in polymer films. Traditionally, mass change is quantified gravimetrically under controlled temperature and humidity [17, 18]. Other methods of moisture content detection include optical spectroscopy [19, 20], mass spectrometry [21-23], chromatography [24-30], and residual gas analysis [31]. While each of these measurement techniques has its own strengths, none are convenient for parallel high-throughput analysis due to the cost and complexity of implementing numerous measuring systems simultaneously. To achieve scalable, high-throughput water uptake analysis, variable-volume and variable-pressure permeation experiments are preferred. In variable-volume permeation, as reported by Brudaker and Kemmermeyer [32], one side of the sample film is exposed to a permeating feed at constant pressure, while the opposite side, attached to an initially

evacuated chamber, is monitored for increasing volume through liquid capillary displacement. Variable-pressure permeation experiments avoid the use of capillaries entirely, since the increasing permeate chamber pressure, rather than the chamber volume, is recorded as a function of time. The rate of pressure change can then be used to determine permeate flux through the exposed film area. As a single-sample, low-throughput technique, this method has been reported by Heilman and colleagues [33], by researchers in industry (Porous Materials, Inc. [34] and the Dow Chemical Company [35]), and has been adopted as a standard analysis method by the American Society for Testing Materials [36]. Below, we describe the experimental setup and theory used for high-throughput, variable-pressure permeation measurements.

2.2. EXPERIMENTAL

2.2.1. High-Throughput Liquid Permeation

The High-Throughput Mass Transport Assay (HT-MTA) has been developed to screen transport of water vapor or liquid. The HT-MTA, shown in Figure 2-1, consists of a custom stainless steel membrane retention mechanism fitted with a single inlet for the upstream feed and 12 downstream permeate chambers, each with a volume of 2 cm^3 and equipped with Honeywell 26PC Series silicon pressure transducers. Films are sealed over the permeate chambers using two Viton® fluoroelastomer gaskets (DuPont Performance Elastomers). Both gaskets are cut with aligned openings, each with a diameter of 0.16 cm to form the film exposure areas. Each downstream port is spaced 0.5 cm, which is expected to reduce permeation interference among adjacent sample locations while maintaining an optimal number of assay points per unit film area. The retention mechanism, downstream chambers, and pressure sensing electronics are

enclosed in a vacuum oven with digital temperature control (Model 1430M, Sheldon Manufacturing, Inc.).

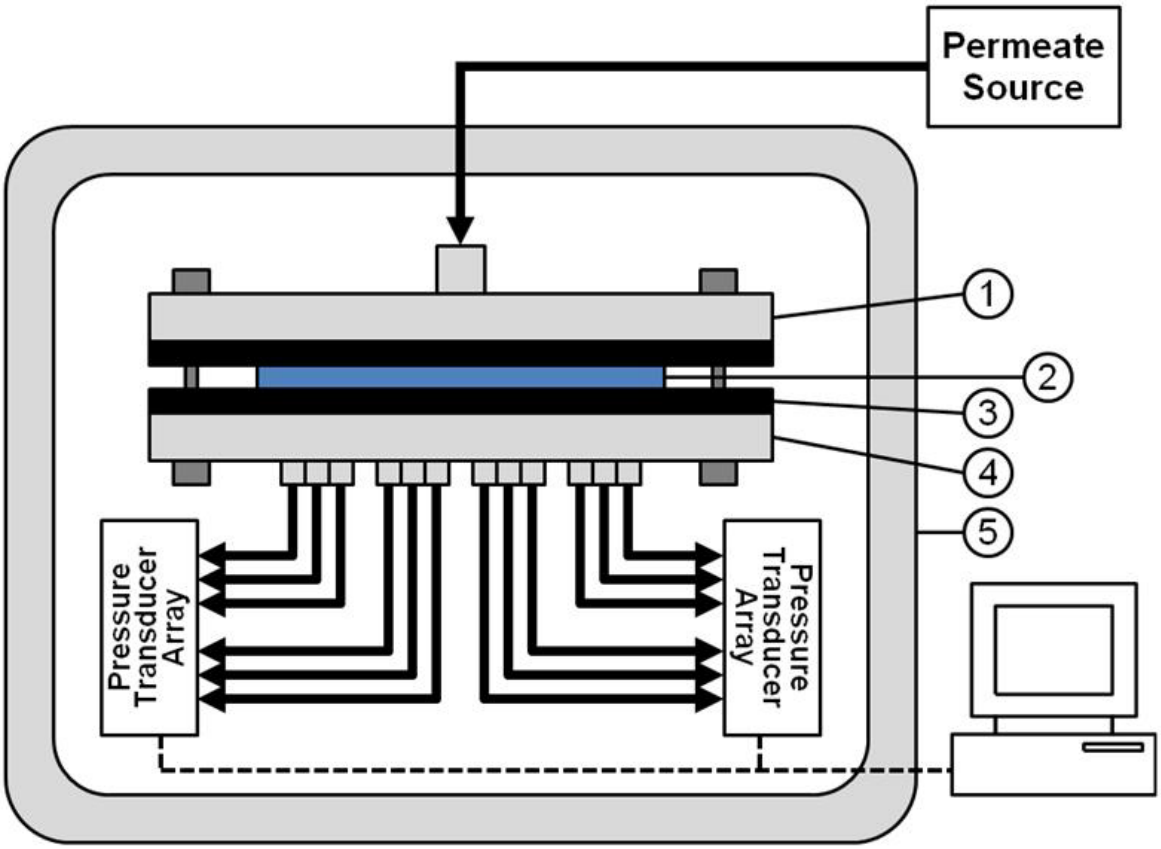

Figure 2-1: Schematic of the High-Throughput Mass Transport Apparatus. 1) Top cover of membrane retention for permeate feed. 2) Membrane. 3) Viton® sealing gaskets with a grid of aligned openings for downstream flow. 4) Bottom cover of membrane retention mechanism with outlets for downstream pressure sensing. 5) Vacuum oven for system drying and temperature control.

Dried samples are placed onto the base of the membrane retention mechanism such that they completely cover each gasket opening before being sealed into place with the top feed inlet. For a single film, a 4x4 cm sheet is sufficient to cover all ports. When multiple samples are tested in parallel, either 4x0.5 or 4x2 cm strips are cut to cover the grid of downstream pressure channels. For all experiments, a single downstream channel covered with the gasket material is used as impermeable reference since the water breakthrough time of Viton® (> 8 h [37, 38]) well exceeds the pervaporation timescale used for films in this study (~2 h). The retention mechanism is held into place with six bolts, each tightened to approximately 4.5 N-m using an adjustable torque wrench. A leak test is used to assure proper sealing around each downstream channel, after which the assay temperature is set in the vacuum oven at atmospheric pressure. To begin the water pervaporation experiments, 6-8 ml of deionized water is fed to the upstream film surface until the feed chamber is filled. The feed is kept at atmospheric pressure while the downstream pressure, initially at atmospheric pressure, is continuously sampled using a National Instruments data acquisition card PXI6031E controlled by a customized LabView interface. Pressure data is collected for at least 1 h, after which the films are removed and the HT-MTA system is thoroughly dried overnight at 60 °C under vacuum.

2.2.2. Transport Characterization

Liquid water sorption into an initially dry, PEM film takes place within a few seconds, such that molar water flux, J_w, through the polymer at any sample location can be measured by an increase in downstream partial vapor pressure, p_w, over a given time, t, according to Equation 2-1:

$$J_w = \frac{1}{A}\frac{dn_w}{dt} = \frac{V_{pc}}{A * R * T}\frac{dp_w}{dt} \qquad \textbf{Equation 2-1}$$

where the permeate vapor is assumed to act as an ideal gas, dn_w/dt is the molar flow rate, A is the exposed film surface area, V_{pc} is the volume of the downstream pressure chamber at temperature, T, and R is the ideal gas constant. For quick sorption, flux will remain constant at early times until the downstream chamber becomes saturated with vapor. During this constant-transport-rate period, Fick's 1st law can be applied to approximate the characteristic diffusion coefficient of water, D_w, according to Equation 2-2:

$$J_w = -D_w \frac{\left(c_{dn} - c_{up}\right)}{\ell} \qquad \textbf{Equation 2-2}$$

where the interfacial upstream and downstream water concentrations, c_{up} and c_{dn}, divided by the swollen film thickness, ℓ, provide the diffusive driving force. While the interfacial concentrations cannot be measured explicitly with the HT-MTA to get diffusion coefficients, upstream and downstream pressures can be used to obtain permeability values, P_w. This is accomplished by using the solution-diffusion model from Wijmans and Baker [39], shown in Equation 2-3:

$$J_w = P_w \frac{\left(p_{sat} - p_{dn}\right)}{\ell} \qquad \textbf{Equation 2-3}$$

where p_{sat} is the water vapor saturation pressure, obtained from Antoine's equation for a given temperature, and p_{dn} is the partial vapor downstream pressure in the permeate chamber. In the HT-MTA, differential pressure monitoring is used to neglect any atmospheric water vapor that might be present at the start of pervaporation experiments. Using the differential pressure basis, the pressure driving force can be written in terms of the downstream differential pressure at any time, p_t', and the differential downstream pressure at infinite time and equilibrium saturation, p_∞':

$$p_{sat} - p_{dn} = p_{\infty}' - p_t' \qquad \textbf{Equation 2-4}$$

In a typical pervaporation setup, the downstream pressure is maintained under vacuum so that p_{dn} remains approximately zero. For the HT-MTA system, where vapor accumulates downstream, p_t' is initially zero. If pseudo steady-state transport takes place at early pervaporation times, i.e. immediately after upstream permeate exposure, such that $p_t' << p_{\infty}'$, Equation 2-3 can be simplified to solve for P_w:

$$P_w = J_w \frac{\ell}{p_{\infty}'} \qquad \textbf{Equation 2-5}$$

The units for permeability are typically expressed in Barrer, where 1 Barrer = 10^{-10} cm^3(STP) cm cm^{-2} s^{-1} $cmHg^{-1}$. It should be noted that under completely dry initial conditions, p_{sat} can be used in place p_{∞}', therefore allowing for quick permeability calculations since the establishment of an equilibrium downstream pressure could then be avoided.

2.2.3. System Functionality

Three types of experiments have been used to demonstrate the functionality of the HT-MTA. To evaluate the device's point-to-point variance, accuracy, and repeatability, the first set of experiments investigated transport through commercially available Nafion® PFSA films at temperatures varying from 30 to 60 °C. In the second set of experiments, Nafion® films were chemically modified with a Fenton's reagent or through ion exchange with either tetrapropylammonium bromide (TPAB) or cetyl trimethylammonium bromide (CeTAB), shown in Figure 2-2.

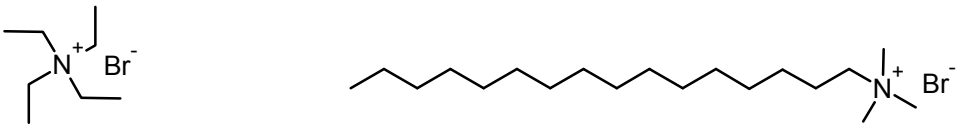

Tetrapropylammonium bromide (TPAB) Cetyltrimethylammonium bromide (CeTAB)

Figure 2-2: Alkyl ammonium bromide salts used for ion exchange with Nafion® 112.

The Fenton's reagent is known to degrade Nafion® films over time, while CeTAB and TPAB are thought to reduce water transport in Nafion® by blocking access to the hydrophilic sulfonic acid pathways. Each of these experiments, repeated two to four times, was performed at 50 °C with unmodified Nafion®, which was always included in the HT-MTA as a reference. In the final set of experiments, the effects of composition on water transport were evaluated using polymer blends of polyvinylidine fluoride (PVDF) and a polyelectrolyte (PE) containing protonated sulfonic acid groups. This binary polymer model has been described recently as a prospective alternative PEM material [40]. Three strips of the PVDF/PE films with PE concentrations ranging from 30 to 60 % by weight were also tested with Nafion® at 50 °C and repeated at least three times. PVDF without polyelectrolyte was also evaluated as an additional control.

2.2.4. Materials and Chemical Treatments

Extruded, pre-protonated Nafion® 112 (Dupont, Inc.) samples were used as the control standard and for temperature-dependent experiments. In its dry state, the sheet had a thickness of 50 ± 1 μm that expanded to 55 ± 1 μm when completely swollen in deionized water. For the accelerated Fenton reagent degradation, a Nafion® sample was immersed in an aqueous solution of 30 ppm $FeCl_3$ and 30 % H_2O_2 at 60 °C overnight. The sample was then washed in deionized water before boiling at 80 °C deionized water for 1.5 h. Samples were stored in water and then dried at room temperature under a vacuum pressure of 635 mmHg overnight prior to permeation tests. For ion exchange treatments, Nafion® samples were immersed in supersaturated aqueous solutions of

either CeTAB or TPAB overnight at 60 °C. The samples were stored in their respective salt solutions, and prior to permeation experiments, were rinsed thoroughly with deionized water and dried under vacuum.

Two types of PVDF powders, Kynar® 731 and 2801, were supplied by Arkema, Inc. Kynar® 731 has a molecular weight of 462,000, whereas Kynar® 2801, a random copolymer of PVDF and 12 wt% hexafluoropropylene (HFP), has a molecular weight of 100,000. The polyelectrolyte (PE), a random copolymer consisting of 70 wt% sulfoethyl methacrylate, 15 wt% hydroxyethyl methacrylate, 8 wt% methyl methacrylate, and 7 wt% styrene dissolved in n-methyl-2-pyrrolidone (NMP), was also supplied by Arkema, Inc, as described previously [16]. The PVDF/PE films were made from stock solutions of each component and dissolved at 10-15 wt% in NMP. The solutions were combined according to the desired PE concentration and allowed to mix at room temperature for 15 min. In order to crosslink the PE, a polymeric hexamethylene diisocyanate (Desmodur® N3300A, supplied by Bayer Corp.) was added to the solution at a 1:0.8 molar ratio of OH:NCO. After mixing for an additional 5 minutes, the solution was coated onto a silicon wafer using a knife-edge coater, described previously [41]. The coated wafer was dried in a convection oven at 175°C for 15 min to remove excess NMP and complete the crosslinking process. Films were lifted from the silicon substrate by immersion in water, and then stored in water until dried for permeation experiments. All PVDF/polyelectrolyte films had a swollen thickness of 25 ± 1 μm.

2.3. RESULTS AND DISCUSSION

2.3.1. HT-MTA Functionality and Transport Evaluation

Standard pervaporation can be described as occurring in four consecutive steps: 1) upstream sorption of liquid permeate into the membrane, 2) diffusion through the

membrane, 3) downstream desorption into a vapor phase, and 4) vapor transport from the membrane surface to the permeate bulk [42, 43]. According to Silva et al. [42] and Binning [44], sorption and desorption steps occur much faster than membrane diffusion for the pervaporation process due to the limiting rate associated with permeate phase change in the membrane. Also, Meuleman et al. [43] noted that vapor transport into the permeate bulk generally occurs significantly faster than the other steps. Therefore, membrane diffusion is most often assumed to be the rate-limiting step and can be directly related to the rise in permeate vapor pressure over time. In a transient, non-circulating pervaporation system like the HT-MTA, where permeate accumulates on the downstream side of the film, the resistances to desorption and vapor diffusion increase over time. Therefore water flux is evaluated immediately after film exposure to minimize the effects of these rate limiting steps.

Parallel downstream differential pressure profiles for water permeation through Nafion® at 30 °C are shown in Figure 2-3. Water is exposed to the top surface of the sample at $t = 0$, and within seconds, vapor transports into the downstream chamber at a constant rate, indicated by the early linear pressure profiles. This almost immediate transition into pseudo steady-state moisture transport confirms that liquid sorption into the dry membrane occurs quickly relative to membrane diffusion.

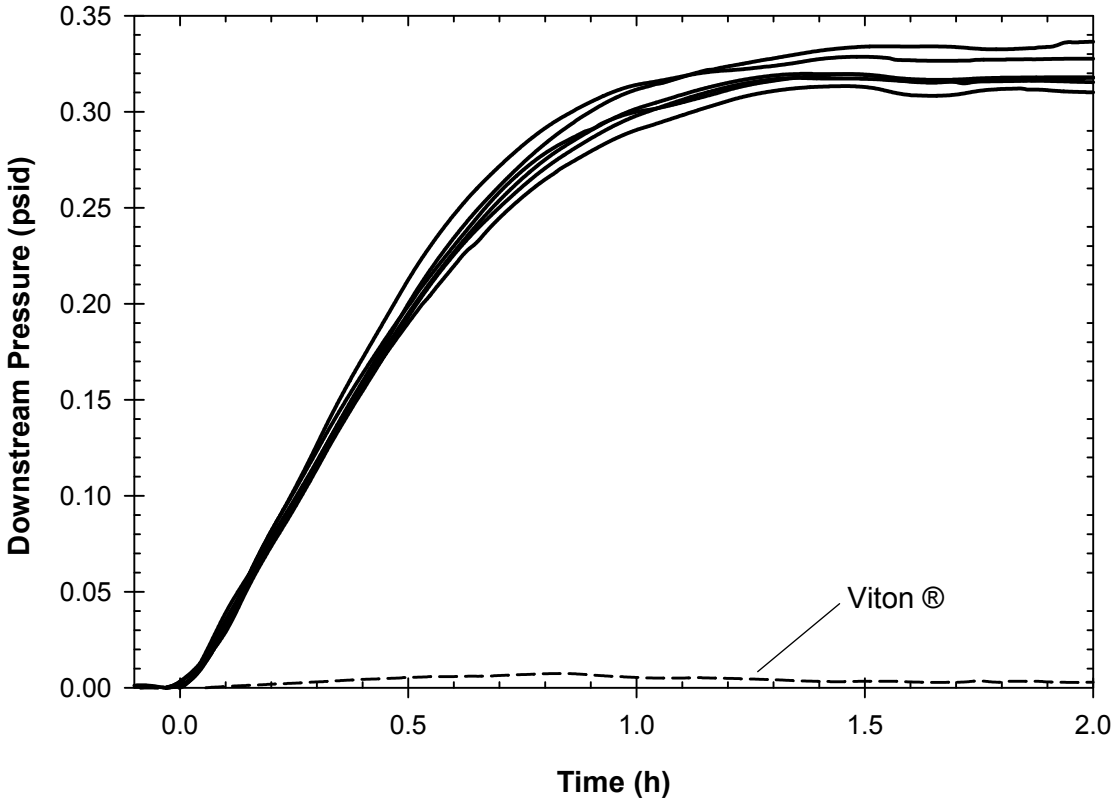

Figure 2-3: Differential downstream pressure profiles from a high-throughput water pervaporation experiment with Nafion® 112 at 30 °C. Water is exposed to the upstream film surface at *t* = 0, and each profile is referenced to Viton® (dashed line).

At later times, the downstream vapor pressures approach values between 0.30 and 0.35 psi, approximately half of the saturation pressure of water at 30 °C. It is possible that the affinity of water to acid groups in the membrane can reduce the saturation pressure of water. However, the difference between p_{∞}' and p_{sat} could also be attributed to atmospheric humidity initially present in the downstream chambers. Typically, atmospheric relative humidity values fluctuate between 30 and 40 %.

Each pressure profile was linearized around the maximum differential rate change to provide a reliable approximation for the pseudo steady-state molar flow rate. Figure 2-4 displays an example linearization from Figure 2-3.

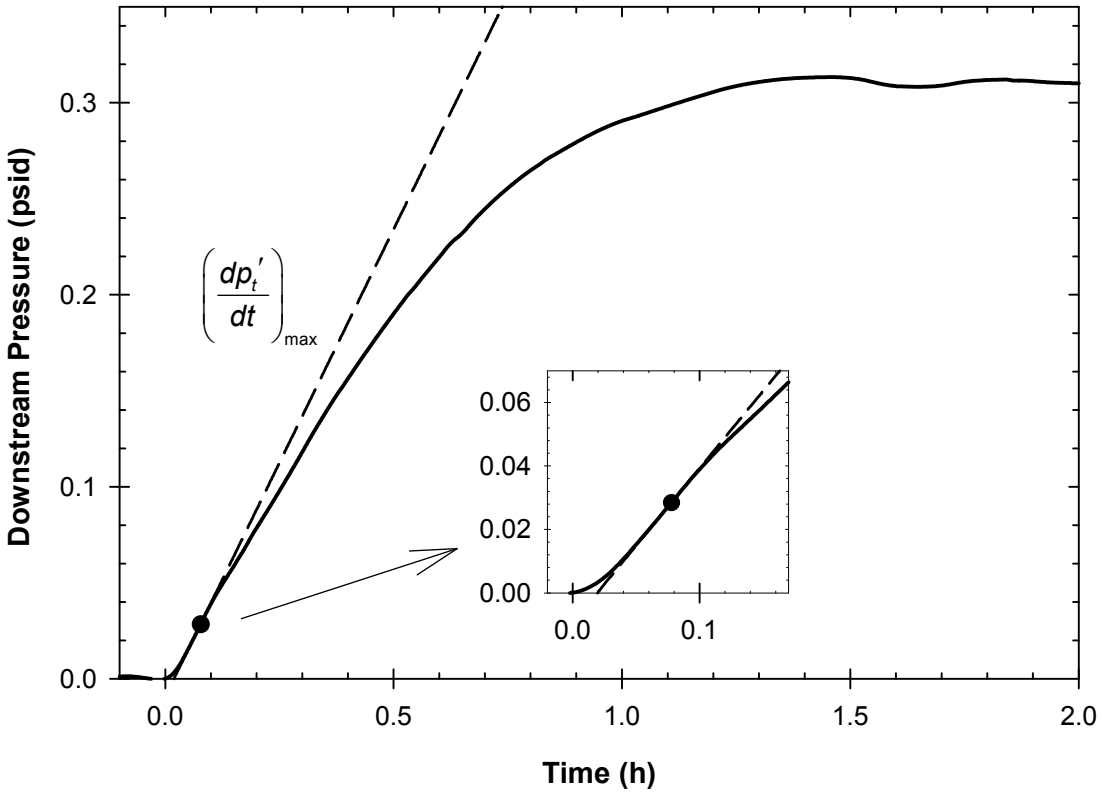

Figure 2-4: Example linearization around the maximum differential rate of pressure change (●).

Using these linear approximations with Equation 2-1 gives an average pseudo steady-state flux of 1.1 x 10^{-5} kg m^{-2} s^{-1} (± 0.1x10^{-5}). This value has been compared with Nafion®/water flux values from other studies that used various film thicknesses, temperatures, and pervaporation configurations, as summarized in Table 2-1. Unfortunately, the variation is large among these studies, spanning three orders of magnitude within the temperature range of 30 to 35 °C. PFSA film thicknesses may contribute to these variations; however, the work from Hensley et al. [45], Romero et al. [46], and Majsztrik et al. [47] (see Table 2-1) suggest that thickness has negligible effects on liquid water flux, at least within the range of 25 to 254 μm. Therefore, the differences among reported values are most likely the result of differing feed and permeate conditions, e.g., stagnant or flowing upstream water source with a either a downstream vacuum trap or a variable flow rate sweeping gas. In the study conducted by Rivin et al. [48], reporting a flux value of 1.2 x10^{-6} kg m^{-2} s^{-1} at 32 °C for a double layer of Nafion® 117, downstream sweep gas was used to maintain a constant concentration driving force across the sample. Using a similar downstream configuration, Romero et al. obtained flux values on the order of 10^{-4} kg m^{-2} s^{-1} at temperatures ranging from 30 to 50 °C. Higher values were obtained by Majsztrik et al., on the order of 10^{-3} kg m^{-2} s^{-1}, also using downstream sweep gas between 30 and 80 °C. The order of magnitude difference between the two previously mentioned studies may be explained by the difference in upstream conditions. Majsztrik et al. reported using a circulating water inlet, while upstream conditions from Romero et al. were stagnant, similar to the HT-MTA. Although the water concentration at the membrane surface remains constant in both cases, the differing upstream configurations and the resulting transport values suggest that upstream fluid velocities influence sorption characteristics.

While stagnant feed conditions may lead to reduced flux values, transport is also likely influenced by downstream conditions. Romero et al. and Majsztrik et al. both

demonstrated that as sweeping gas flow rates approach stagnant conditions, transport rates drop to values within 10^{-5} and 10^{-4} kg m^{-2} s^{-1}, very close to those values reported in this study. We expected that reduced downstream flow conditions would also compare well to experiments using downstream evacuation since partial vapor pressures and convective transport are minimized. However, Ames et al. [49] and Hensley et al.[45], who used upstream circulation and downstream evacuation, both report very high flux values on the order of 10^{-3} kg m^{-2} s^{-1} at 24 and 35 °C, respectively. These values are much closer to values obtained by Majsztrik et al. under high downstream convection. In these three studies, upstream circulation was maintained during pervaporation, again suggesting that convection may also play a role in upstream water sorption and overall transport characteristics.

Table 2-1: Reported Average Flux Values for Liquid Water through Nafion®

Reference	Upstream Config.	Downstream Config.	Thickness	Temp. (°C)	J (x10^5 kg s^{-1} m^{-2})	P (x10^{-4} Barrer) [a]
Reed and Meredith (this work)	stagnant liquid at atm. pressure	stagnant dry air at atm. Pressure	55 µm	30	1.1 ± 0.1	4.3 ± 0.4
				40	1.7 ± 0.2	8.1 ± 1.1
				50	6.1 ± 0.5	12.5 ± 1.1
				60	11.9 ± 2.6	16.2 ± 4.5
Rivin et al. [48]	not given	sweep gas at 1 l/min	356 µm	32	0.12	1.6
Ames et al. [49]	flowing liquid	vacuum and cold trap	25 µm	24	94	120
Hensley et al. [45]	flowing liquid	vacuum and cold trap	25 µm	35	210	150
			51 µm	35	280	420
			127 µm	35	180	680
			178 µm	35	180	950
Romero et al. [46]	stagnant liquid at atm. pressure	sweep gas at 1 l/min	51 µm	50	41	28
			127 µm	30	14	72
				40	22	62
				50	65	69
			183 µm	50	25	62
		sweep gas at 0-50 ml/min [b]	127 µm	30 – 50	~9	~26
Majsztrik et al. [47]	flowing liquid at atm. pressure	sweep gas at 1.1 l/min	51 µm	30	170	330
				50	380	260
				70	680	190
				80	617	110
			127 µm	30	130	630
				50	280	480
				70	450	300
				80	500	220
			254 µm	30	140	1400
				50	250	850
				70	400	540
				80	500	450
		sweep gas at 0-50 ml/min [b]	51 -254 µm	30	5 – 7	10 – 170
				80	170 – 250	30 – 220

[a] Calculated using Equation 2-3 or Equation 2-5

[b] Estimated from graphical data at the lowest given sweep gas flow rate

Flux values from Table 2-1 were normalized with their respective driving forces to estimate water permeability through Nafion® at various temperatures according to Equation 2-3 and Equation 2-5. As could be expected, variation among reported permeability values is somewhat reduced compared to water flux, while general observations made above concerning the effects of pervaporation conditions remain the same. The permeability calculations from HT-MTA experiments compare very well with values from Romero et al. and Majsztrik et al. under low downstream flow conditions, while values under high downstream convective flow and vacuum trapping are somewhat higher than ours. Therefore, due to variations in pervaporation methods, transport characteristics such as permeate flux and membrane permeability may not be compatible among different studies, but can still be used to screen for those trends that can help in identifying structure/property relationships for membrane optimization.

2.3.2. Temperature Dependence of Water Transport

High-throughput water pervaporation experiments were performed for Nafion® films between 30 and 60 °C to investigate the HT-MTA's ability to detect the effects of temperature on flux and permeability. The results from 24 experiments, each sampling up to 12 locations simultaneously, are averaged in Table 2-1. The HT-MTA results for flux and permeability show expected trends with temperature that are typical in mass transport experiments. Detailed correlations show that both flux and permeability obey the Arrhenius model according to Equation 2-6 and Equation 2-7 [50, 51]:

$$J = J_o \exp\left(\frac{-E_J}{RT}\right) \qquad \textbf{Equation 2-6}$$

$$P = P_o \exp\left(\frac{-E_P}{RT}\right) \qquad \textbf{Equation 2-7}$$

where E_J and E_P are the activation energies for the flux and permeability, respectively, indicating each property's temperature sensitivity. J_o and P_o are the respective pre-exponential factors. Arrhenius plots of ln(J) and ln(P) vs. $1/T$ are shown in Figure 2-5 for the temperature experiments from this study, as well as those conducted by Romero et al. and Majsztrik et al., previously cited in Table 2-1.

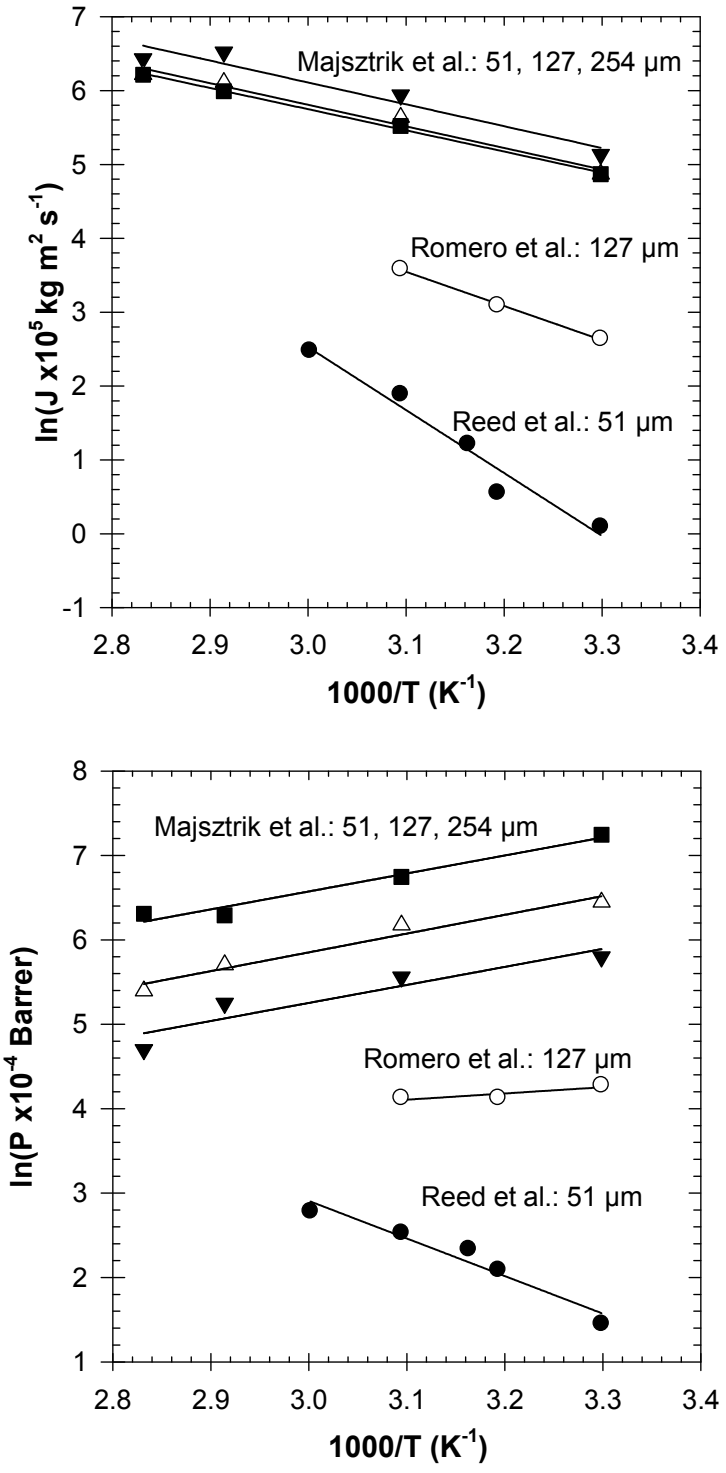

Figure 2-5: Arrhenius plots for water flux (a) and permeability (b), based on Nafion® pervaporation data from this study for 55 μm thick films(●), Romero et al. for 127 μm thick films (○), and Majsztrik et al. for 51 (▲), 127 (△), and 254 μm thick films (■).

These profiles were used with linear regressions to determine apparent values for E_J and E_P, which are displayed with their respective R^2 correlation values in Table 2-2. The flux/temperature relationship determined using the HT-MTA follows an expected Arrhenius model, but with a higher temperature dependence than that reported in the two literature comparison studies. The increased apparent activation energy for flux is most likely due to accumulation of downstream fluid, which increases the minimal energy required to transport water molecules through the film. Permeability also shows a positive Arrhenius dependence on temperature in the HT-MTA results, contrary to observations made in literature, where permeability of liquid water through Nafion® membranes decreases with increasing temperature, resulting in negative E_P values. The negative permeability-temperature correlation is common in pervaporation experiments and has been previously explained by Feng and Huang [50], who estimated E_P using Equation 2-3 and the Clausius-Clapeyron equation below to introduce the enthalpy of vaporization, ΔH_{vap}:

$$p_{sat} = B_o \exp\left(\frac{-\Delta H_{vap}}{RT}\right) \qquad \textbf{Equation 2-8}$$

where B_o is the pre-exponential factor. Combining Equation 2-8 with Equation 2-5, Equation 2-6, and Equation 2-7 for the case when $p_\infty = p_{sat}$, gives:

$$P = P_o \exp\left(\frac{-E_P}{RT}\right) = \frac{J_o}{\ell B_o} \exp\left(\frac{-E_J + \Delta H_{vap}}{RT}\right) \qquad \textbf{Equation 2-9}$$

$$E_P = E_J - \Delta H_{vap} \qquad \textbf{Equation 2-10}$$

For the given temperature range, enthalpy of vaporization remains relatively constant at 42 kJ/mol. If $E_J < \Delta H_{vap}$, which is the case for cited literature values, then E_P is negative. Since water flux is more sensitive to temperature in the HT-MTA, then E_P and the the response of permeability to temperature becomes more positive. Note that in Table 2-2, the difference between E_J and E_P from each study compares well with ΔH_{vap}, which is consistent with Equation 2-10.

Table 2-2: Activation Energies for Flux and Permeability Based on Linear Regressions of Arrhenius Model

Reference	Thickness	E_J (kJ/mol)	$(R^2)_J$	E_P (kJ/mol)	$(R^2)_P$
Reed and Meredith (this work)	55 μm	70.9	0.9589	37.0	0.9452
Romero et. al.[46]	127 μm	38	0.9981	-6	0.7658
Majstrik et al. [47]	51 μm	25	0.9362	-18	0.8694
	127 μm	24	0.9779	-19	0.9604
	254 μm	24	0.9973	-18	0.9655

Alternatively, E_P values can be explained with activation energies of diffusivity (E_D) and solubility (E_S) using their respective Arrhenius models to get Equation 2-11.

$$E_P = E_D + E_S \qquad \textbf{Equation 2-11}$$

In general, as temperature increases permeate solubility decreases in polymer membranes so that E_S is negative. Therefore, if the solubility coefficient is more sensitive to temperature than the diffusion coefficient, then E_P will also be negative. It has been observed that the sensitivity of solubility to temperature, and thus the E_P value, is strongly affected by the conditions of the mass transport experiment [52]. For example, many studies have investigated the permeability of methanol through PFSA membranes

using both pervaporation and permeation, which differs from pervaporation by using a well-mixed, dilute control volume of liquid on the downstream side of the membrane instead of evacuation or gas convection. The E_P value determined by pervaporation of concentrated methanol was negative in the temperature range of 35 to 60 °C (~-23 kJ/mol), close to that of pure water in the same measurement apparatus (~-30 kJ/mol) [51]. However, numerous studies have shown that the E_P from methanol permeation experiments using commercial PFSAs is positive in the same temperature range, with values ranging from 14 to 19 kJ/mol [53-56]. The similarity in permeability-temperature trends between the liquid permeation method and HT-MTA suggests that the positive correlation could be related to the accumulation of permeate downstream, which could reduce the temperature sensitivity of solubility. Therefore, the transport phenomena taking place in the HT-MTA more closely reflects a standard permeation experiment with downstream permeate accumulation, rather than a standard pervaporation with downstream evacuation or gas convection.

2.3.3. Effects of Chemical Modifications

Nafion® films treated with CeTAB and TPAB were evaluated for transport characteristics in parallel with untreated controls at 50 °C. Each experiment was repeated once, and the results are shown in Figure 2-6. As expected, both ion treatments produce significantly lower transport coefficients than the untreated control, consistent with the expected transport inhibition in the presence of hydrocarbon cations associated with SO_3^- groups in the membrane. There was no significant difference between flux or permeability values obtained for CeTAB and TPAB.

Chemical degradation was conducted by exposing films to a Fenton's reagent, which has been shown to degrade Nafion® by free hydroxyl radical attack [57]. The Fenton-degraded sample displayed slightly higher than normal flux and permeation characteristics at 50 °C, as shown in Figure 2-6. Increased water transport after

prolonged reagent exposure is likely the result of polymer chain scission that allows for increased chain mobility. It should also be noted that although transport increases with Fenton degradation, conductivity is significantly reduced from 80 to 20 mS/cm, measured using the four-point probe high-throughput conductivity measurement apparatus. This observation indicates possible loss or rearrangement of sulfonic acid groups resulting in decreased proton transport capacity.

As mentioned previously, all experiments with chemically-modified Nafion® films were accompanied by unmodified Nafion® and Viton®. In each case, HT-MTA could distinguish treated films from the control samples by significant differences in flux and permeability. These results suggest that “crosstalk” is negligible or nonexistent between adjacent pressure ports, and also demonstrates the ability of HT-MTA to efficiently characterize multiple films in parallel.

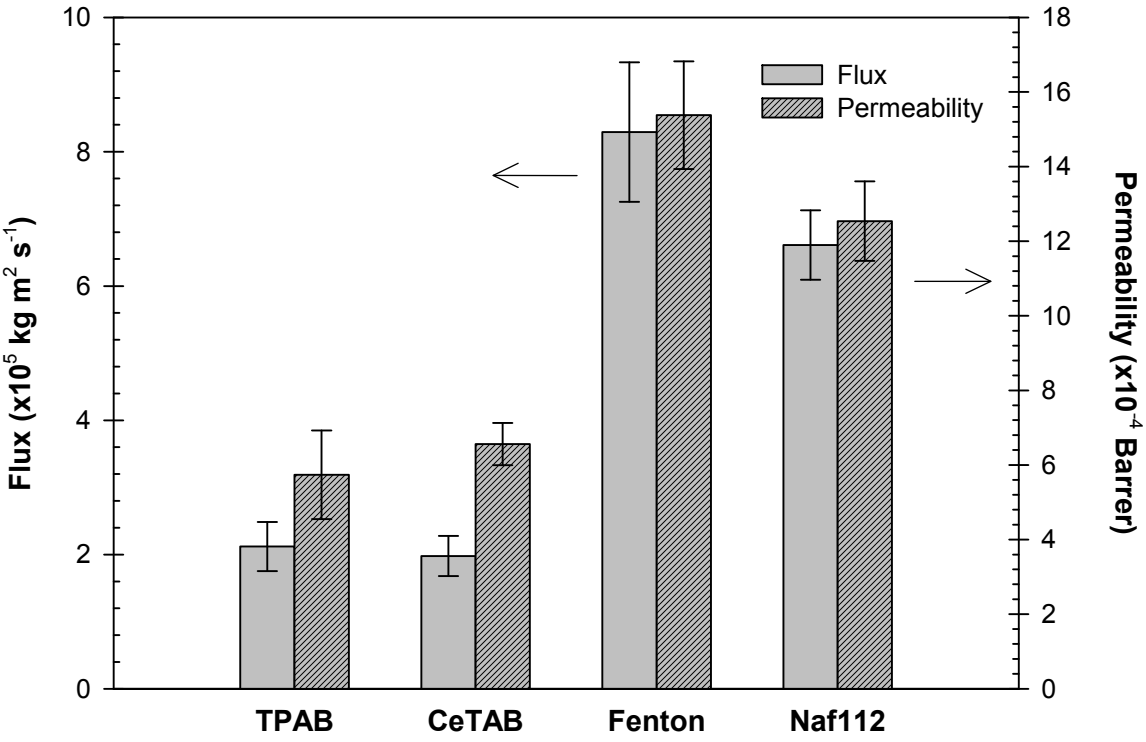

Figure 2-6: Transport characteristics of Nafion® 112 films either modified through the addition of TPAB and CeTAB salts, or degraded using a standard Fenton's reagent. All liquid water pervaporation experiments where carried out at 50 °C with unmodified Nafion® 112 as a control. Error bars represent 95 % confidence intervals.

2.3.4. Composition effects in PVDF/polyelectrolyte blends

Multiple blends of PVDF and PE at various compositions were tested in parallel along with Nafion® and Viton® as a control and reference, respectively. Two types of PVDF/PE blends were evaluated, each using a different PVDF formulation. Kynar® 2801 films were made with 30, 45, 55, and 60 wt% PE. Each of these films were cut to cover a single column of three downstream permeation ports, leaving two ports for the Nafion® sample, and one port for Viton®. The results from these experiments are shown in Figure 2-7. The film with 60 wt% PE film was too brittle for repeated experiments, so fewer data points were obtained at this concentration. For comparison purposes, Kynar® 2801 was casted from solvent without polyelectrolyte and the film (10 μm thickness) was also evaluated using the HT-MTA. No water transport was observed over the experimental time period for the pure Kynar® film, as expected. Therefore, the polyelectrolyte provides the dominant mode of water transport in PVDF/PE blends. In Figure 2-7, both water flux and permeability increase with PE content up to a PE loading of 45 wt%. Analysis of variance shows that the 30 and 60 wt% PE films have significantly lower flux and permeability values than the 45 and 55 wt% PE films (p-value < 0.05), with no significant difference within both groups. Therefore, the rate of water transfer across PVDF/PE films likely to be maximized near 45 to 55 wt% PE, suggesting that these polymer blends display an optimal degree of phase separation that facilitates water transport. For example, it is possible that at low concentrations of PE, continuous ionic channels do not form due to a lack of phase continuity, and at high PE concentrations, the PE aggregates into isolated domains that limit uniform transport. This phenomenon has been shown previously for other proton-conducting polymer blends [58, 59].

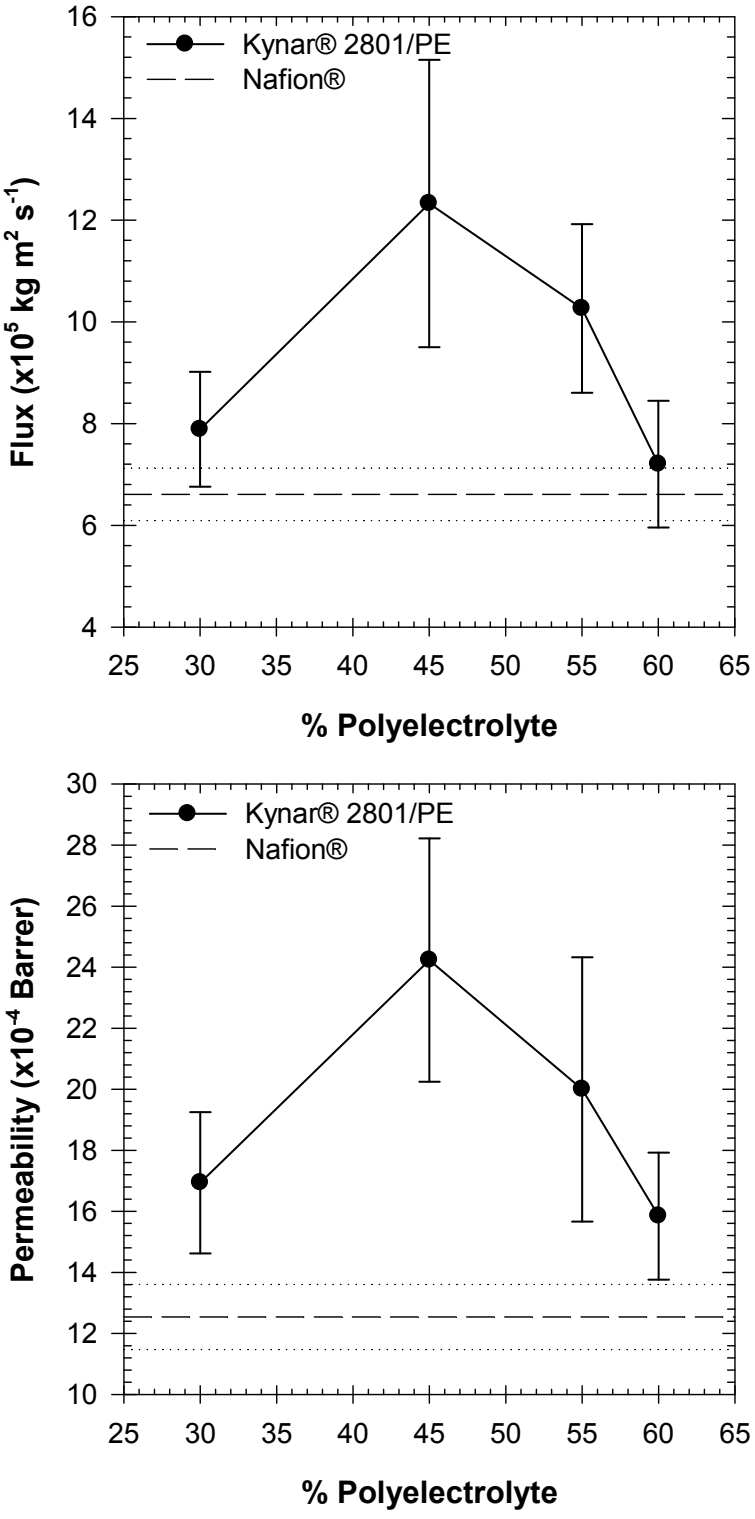

Figure 2-7: Transport characteristics from parallel liquid water permeation experiments through blends of Kynar® 2801 and PE at 50 °C, with Nafion® 112 as a reference. Error bars represent 95 % confidence intervals.

Kynar® 731 films were made with 30, 40, and 50 wt% PE, and the results from the parallel permeation experiments are shown in Figure 2-8. The change in PVDF did not affect water transport significantly at equivalent PE concentrations. However, with the Kynar® 731 blends, statistical analysis shows that average flux and permeability for the 30 wt% film was less than the 40 and 50 wt% PE films, with no significant difference between the 40 and the 50 wt% PE films. These results are consistent with those from the Kynar® 2801 blends, as there is evidence of maximized water transport above 40 wt% PE. The water transport trends are consistent with the conductivity trends observed by Zapata et al. [16] for the same PVDF/PE blends, where conductivity generally maximized near 55 – 60 wt% PE.

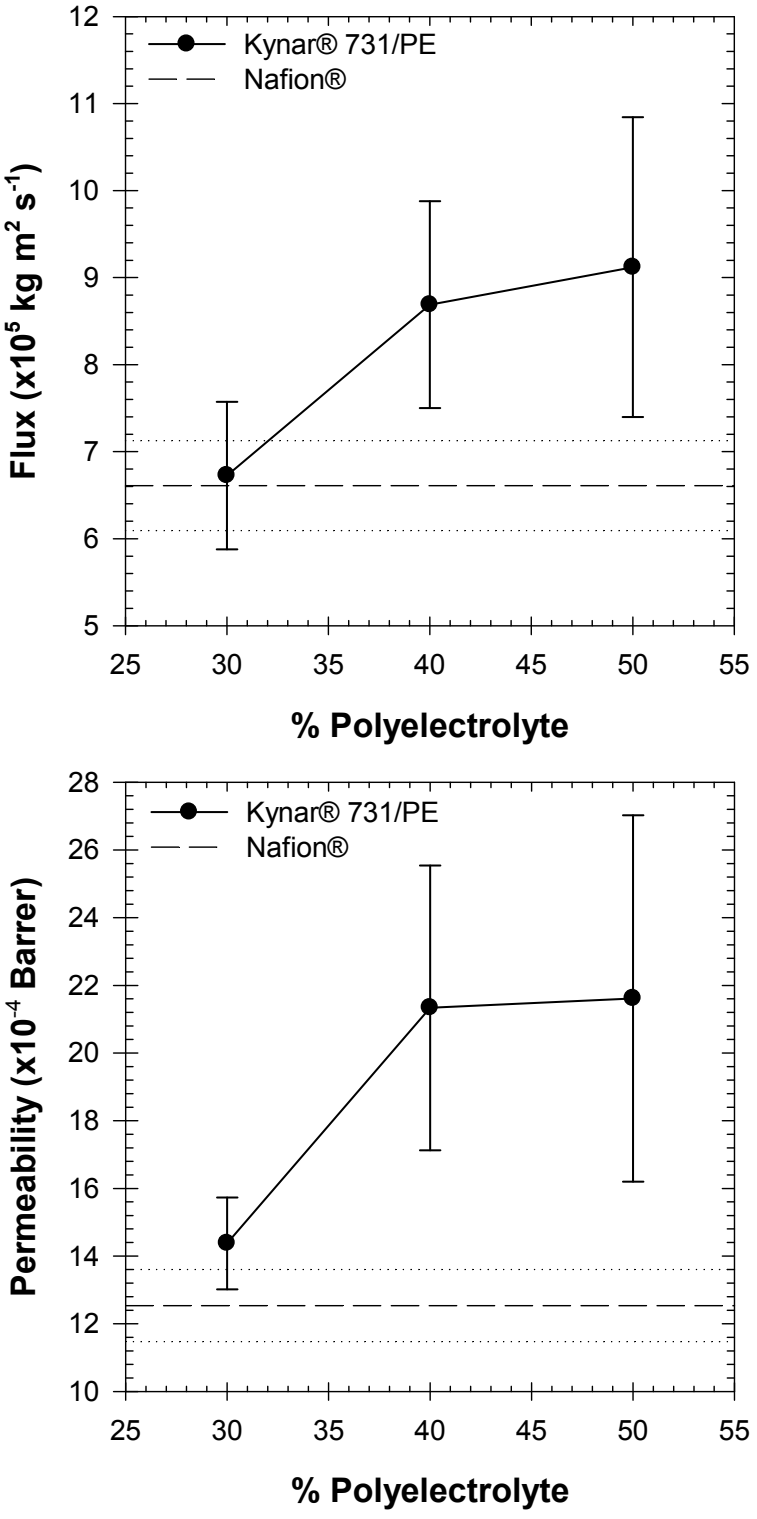

Figure 2-8: Transport characteristics from parallel liquid water permeation experiments through blends of Kynar® 731 and PE at 50 °C, with Nafion® 112 as a reference. Error bars represent 95 % confidence intervals.

2.4. CONCLUSIONS

A high-throughput mass transport assay has been developed that is capable measuring pseudo steady-state flux and permeability of water through hydrophilic membranes. HT-MTA utilizes cost-efficient design with parallel channels suitable for both combinatorial and homogeneous films to achieve steady state transport conditions much quicker than conventional pervaporation techniques. The functionality of the device has been demonstrated with the evaluation of liquid water transport through Nafion® and model polymer blends of PVDF and an acrylic, proton-conducting polyelectrolyte. For Nafion® films, the flux and permeability values were generally about one to two orders of magnitude lower than many of the previous studies of water pervaporation through Nafion®. The difference is attributed to the downstream configuration of the HT-MTA, which accumulates stagnate permeate vapor for pressure measurement. This configuration is somewhat analogous to a standard liquid permeation experiment, and the resemblance was confirmed by trends in permeability with respect to temperature, which display a positive correlation unlike typical pervaporation techniques. Still, despite the deviation from experimental values in cited pervaporation studies, HT-MTA provides a rapid method by which trends in transport behavior can be identified. The effects of chemical modification and rapid degradation on water transport have been characterized for Nafion® films. The dependence of flux and permeability on temperature were found to follow Arrhenius models used to determine respective transport activation energies. Also, for two types of PVDF/PE blends, the dependence of water flux and permeability on PE content was found to be consistent with trends in proton conductivity from previous work.

2.5. REFERENCES

1. Powell, C.E. and G.G. Qiao, *Polymeric CO2/N2 gas separation membranes for the capture of carbon dioxide from power plant flue gases.* Journal of Membrane Science, 2006. **279**(1-2): p. 1-49.

2. Freeman, B.D., *Basis of Permeability/Selectivity Tradeoff Relations in Polymeric Gas Separation Membranes.* Macromolecules, 1999. **32**(2): p. 375-380.

3. Matsuura, T., *Progress in membrane science and technology for seawater desalination -- a review.* Desalination, 2001. **134**(1-3): p. 47-54.

4. Kamachi, M., M. Kurihara, and J.K. Stille, *Synthesis of Block Polymers for Desalination Membranes. Preparation of Block Copolymers of 2-Vinylpyridine and Methacrylic Acid or Acrylic Acid.* Macromolecules, 2002. **5**(2): p. 161-167.

5. Baker, R.W., *Future Directions of Membrane Gas Separation Technology.* Industrial & Engineering Chemistry Research, 2002. **41**(6): p. 1393-1411.

6. Zhang, J., et al., *High temperature PEM fuel cells.* Journal of Power Sources, 2006. **160**(2): p. 872-891.

7. Kreuer, K.D., *On the development of proton conducting polymer membranes for hydrogen and methanol fuel cells.* Journal of Membrane Science, 2001. **185**(1): p. 29-39.

8. Hamrock, S.J. and M.A. Yandrasits, *Proton exchange membranes for fuel cell applications.* Polymer Reviews, 2006. **46**(3): p. 219-244.

9. Smitha, B., S. Sridhar, and A.A. Khan, *Solid polymer electrolyte membranes for fuel cell applications - A review.* Journal of Membrane Science, 2005. **259**(1-2): p. 10-26.

10. Hickner, M.A., et al., *Alternative polymer systems for proton exchange membranes (PEMs).* Chemical Reviews, 2004. **104**(10): p. 4587-4611.

11. Dobrovol'skii, Y., et al., *Proton-exchange membranes for hydrogen-air fuel cells.* Russian Journal of General Chemistry, 2007. **77**(4): p. 766-777.

12. Dobrovolsky, Y.A., et al., *Achievements in the field of proton-conductive portion electrolyte membranes.* Russian Journal of Electrochemistry, 2007. **43**(5): p. 489-501.

13. Shao, Y., et al., *Proton exchange membrane fuel cell from low temperature to high temperature: Material challenges.* Journal of Power Sources, 2007. **167**(2): p. 235-242.

14. Sormana, J.-L. and J.C. Meredith, *High-throughput discovery of structure-mechanical property relationships for segmented poly(urethane-urea)s.* Macromolecules, 2004. **37**(7): p. 2186-2195.

15. Chattopadhyay, S. and J.C. Meredith, *Combinatorial screening of organic electronic materials: Thin film stability.* Measurement Science and Technology, 2005. **16**(1): p. 128-136.

16. Zapata, P., P. Basak, and J.C. Meredith, *High-Throughput Screening of Ionic Conductivity in Polymer Membranes.* Electrochimica Acta, 2009. **54**(15): p. 3899-3909.

17. Watari, T., et al., *Water vapor sorption and diffusion properties of sulfonated polyimide membranes.* Journal of Membrane Science, 2003. **219**(1-2): p. 137-147.

18. BiyIkoglu, A., *Review of proton exchange membrane fuel cell models.* International Journal of Hydrogen Energy, 2005. **30**(11): p. 1181-1212.

19. Linossier, I., et al., *Measuring Water Diffusion in Polymer Films on the Substrate by Internal Reflection Fourier Transform Infrared Spectroscopy.* Journal of Applied Polymer Science, 1997. **66**(13): p. 2465-2473.

20. Fushinobu, K., et al., *Optical Measurement Technique of Water Contents in Polymer Membrane for PEFCs.* Journal of Fuel Cell Science and Technology, 2006. **3**: p. 13-17.

21. Schäfer, T., J. Vital, and J.G. Crespo, *Coupled pervaporation/mass spectrometry for investigating membrane mass transport phenomena.* Journal of Membrane Science, 2004. **241**(2): p. 197-205.

22. Bakker, W.J.W., et al., *Permeation characteristics of a metal-supported silicalite-1 zeolite membrane.* Journal of Membrane Science, 1996. **117**(1): p. 57-78.

23. Tanaka, K., et al., *Isotopic-transient permeation measurements in steady-state pervaporation through polymeric membranes.* Journal of Membrane Science, 2002. **197**(1): p. 173-183.

24. O'Brien, K.C., et al., *A new technique for the measurement of multicomponent gas transport through polymeric films.* Journal of Membrane Science, 1986. **29**(3): p. 229-238.

25. Jordan, S.M. and W.J. Koros, *Permeability of pure and mixed gases in silicone rubber at elevated pressures.* Journal of Polymer Science Part B: Polymer Physics, 1990. **28**(6): p. 795 - 809.

26. Ziegel, K.D., H.K. Frensdorft, and D.E. Blair, *Measurement of hydrogen isotope transport in poly(vinyl fluoride) films by the permeation-rate method.* Journal of Polymer Science Part A-2: Polymer Physics, 1969. **7**(5): p. 809 - 819.

27. Pasternak, R.A., J.F. Schimscheimer, and J. Heller, *A dynamic approach to diffusion and permeation measurements.* Journal of Polymer Science Part A-2: Polymer Physics, 1970. **8**(3): p. 467-479.

28. Yasuda, H. and K. Rosengren, *Isobaric measurement of gas permeability of polymers.* Journal of Applied Polymer Science, 1970. **14**(11): p. 2839-2877.

29. Pye, D.G., H.H. Hoehn, and M. Panar, *Measurement of gas permeability of polymers. II. Apparatus for determination of permeabilities of mixed gases and vapors.* Journal of Applied Polymer Science, 1976. **20**(2): p. 287 - 301.

30. Chern, R.T., et al., *Selective permeation of CO2 and CH4 through kapton polyimide: Effects of penetrant competition and gas-phase nonideality.* Journal of Polymer Science: Polymer Physics Edition, 1984. **22**(6): p. 1061 - 1084.

31. Tremblay, P., et al., *Gas permeability, diffusivity and solubility of nitrogen, helium, methane, carbon dioxide and formaldehyde in dense polymeric membranes using a new on-line permeation apparatus*, in *Journal of Membrane Science*. 2006. p. 1-40.

32. Brubaker, D.W. and K. Kammermeyer, *Apparatus for Measuring Gas Permeability of Sheet Materials.* Analytical Chemistry, 1953. **25**(3): p. 424 - 426.

33. Heilman, W., et al., *Permeability of Polymer Films to Hydrogen Sulfide Gas.* Industrial & Engineering Chemistry, 1956. **48**(4): p. 821 - 824.

34. Jena, A. and K. Gupta, *Characterization of water vapor permeable membranes.* Desalination, 2002. **149**(1): p. 471-476.

35. Brown, W.E. and W.J. Sauber, *Gas transmission by plastics films.* Modern Plastics, 1959. **36**(12): p. 107,110,112-114 ,116,190.

36. *ASTM D 1434-56T* 1956.

37. Forsberg, K. and L.H. Keith, *Chemical Protective Clothing Performance Index Book*. 1 ed. 1989, New York: John Wiley & Sons. 308.

38. Forsberg, K., *Quick selection guide to chemical protective clothing*. 2nd ed. ed, ed. S.Z. Mansdorf. 1993, New York: Van Nostrand Reinhold.

39. Wijmans, J.G. and R.W. Baker, *A simple predictive treatment of the permeation process in pervaporation.* Journal of Membrane Science, 1993. **79**(1): p. 101-113.

40. Nagarale, R.K., G.S. Gohil, and V.K. Shahi, *Recent developments on ion-exchange membranes and electro-membrane processes.* Advances in Colloid and Interface Science, 2006. **119**(2-3): p. 97-130.

41. Meredith, J.C., A. Karim, and E.J. Amis, *High-Throughput Measurement of Polymer Blend Phase Behavior.* Macromolecules, 2000. **33**(16): p. 5760-5762.

42. Silva, V.S., et al., *Mass transport of direct methanol fuel cell species in sulfonated poly(ether ether ketone) membranes.* Electrochimica Acta, 2006. **51**(18): p. 3699-3706.

43. Meuleman, E.E.B., et al., *EPDM as a selective membrane material in pervaporation.* Journal of Membrane Science, 2001. **188**(2): p. 235-249.

44. Binning, R., et al., *Separation of Liquid Mixtures by Permeation.* Ind. Eng. Chem., 1961. **53**(1): p. 45-50.

45. Hensley, J.E., et al., *The effects of thermal annealing on commercial Nafion® membranes.* Journal of Membrane Science, 2007. **298**(1-2): p. 190-201.

46. Romero, T. and W. Mérida, *Water transport in liquid and vapour equilibrated Nafion(TM) membranes.* Journal of Membrane Science, 2009. **338**(1-2): p. 135-144.

47. Majsztrik, P., A. Bocarsly, and J. Benziger, *Water Permeation through Nafion Membranes: The Role of Water Activity.* The Journal of Physical Chemistry B, 2008. **112**(51): p. 16280-16289.

48. Rivin, D., et al., *Solubility and transport behavior of water and alcohols in Nafion(TM).* Polymer, 2001. **42**(2): p. 623-635.

49. Ames, R.L., et al., *Nitric Acid Dehydration Using Mixed Perfluorosulfonate and -carboxylate Ionomer Membranes.* Industrial & Engineering Chemistry Research, 2005. **44**(10): p. 3672.

50. Feng, X. and R.Y.M. Huang, *Estimation of activation energy for permeation in pervaporation processes.* Journal of Membrane Science, 1996. **118**(1): p. 127-131.

51. Gorri, D., et al., *Water and methanol permeation through short-side-chain perfluorosulphonic acid ionomeric membranes.* Journal of Membrane Science, 2008. **322**(2): p. 383-391.

52. Gorri, D., R. Ibáñez, and I. Ortiz, *Comparative study of the separation of methanol-methyl acetate mixtures by pervaporation and vapor permeation using a commercial membrane.* Journal of Membrane Science, 2006. **280**(1-2): p. 582-593.

53. Tricoli, V., N. Carretta, and M. Bartolozzi, *A Comparative Investigation of Proton and Methanol Transport in Fluorinated Ionomeric Membranes.* Journal of The Electrochemical Society, 2000. **147**(4): p. 1286-1290.

54. Tricoli, V. and F. Nannetti, *Zeolite-Nafion composites as ion conducting membrane materials.* Electrochimica Acta, 2003. **48**(18): p. 2625-2633.

55. Kim, Y.S., et al., *Sulfonated poly(arylene ether sulfone) copolymer proton exchange membranes: composition and morphology effects on the methanol permeability.* Journal of Membrane Science, 2004. **243**(1-2): p. 317-326.

56. Li, L., J. Zhang, and Y. Wang, *Sulfonated poly(ether ether ketone) membranes for direct methanol fuel cell.* Journal of Membrane Science, 2003. **226**(1-2): p. 159-167.

57. Healy, J., et al., *Aspects of the Chemical Degradation of PFSA Ionomers used in PEM Fuel Cells.* Fuel Cells, 2005. **5**(2): p. 302-308.

58. Kim, B. and B. Jung, *Partially Sulfonated Polystyrene and Poly(2,6-dimethyl-1,4-phenylene oxide) Blend Membranes for Fuel Cells.* Macromolecular Rapid Communications, 2004. **25**(13): p. 1263-1267.

59. Hong, L. and N. Chen, *Proton-conducting polymer membrane based on sulfonated polystyrene microspheres and an amphiphilic polymer blend.* Journal of Polymer Science Part B: Polymer Physics, 2000. **38**(11): p. 1530-1538.

Chapter 3
Effects of Accelerated Degradation Protocols on Nafion® Properties

Reproduced with permission from Keith Reed and J.C. Meredith
Unpublished work (*to be submitted for publication*)

The previous chapter described the development of a high-throughput mass transport assay, which is an essential addition to the proton exchange membrane characterization toolset. In this chapter, the utility of this toolset is demonstrated through a detailed analysis of Nafion® degradation, which plays a major role in fuel cell durability. A combination of analysis techniques was employed to explore effects of degradation on Nafion®, and possible degradation mechanisms. To decompose membrane samples without costly, time-intensive fuel cell operation experiments, accelerated aging tests are often used. Here, a Fenton's degradation assay was carried out with various reactant compositions, in order to optimize the conditions for miniaturized samples utilized in a high-throughput assay. The results support Nafion® degradation mechanisms previously suggested, and provide information to correlate accelerated degradation techniques with long-time film durability tests.

3.1. INTRODUCTION

Alternative energy resources are currently receiving widespread attention for reducing the release of harmful emissions into the atmosphere and eliminating petroleum dependence [1]. Accomplishing these goals in the near future has been realized through the advances made in fuel cells, which in various forms convert chemical energy into electrical energy. Among the collection of fuel cell technologies, the proton exchange membrane fuel cell (PEMFC) is considered highly attractive due to its low operating temperature, CO_2 tolerance, high power density, and potential for cost-effective performance [2]. These factors make the PEMFC a versatile power source, especially fit for transportation, while also suitable for stationary and portable applications [3]. Unfortunately for transportation applications, PEMFCs achieved to date are far from being commercially viable, in large part due to the chemical and physical limitations of the polymer electrolyte. DuPont's Nafion® membrane, a perfluorosulfonic acid (PFSA) polymer (see Figure 3-1), is considered to be the state-of-the-art PEMFC material for its high proton conductivity and chemical resistance, but lacks the long term durability to achieve cost-effective performance [4].

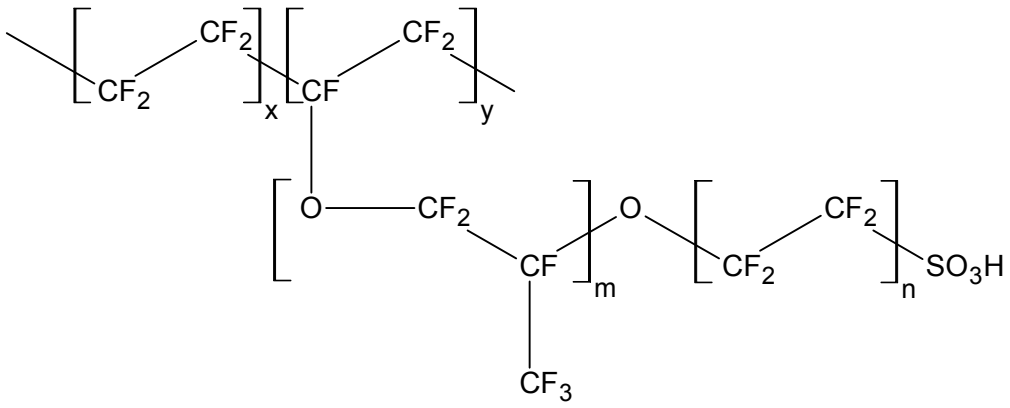

Figure 3-1: Chemical structure of Nafion®.

Since electrolyte durability is critical to the overall operation of the fuel cell, much attention has been directed toward studying the mechanisms of Nafion® degradation during operation, for which much still remains unknown [5]. The conventional *in situ* method of onboard monitoring, while a useful tool for performance evaluation, is both costly and time-intensive when considering fuel consumption and evaluation life cycles, which are intended to last at least 5000 h [6]. For this reason, researchers have investigated the use of *ex situ* accelerated membrane degradation experiments to quickly assess the process. A popular approach is to expose membranes to a Fenton's reagent, which is a solution that rapidly generates peroxide (•OH) and hydroperoxide (•OOH) radicals from hydrogen peroxide and a metal cationic catalyst, typically iron(II). The reaction, originally suggested by Haber and Wiess [7], proceeds as follows:

$$Fe^{2+} + H_2O_2 \rightarrow Fe^{3+} + \bullet OH + OH^- \quad \textbf{Equation 3-1}$$

$$Fe^{2+} + \bullet OH \rightarrow Fe^{3+} + OH^- \quad \textbf{Equation 3-2}$$

$$H_2O_2 + \bullet OH \rightarrow \bullet OOH + H_2O \quad \textbf{Equation 3-3}$$

$$Fe^{2+} + \bullet OOH \rightarrow Fe^{3+} + OH^- \quad \textbf{Equation 3-4}$$

$$Fe^{3+} + \bullet OOH \rightarrow Fe^{2+} + H^+ + O_2 \quad \textbf{Equation 3-5}$$

Free radical attack on the on PFSA membranes has been previously demonstrated to take place during long-time operation, initiated by the production of hydrogen peroxide at the electrodes in the presence of trace metal impurities [4, 8-11]. The Fenton test therefore allows one to manipulate the extent and rate at which free radical attack will take place by controlling the concentrations of hydrogen peroxide and metal catalyst, respectively. Unfortunately, a generalized correlation between *ex situ* accelerated testing and real-time *in situ* fuel cell membrane durability has yet to be discovered [12]. Furthermore, while there has been some work on the effect of individual reagent

components on Nafion's® chemical structure [13, 14], there is very little information available regarding the combined effects of both reagent concentrations on Nafion's® performance properties. For these reasons, the information obtained from accelerated durability tests has not been fully utilized. In this chapter, we utilize a customized set of rapid, high-throughput characterization techniques, among other characterization tools, to show how variations in Fenton testing protocols affect Nafion® films. Basic chemical effects are evaluated in addition to changes in performance properties, namely mechanical strength, proton conductivity, and water transport.

3.2. EXPERIMENTAL

3.2.1. Ex Situ Degradation

Nafion® 112 (Dupont), with a thickness of 51 μm was used for all degradation experiments. Films were pre-treated in a 1 M solution of sulfuric acid (ACS reagent grade, from Sigma-Aldrich) for 2 h at 80 °C, followed by three cycles of rinsing in deionized water at 80 °C for 30 min each. Prior to the start of experiment, films were swollen in 150 ml of a 15 or 30 % solution of hydrogen peroxide (ACS reagent grade, from VWR International) for 1 h at 80 °C. To initiate the formation of hydroxyl and peroxide radicals, iron (II) sulfate heptahydrate (ACS reagent grade) was added to the solutions at various concentrations. The degradation reagent was maintained at 80 °C for 12 h, after degraded films were rinsed and re-protonated in 1 M H_2SO_4 for 2 h at 80 °C to remove all metal ions from the films. Re-protonated samples were rinsed thoroughly and stored in deionized water.

3.2.2. Post Degradation Supernatant Analysis

The supernatant from each degradation experiment was analyzed for anion content using an ICS-2000 Ion Chromatography System (Dionex Corporation). The

fluoride ion peak at approximately 3.1 min is the first anion to emerge from chromatograph column and was quantified using a calibration curve generated with fluoride standards (Ricca Chemical). The concentration of hydrogen cations was estimated using a Corning Pinnacle 542 pH/conductivity meter.

3.2.3. Fourier Transform Infrared (FTIR) Analysis

Nafion® samples were measured for FTIR using a VERTEX 80v using a Hyperion 3000 Microscope with an attenuated total reflectance (ATR) attachment (Bruker Optics). Spectra were collected at room temperature and pressure after 64 scans with a resolution of 4 cm^{-1}. An air background was subtracted from all measurements.

3.2.4. Scanning Electron Microscopy (SEM)

High resolution images of degraded Nafion® films were obtained using a LEO 1530 thermally-assisted field emission scanning electron microscope (SEM), operated at 10keV. Samples were cryogenically broken in liquid nitrogen and metalized using gold sputtering prior to imaging.

3.2.5. High-Throughput Measurement of Mechanical Properties

Degraded Nafion® films were characterized for mechanical strength in the dry state using a custom, fully automated, high-throughput mechanical testing apparatus (HTMECH). A detailed description of HTMECH is described elsewhere [15] and a basic overview of the instrument is given here. Samples were mounted between two steel plates perforated with a 10 x 10 grid of holes that are 3.00 mm in diameter. The sample holder is affixed to a linear motor that moves along the z-axis. At the base of the instrument is a hemispherical-tip needle (1.00 mm in diameter) connected to a force-sensitive load cell that moves along the x and y-axis. After the needle was positioned below the desired sample location on the grid, the holder was brought down to the needle at defined velocity. Sample indentation generates a force vs. time profile that describes the evolution of axisymmetric biaxial deformation and failure. Analysis of this

profile was performed using a customized algorithm that allows for the assessment of properties such as elastic modulus, tensile strength, ultimate elongation, and toughness. Mechanical characterization tests were performed at a constant speed of 15 mm/s under ambient conditions.

3.2.6. High-Throughput Proton Conductivity Measurements

Proton conductivity measurements were performed with electrochemical impedance spectroscopy (EIS) using a customized, fully automated, high-throughput conductivity (HTC) measurement device, described in detail elsewhere [16]. Swollen film samples were placed in a well-like, electrically insulating sample holder and held in place with a grid-like retention mechanism. The sample holder was filled with enough deionized water at room temperature to completely cover films and prevent dehydration. Before measuring conductivity, localized thickness measurements were taken using an Omega GP901-2 linear displacement digital gauging probe with a flat-tip, 0.12 μm resolution, and low spring constant to reduce sample compression (Omega Engineering, Inc.). To measure conductivity, the hydrated membrane was excited with an alternating current (AC) signal from the outer point-electrodes of a commercially available, tungsten carbide 4-point probe head (Jandel Engineering Ltd.). The response voltage from this AC excitation was measured with the inner point-electrodes, allowing for the calculation of complex impedance. Since electrodes are equally spaced apart, proton conductivity was estimated from complex impedance using the following simplified model:

$$\sigma \approx \frac{1}{Z}\frac{\ln(2)}{\pi h} \qquad \textbf{Equation 3-6}$$

where σ is the membrane proton conductivity, Z is the membrane's complex impedance, and h is the membrane thickness. All proton conductivity measurements were determined at room temperature with an excitation signal of 1 kHz and averaged over a 10 second stabilization period.

3.2.7. Water Transport Properties

Films were characterized for fractional water uptake, dimensional swelling, flux, and permeability. For water uptake and swelling analysis, dry samples were measured for thickness and mass, boiled for 1 h in deionized water at 80 °C, cooled to room temperature over night, and then lightly blotted with Kimwipes® to remove excess water before quickly measuring mass and thickness again. Fractional water uptake was calculated using the wet and dry masses, according to the following equation:

$$q_m = \frac{m_{wet} - m_{dry}}{m_{dry}} \qquad \textbf{Equation 3-7}$$

where q_m is fractional water uptake, and m is the film mass. Similarly, the change in thickness was used to determine the dimensional swelling ratio, according to the following equation:

$$q_\ell = \frac{\ell_{wet}}{\ell_{dry}} \qquad \textbf{Equation 3-8}$$

where q_ℓ is the swelling ratio, and ℓ is film thickness.

Water flux and permeability were obtained through liquid pervaporation experiments using a high-throughput mass transport assay (HT-MTA). Details on the operation of the HT-MTA are given in the previous chapter and are briefly outlined here. Film samples were held into place with two Viton® rubber sheets supported by stainless plates. Both the rubber sheets and backing plates are perforated with a grid of through-holes that are each 0.16 cm in diameter. On the bottom-side of the retention mechanism, each through-hole is fitted with a stainless steel tube and a Honeywell 26PC Series silicon differential pressure transducer that act as the downstream variable pressure chamber with an internal volume 2 cm^3. The top-side plate of the retention mechanism is fitted with an inlet for liquids or gases, allowing for continuous upstream permeate exposure. To begin high-throughput pervaporation experiments, liquid water was

injected on the upstream side of retention mechanism at atmospheric pressure, with each downstream chamber initially at atmospheric pressure, such that the downstream differential pressure, p_w', was equal to zero. Water vapor immediately diffuses into these chambers causing downstream pressure to rise until saturation. For hydrophilic thin films, where water sorption occurs very quickly with respect to the time needed to reach downstream saturation, steady-state water flux, J_W can be approximated by the initially linear pressure rate, according to the following equation:

$$J_W = \frac{V_{pc}}{A * R * T} \frac{dp_W'}{dt} \qquad \textbf{Equation 3-9}$$

where the permeate vapor is assumed to act as ideal gas, dp_W'/dt is the initial steady-state pressure rate, A is the exposed film surface area based on the through-hole diameter, V_{pc} is the volume of the downstream pressure chamber at temperature, T, and R is the ideal gas constant. Liquid water permeability, P_W can then be calculated using the solution-diffusion model with a pressure driving force equal to the differential pressure at equilibrium, p_∞':

$$P_W = J_W \frac{\ell}{p_\infty'} \qquad \textbf{Equation 3-10}$$

The units for permeability are typically expressed in Barrer, where 1 Barrer = 10^{-10} cm^3(STP) cm cm^{-2} s^{-1} $cmHg^{-1}$.

3.3. RESULTS AND DISCUSSION

3.3.1. Free Radical Degradation Pathways

There are three possible pathways for peroxide and hydroperoxide radicals to react with PFSA membranes: chain unzipping, chain scission, and side-group attack [17]. Chain unzipping can be initiated on H-containing end groups (i.e., -CHF_2 and

-COOH) that are present in small concentrations as a result of the Nafion® manufacturing process [5, 10, 12, 18-21]. In the presence of free radicals, these end-groups can react to produce HF and CO_2 according to the following example:

$$R\text{-}CF_2COOH + \bullet OH \rightarrow R\text{-}CF_2\bullet + CO_2 + H_2O \quad \textbf{Equation 3-11}$$

$$R\text{-}CF_2\bullet + \bullet OH \rightarrow R\text{-}CF_2OH \quad \textbf{Equation 3-12}$$

$$R\text{-}CF_2OH \rightarrow R\text{-}COF + HF \quad \textbf{Equation 3-13}$$

$$R\text{-}COF + H_2O \rightarrow R\text{-}COOH + HF \quad \textbf{Equation 3-14}$$

As shown in the mechanism above, the carboxylate group is regenerated and the reaction propagates, eventually decomposing the polymer into low molecular weight compounds. Chain unzipping is generally agreed to be more dominant than chain scission reactions and side-group attack [22]. Although the exact mechanisms for chain scissioning have yet to be identified it involves the free radical attack of CF_2-CF_2 bonds, while radical side-group attacks can occur at C-S bonds or more susceptible ether linkages. Each of these possible free radical reactions have been considered in explaining the various Fenton-induced property changes observed in this study.

3.3.2. Ionic Loss from Nafion® Degradation

When trace amounts of Fe_2SO_4 were added to swollen Nafion® films in hydrogen peroxide solutions at 80 °C, gas evolved intensively due to the formation of oxygen during the Haber-Weiss reaction (see Equation 3-5). The iron catalyst, initially aqua-blue in color, became a reddish-brown over time, confirming the change in the iron oxidation state. After carrying out the decomposition reactions for 12 h with Nafion®, the depleted reagents were analyzed for polymer decomposition components. The post-degradation pH values ranged from 2.4 to 2.7, consistent with the production of acid by-products (Equation 3-5) and the possible release of protons from the sulfonic acid groups on

polymer side chains. Fluoride losses were determined by ion chromatography and plotted in Figure 3-2 for each Fenton reagent concentration. These results indicate higher fluoride losses in solutions with the 30 % H_2O_2, which is expected since more peroxide and hydroxyperoxide radicals were available during the accelerated decomposition process. For both H_2O_2 concentrations, the fluoride release from the PFSA samples increased with iron(II) content up to 50 ppm Fe^{2+}, and then decreased thereafter. This relationship between fluoride loss and Fe^{2+} concentration has been previously observed by Kodama et al. [13] and Chen et. al. [14]. Kodama et al. proposed that higher concentrations of Fe^{2+} produce free radicals at a rate where polymer attack sites become limited. The excess free radicals would then naturally deplete before reacting with Nafion®, thereby reducing the amount fluoride loss during degradation. Another possibility, suggested by Chen et al., is that the higher iron(II) concentration favors chain scissioning over chain unzipping, such that large polymer fragments become more abundant while the number of fluoride ions generated by end-group reactions is reduced.

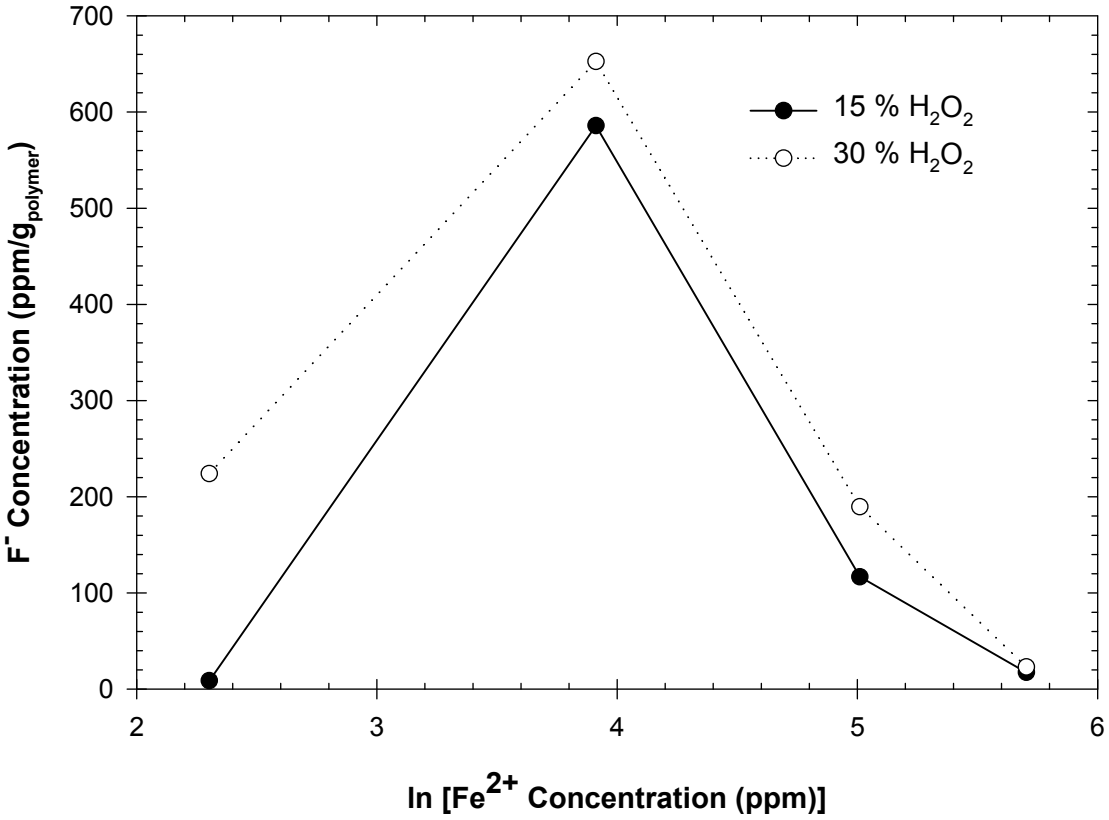

Figure 3-2: Fluoride ion content of aqueous Fe^{2+}/H_2O_2 solutions after degradation of Nafion® 112 at 80 °C for 12 h.

No *R*-SO_3^- polymer fragments could be detected in any of the depleted reagents with ion chromatography, which has a detection limit on the order of 0.1 ppm. While this might suggest that no radical reactions took place on polymer side-chains directly, it is possible that the sulfonated fluorocarbon chains were overshadowed by the large SO_4^{2-} peak from the metal ionic salt in solution. For this reason, FTIR analysis was used to evaluate the relative loss of chemical bonds in degraded films. The spectra, shown in Figure 3-3, indicated no significant changes in the Nafion® polymer structure after degradation, even for the C-F vibration bands at 1204, 1150, and 982 cm^{-1}, which ion chromatography had shown to be affected by accelerated degradation. Similar results have been obtained by Kindu et al. for the degradation of PFSA films in the presence of Fe^{2+} and H_2O_2 [19], who showed that fresh and degraded Nafion® samples had no significant changes in FTIR spectra, ion exchange capacity, or backbone-to-side-chain ratio, despite visible signs of degradation and significant fluoride losses. They concluded that free radical degradation might have cleaved polymer backbones and side chains in proportion such that the only significant chemical change during degradation was the average molecular mass. Such changes are consistent with free radical chain scissioning, but the stability of the C-F bonds in Figure 3-3 is still an anomaly. An estimate of fluoride concentrations in the supernatents showed that fluoride loss from degraded samples was on the order of 10^{-3} mol/l polymer, which is close to the detection limit of the FTIR instrument [23]. The relative proportions of chemical bonds could also be retained if chain unzipping completely decomposed some polymer chains, i.e. those chains with vulnerable H-containing end groups, while leaving the other chains unaltered.

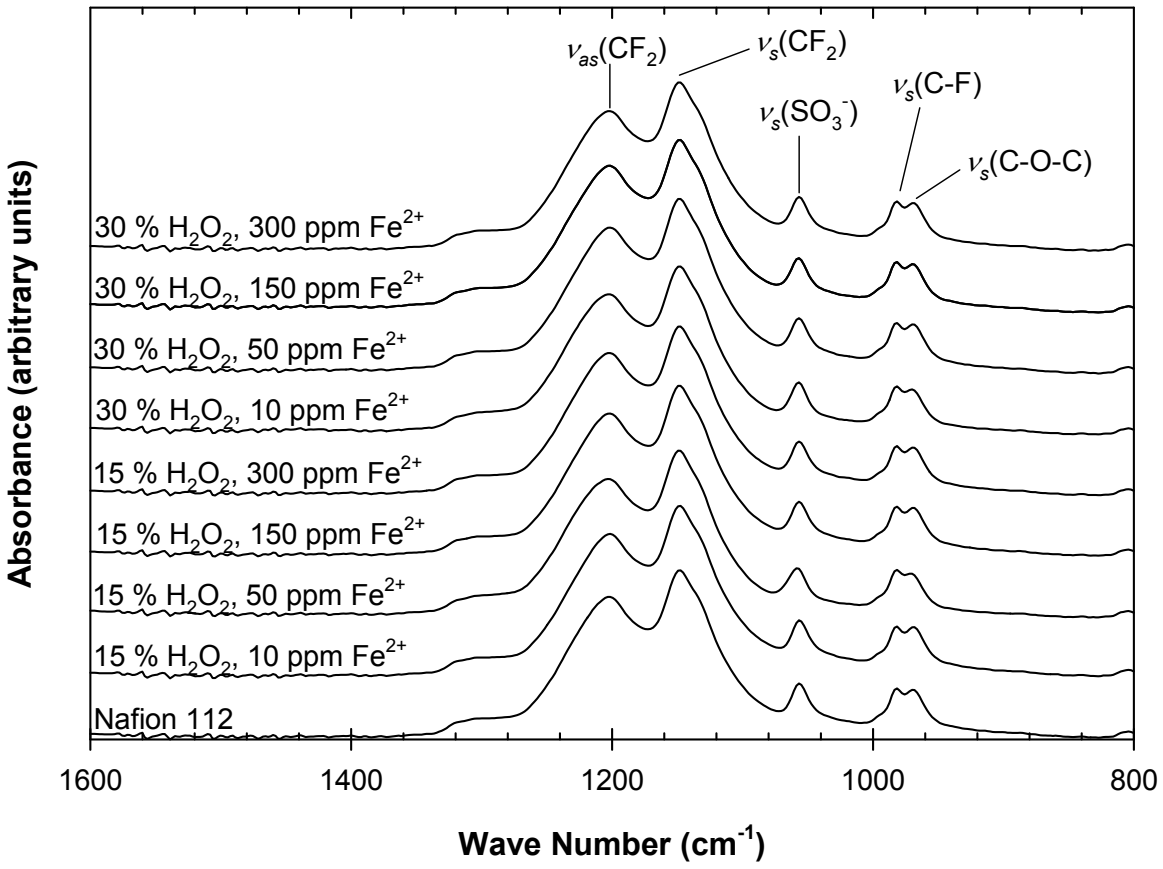

Figure 3-3: FTIR spectra of degraded Nafion® samples after exposure to aqueous solutions of hydrogen peroxide and iron(II) sulfate at 80 °C for 12 h.

3.3.3. Structural Changes from Nafion® Degradration

Films exposed to the higher concentration of H_2O_2 undergo a dramatic change in optical properties from initially clear and transparent to white and opaque. To investigate how this color change related to the structural properties, film morphologies were examined with SEM imaging of fresh and degraded PFSA samples. Select cross-sectional and surface images are shown in Figure 3-4 and Figure 3-5, respectively. The results show that the color change is related to the small bubbles that developed in films immersed in 30 % H_2O_2 solutions. The resulting voids within the polymer film refract light in a manner that causes the observed change in color. Based on surface micrographs, these voids also produced pinholes at the surface that may affect transport of liquids and gases, which will be discussed later. Similar observations were made by Tang et al., who concluded that voids formed during accelerated durability tests were the result of decomposed polymer repeat units [4]. While such decomposition can occur from any of the free radical attack pathways that have been suggested, the chemical analysis discussed previously shows that void formation is most likely the result of complete chain unzipping. It was also observed from the SEM micrographs that among the films aged in 30 % H_2O_2, the 50 ppm Fe^{2+} solution induced larger film pores while the other Fe^{2+} concentrations caused many small pores. These results are consistent with the suggestion that the effects of free radical degradation were maximized on Nafion® films at 50 ppm Fe^{2+}.

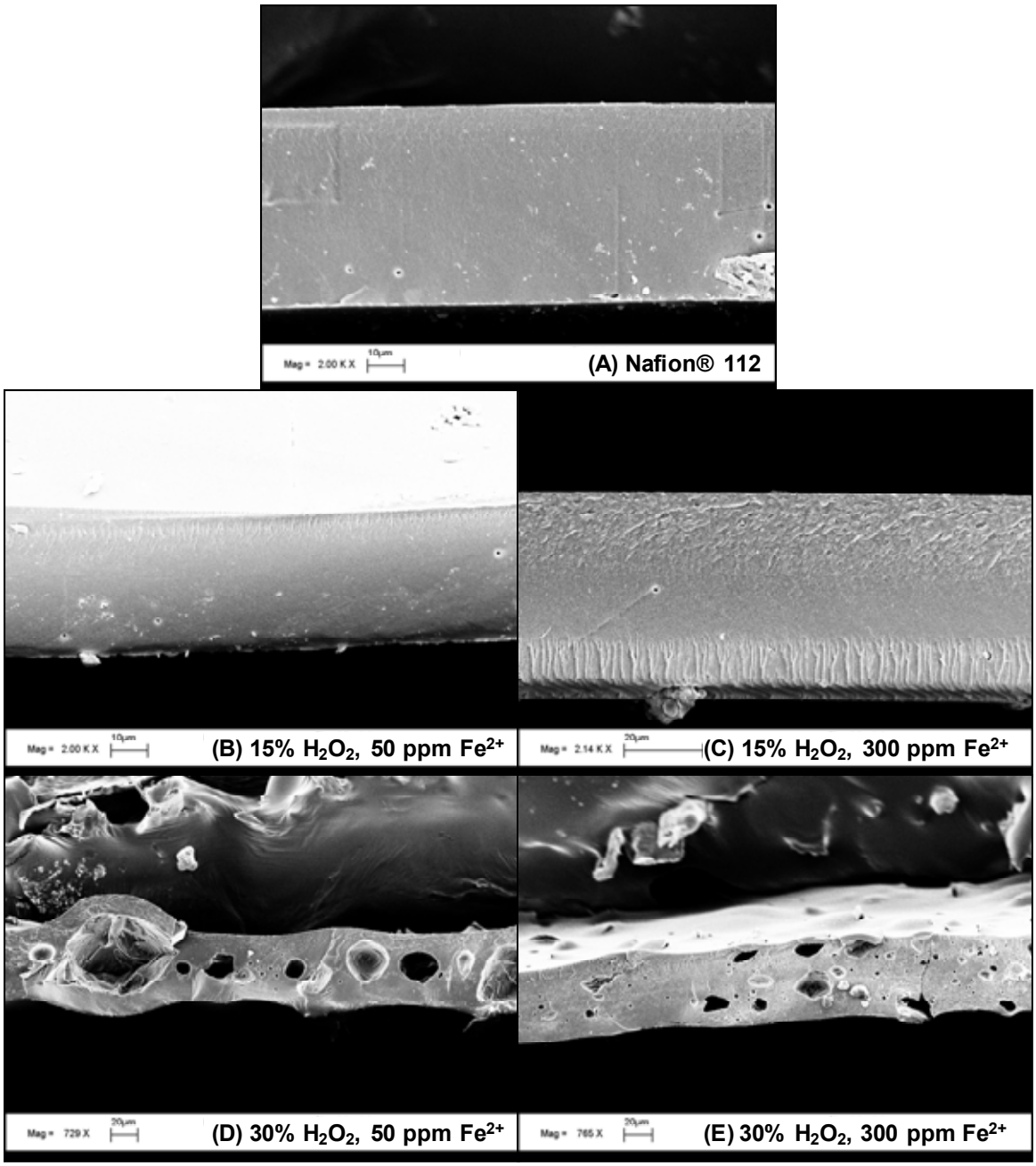

Figure 3-4: Cross-sectional images of select Nafion® 112 samples before (A) and after (B-E) exposure to various aqueous solutions of Fe^{2+}/H_2O_2 at 80 °C for 12 h. Micrographs for (D) and (E) were taken at a lower magnification show to representative morphological changes.

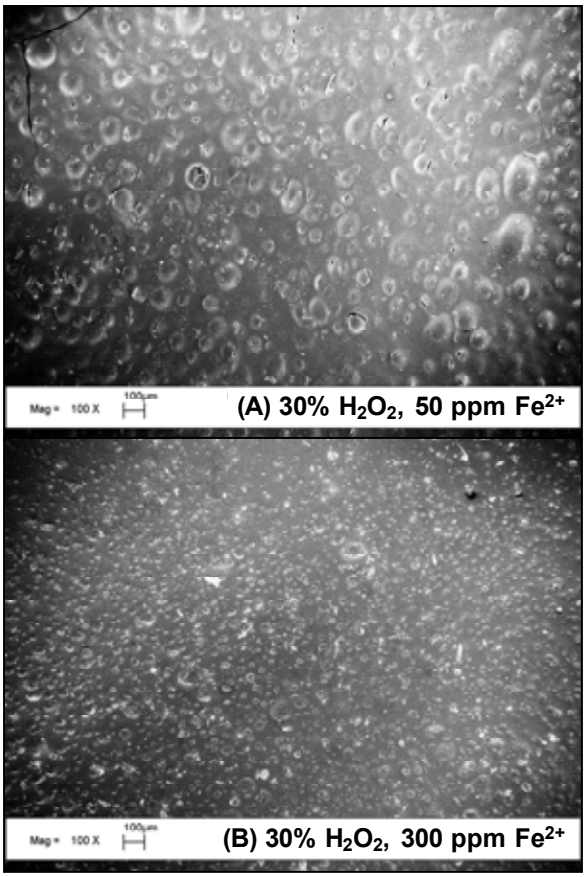

Figure 3-5: Surface images of select Nafion® 112 samples after exposure to 30 % H_2O_2 solution with 50 ppm (A) and 300 ppm Fe^{2+} (B).

3.3.4. Degradation Effects on Mechanical Properties

The mechanical properties of each degraded film were averaged from needle indentation experiments at 5 sample locations. The resulting force versus time and stress versus strain profiles were used to determine normalized maximum force (Figure 3-6), tensile strength (Figure 3-7), elastic modulus (Figure 3-8), ultimate elongation (Figure 3-9), and toughness (Figure 3-10) of films exposed to the 8 different Fenton reagent compositions. In general, catalyst concentration, controlling the rate of free radical formation, had very little to no effect on mechanical properties. On the other hand, hydrogen peroxide concentration, which controls the total amount of free radicals generated, had a significant effect on all mechanical properties. The normalized maximum force and tensile strength of the PFSA films remained relatively stable after immersion in 15 % H_2O_2, but were reduced by ~50 % in solutions with 30 % H_2O_2. This reduction in polymer strength at the higher hydrogen peroxide concentration can be explained by the pores observed in the SEM images. The elastic modulus dropped by approximately 20 % in the 15 % H_2O_2 solutions, and was reduced by 50 % in the 30 % H_2O_2 solutions. These results support possible reductions in chain entanglements as a result of chain scissioning, which also increases chain mobility under stress. The increase in ultimate elongation for films degraded with 15 % H_2O_2 also supports better chain mobility. On the other hand, for the durability tests using 30% H_2O_2 solutions, films had ultimate elongations that were lower than the original sample. This indicates that despite increased chain mobility induced with higher H_2O_2 concentration, the presence of voids in the films significantly reduced the total strain capacity of the degraded polymers. Therefore, it was expected that the weaker and less elastomeric films from the 30 % H_2O_2 solutions would also have lower toughness values after aging. Meanwhile, films reacted with 15 % H_2O_2, having similar strength and morphology to the original

polymer but with higher ductility, were expected to have increased toughness values relative to native Nafion®.

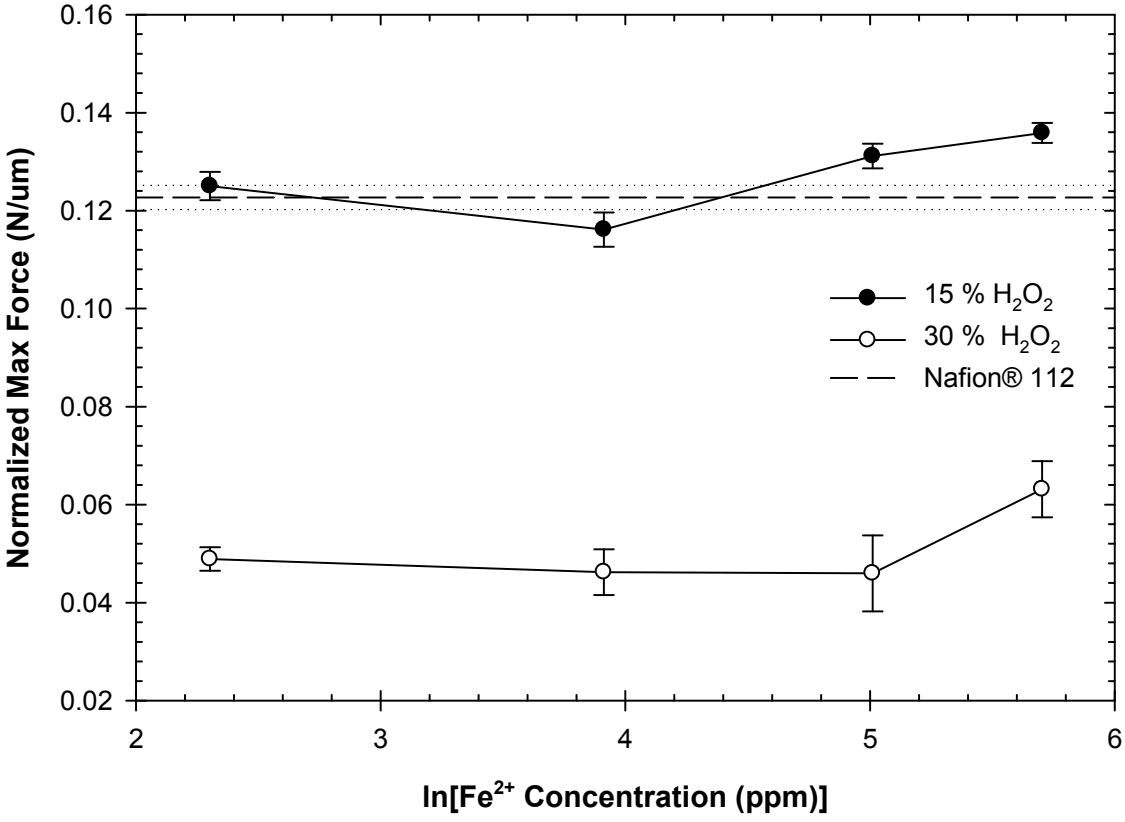

Figure 3-6: Normalized maximum force of Nafion® 112 films after exposure to various aqueous solutions of Fe^{2+}/H_2O_2 at 80 °C for 12 h. Error bars represent 95 % confidence intervals

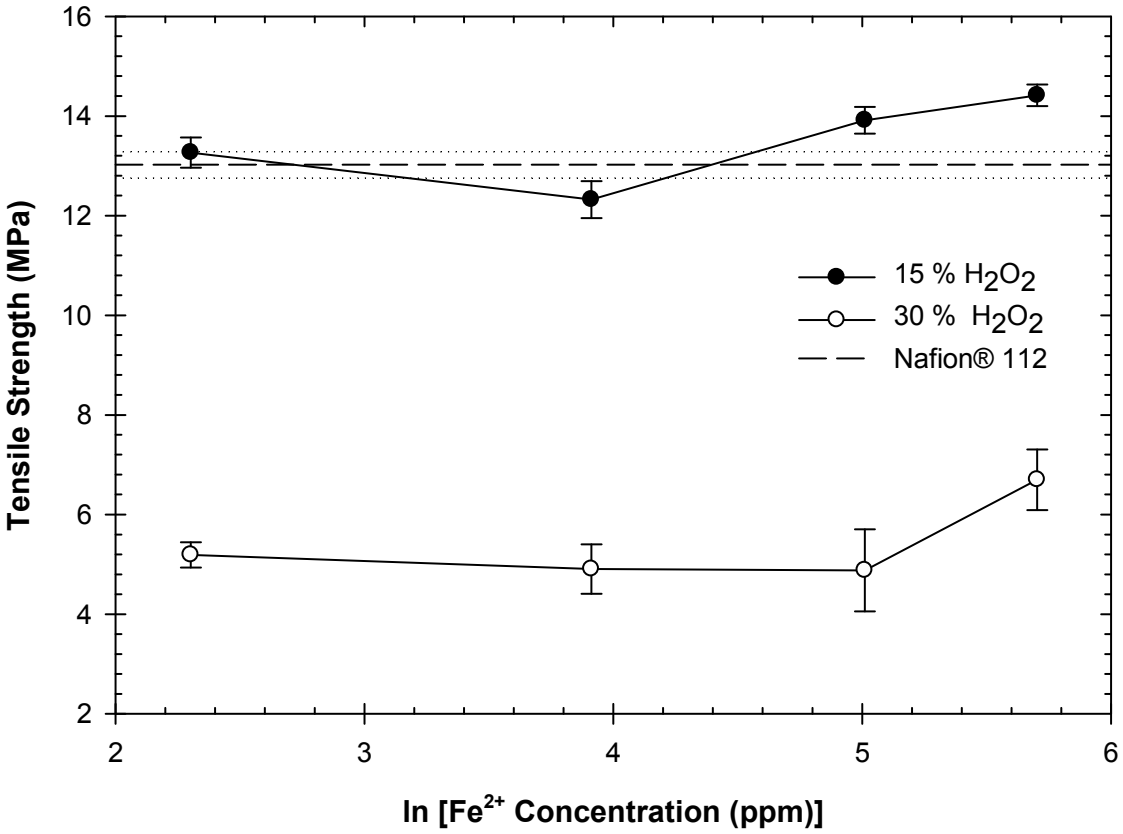

Figure 3-7: Tensile strength of Nafion® 112 films after exposure to various aqueous solutions of Fe^{2+}/H_2O_2 at 80 °C for 12 h. Error bars represent 95 % confidence intervals.

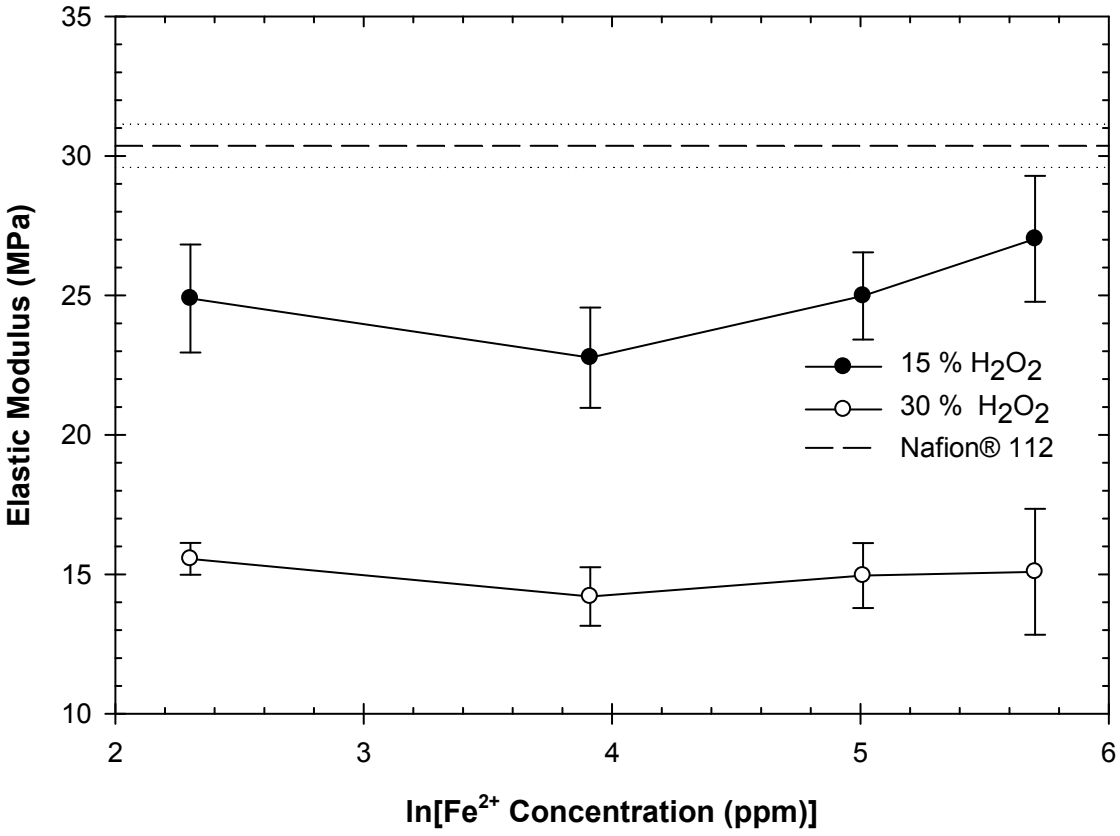

Figure 3-8: Elastic Modulus of Nafion® 112 films after exposure to various aqueous solutions of Fe^{2+}/H_2O_2 at 80 °C for 12 h. Error bars represent 95 % confidence intervals.

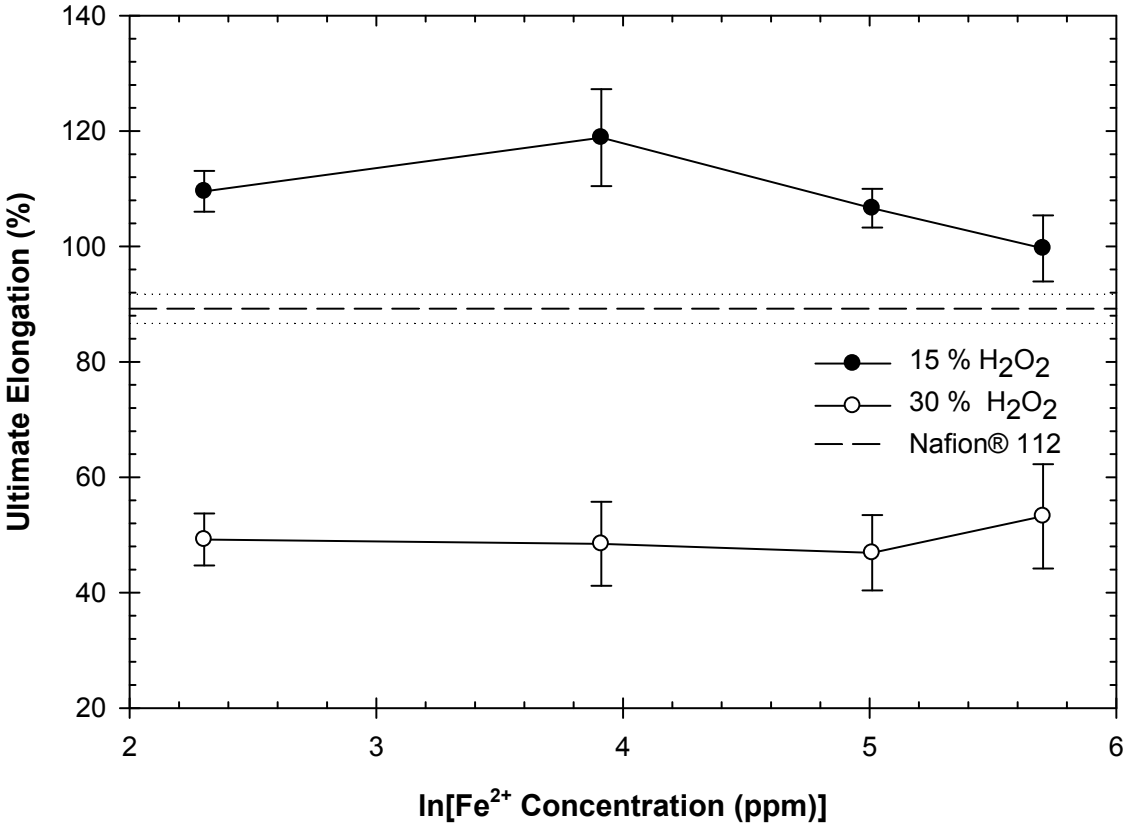

Figure 3-9: Ultimate elongation of Nafion® 112 films after exposure to various aqueous solutions of Fe^{2+}/H_2O_2 at 80 °C for 12 h. Error bars represent 95 % confidence intervals.

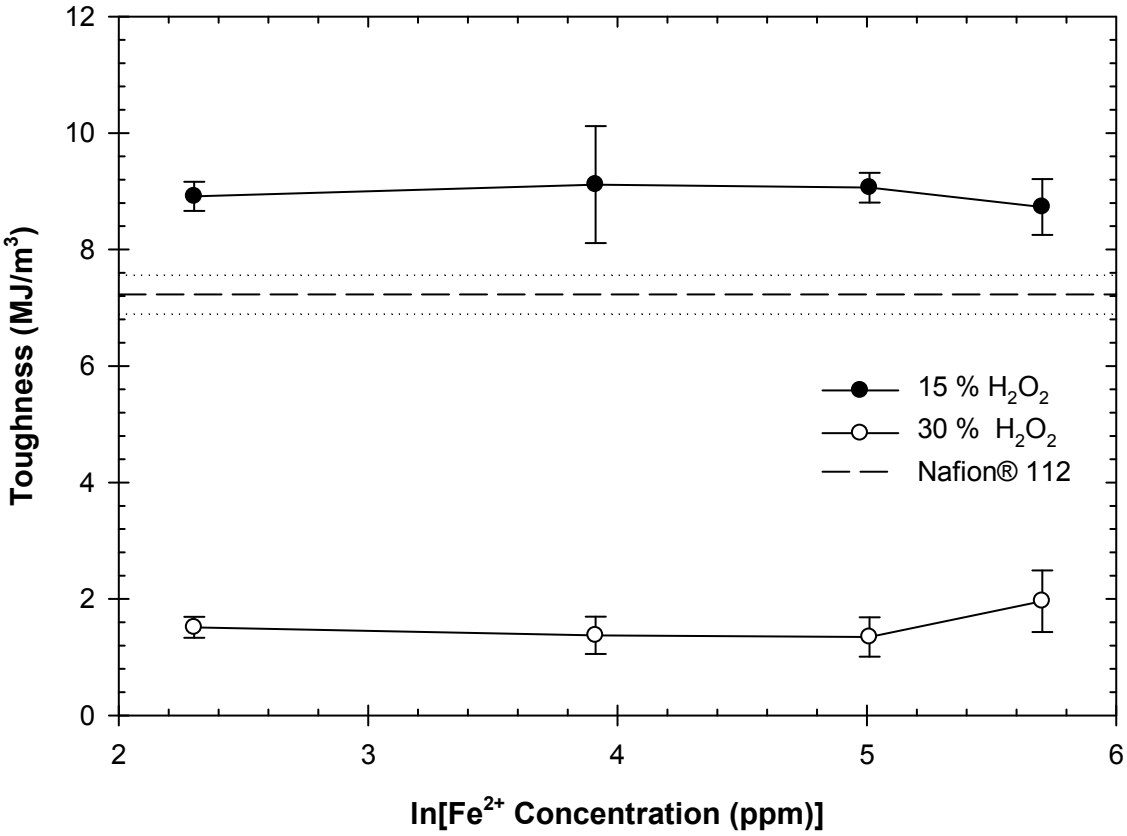

Figure 3-10: Toughness of Nafion® 112 films after exposure to various aqueous solutions of Fe^{2+}/H_2O_2 at 80 °C for 12 h. Error bars represent 95 % confidence intervals.

3.3.5. Degradation Effects on Proton Conductivity

Proton conductivity measurements were averaged over 4 sample locations on Nafion® films that were previously exposed to various degradation reagents. The results are presented in Figure 3-11. Although proton conductivities were expected to generally decrease under each degradation condition, conductivity values increased slightly after exposure to the 15 % H_2O_2 solutions for all iron concentrations except 50 ppm Fe^{2+}, which showed a significant reduction in proton conductivity. The higher proton conduction 15 % H_2O_2 may also be the result of increased chain mobility that could allow for improved rearrangement of sulfonic acid groups serving as chemical channels for proton transport. Under harsher reagent conditions with a higher concentration of H_2O_2, additional sulfonic acid mobility may lead extensive sulfonic acid aggregation that can cause a loss of percolated networks for proton transport. Also, the voids produced as result to exposure to the higher concentrated H_2O_2 solutions might act as physical obstructions in the ionic pathways. These explanations agree with the ion chromatography and FTIR results that suggest that there were no significant losses of sulfonic acid side chains from the films.

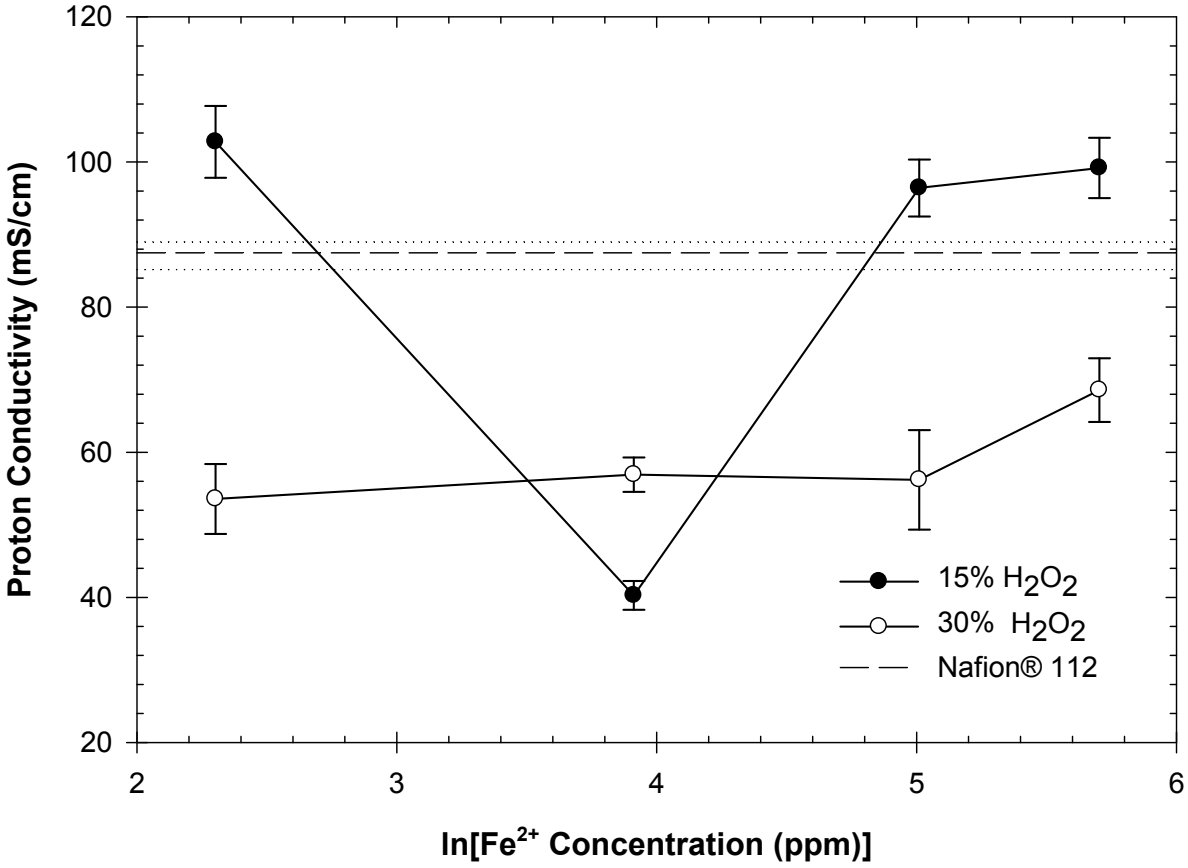

Figure 3-11: Proton conductivity of Nafion® 112 films after exposure to various aqueous solutions of Fe^{2+}/H_2O_2 at 80 °C for 12 h. Error bars represent 95 % confidence intervals.

3.3.6. Degradation Effects on Water Transport

The effect of accelerated free radical degradation on water transport was evaluated on Nafion® films using multiple techniques. Water uptake (see Figure 3-12), based on dry and swollen film masses increased for all degradation experiments as expected. The overall increase of the water storage capacity in degraded films is likely due to improved polymer chain flexibility resulting from chain scissions, as discussed previously. For each Fe^{2+} concentration, the films exposed to 30 % H_2O_2 gave the highest uptake values, most likely due to the presence of voids in the film. The additional free space resulted in the increased free water retention capacities of degraded samples. It was observed that water uptake changes for PFSA films immersed in 30 % H_2O_2 solutions were similar to the trends in pore size and fluoride loss with respect to iron(II) content. For the solution with 50 ppm Fe^{2+}, for which each of these properties reaches a maximum value, the rate of free radical attack was optimized. This is further evidence of optimized free radical attack under specific regent conditions which may be significant for quickly inducing film changes representative of worst-case decomposed performance.

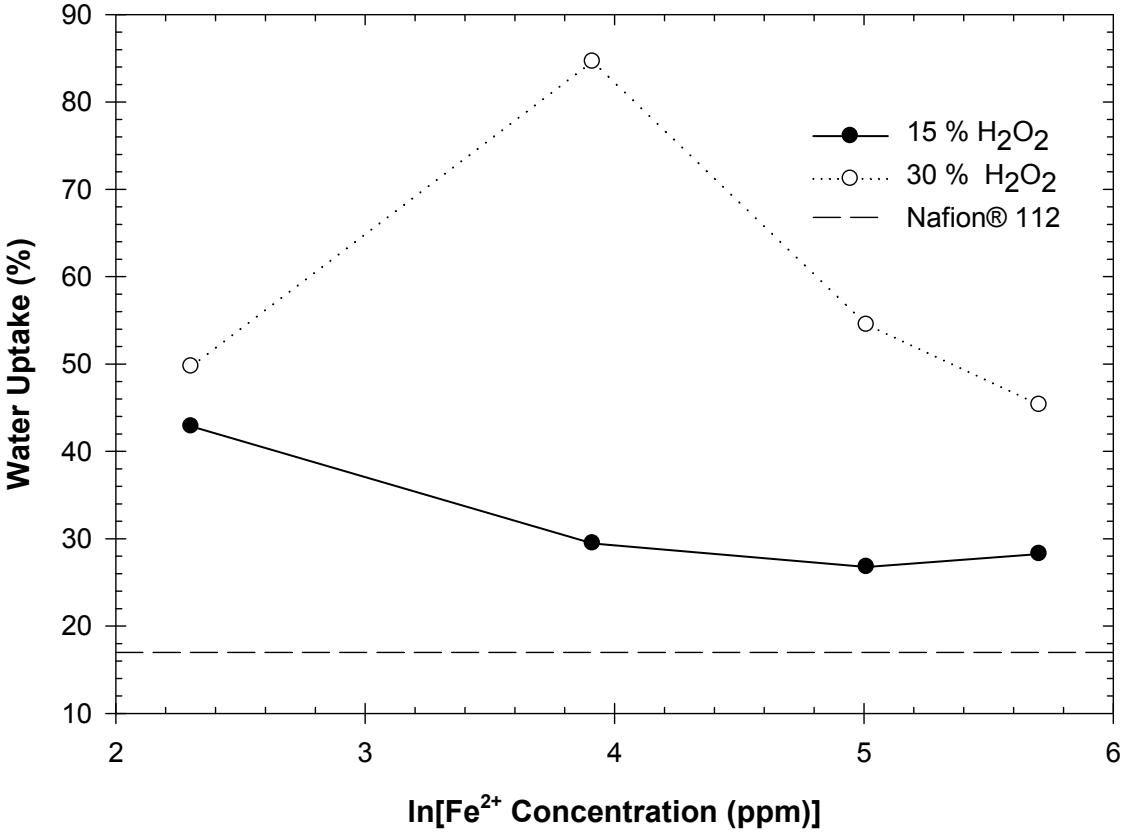

Figure 3-12: Post-degradation water uptake based on dry and swollen film masses at room temperature.

The degraded Nafion® swelling ratios, shown in Figure 3-13, do not follow the same trends as water uptake. For films degraded with 30 % H_2O_2, the swelling ratios were somewhat higher than the original polymer at 10ppm Fe^{2+}, but for higher Fe^{2+} concentrations, the swollen thickness changes were less than the original polymer. This phenomenon may be related to changes in the polymer morphology, which has been shown with SEM imaging to change with Fe^{2+} content. The voids formed during the Fenton tests are capable of retaining water, but these sections of the polymer films do not expand or contract with water uptake, thereby causing reduced dimensional changes in the swollen state. For this reason, films degraded with 15 % H_2O_2 solutions, which were relatively defect free, consistently displayed increased in swelling ratios after accelerated aging experiments.

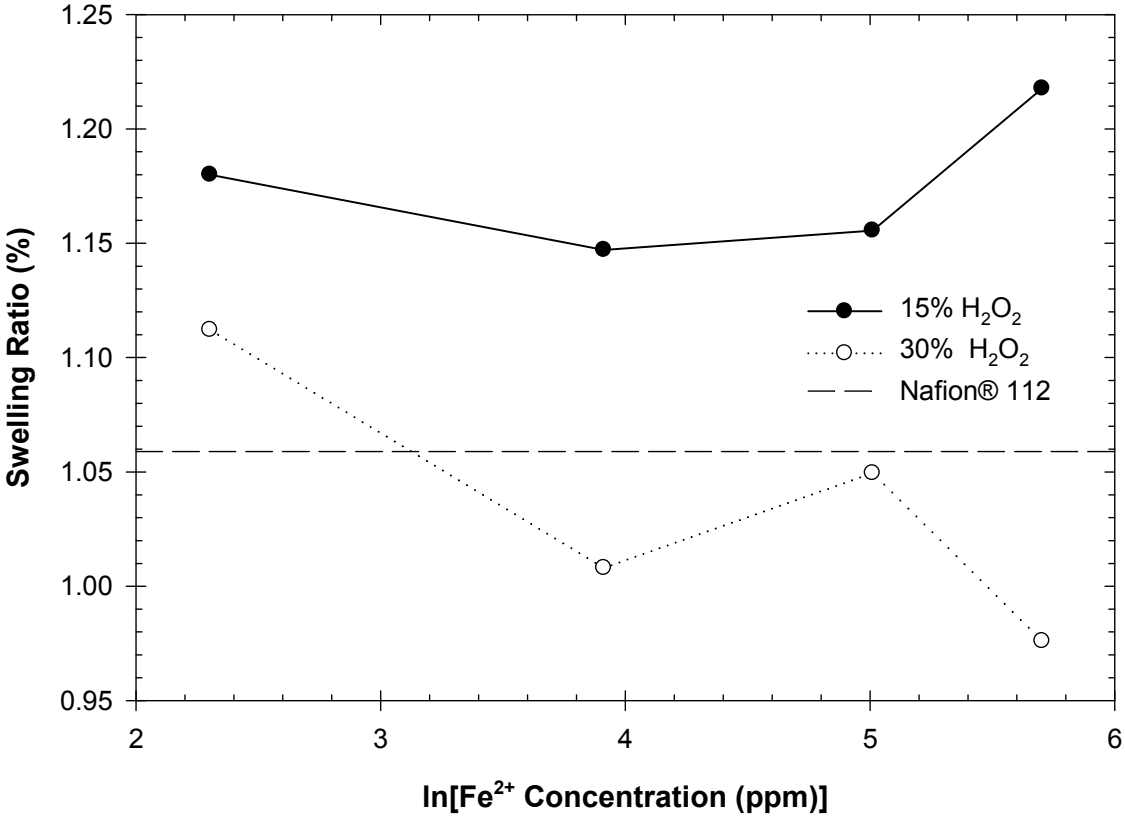

Figure 3-13: Post-degradation swelling ratios based on dry and swollen film thicknesses at room temperature.

Liquid water flux and permeability values were averaged over 12 sample locations and are displayed in Figure 3-14 and Figure 3-15. The decomposed films generally experienced little to no change as a result of free radical degradation. Both properties were expected to change proportionally with proton conductivity, since some rearrangement of sulfonic acid segments is thought to facilitate water transport. Furthermore, higher water transport and liquid breakthrough were expected with films exposed to 30 % H_2O_2 since SEM micrographs indicated the formation of pinholes on degraded film surfaces. The results suggest that water transport pathways may not be directly affected by the same ionic channel alignment that facilitates proton transport. Also, the flux similarities between unmodified Nafion® and the degraded, porous Nafion® films suggest that water molecules remained in the continuous polymer phase while moving through membranes so that no liquid water breakthrough could occur.

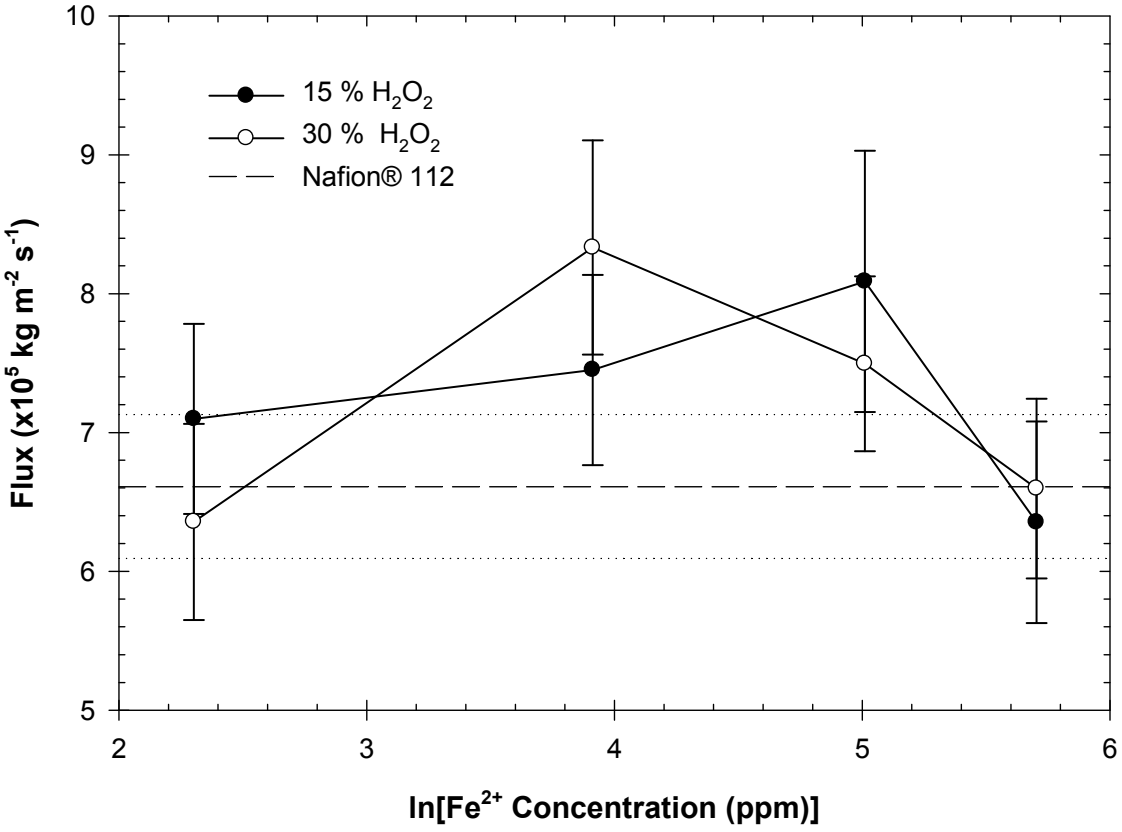

Figure 3-14: Water flux through Nafion® films degraded with various H_2O_2/Fe^{2+} compositions. Flux was determined from high-throughput pervaporation at 50 °C and averaged over 12 samples locations. Error bars represent 95 % confidence intervals.

Interestingly, flux only increased when films were exposed to the solutions consisting of 15 % H_2O_2 with 100 ppm Fe^{2+} and 30 % H_2O_2 with 50 ppm Fe^{2+}, while all other reagents led to insignificant flux changes. Permeability values, on the other hand, were unaffected by degradation in 15% H_2O_2, but were reduced somewhat in 30 % H_2O_2 solutions for all iron(II) concentrations except 50 ppm, where the permeability increased after accelerated decomposition. For that particular sample, which also had the greatest increase in water uptake, it is likely that substantial polymer defects caused higher water transport. In general, rapid decomposition with higher H_2O_2 concentrations should limit water transport through the continuous polymer phase of Nafion® films since internal voids can obstruct water channels. Decreased permeability values from immersion in 30 % H_2O_2 are also fairly consistent with the reduction in swelling ratios under these degradation conditions. According to Equation 3-10, if flux is unaffected by free radical degradation, and the driving force decreases with reduced swelling thickness, then the permeability should also decrease as result of degradation.

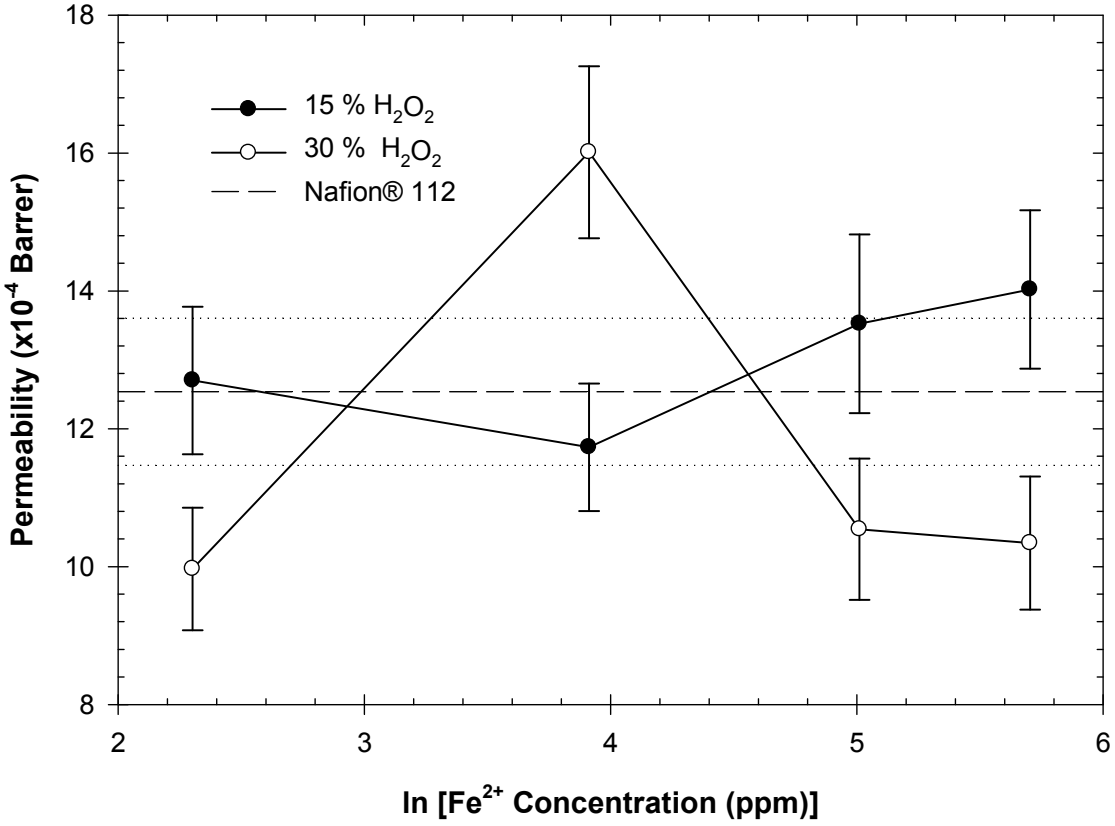

Figure 3-15: Water permeability through Nafion® films degraded with various H_2O_2/Fe^{2+} compositions. Permeability was determined from high-throughput pervaporation at 50 °C and averaged over 12 samples locations. Error bars represent 95 % confidence intervals.

3.4. CONCLUSIONS

In an effort to better understand the free radical degradation pathways taking place in Nafion® during fuel cell operation, variations in the Fenton testing protocols were explored. Analysis of the chemical and performance properties of rapidly aged samples show that the hydrogen peroxide concentrations had a significant impact on accelerated testing. The more concentrated hydrogen peroxide solutions induced increased fluoride loss from the film, along with lower conductivity, and reduced mechanical stability due to severe morphological changes. Accelerated durability testing in the more dilute hydrogen peroxide concentration resulted in films with slightly increased proton conductivities, and for some concentrations of Fe^{2+}, slightly improved mechanical properties. These enhancements under relatively mild accelerated degradation conditions are most likely the result of increased polymer chain mobility from reduced chain entanglements that did not comprise overall film morphologies. Significant changes in fluoride loss, proton conductivity, and water transport were observed for Nafion® films degraded with 50 ppm Fe^{2+}, suggesting that an optimal rate of free radical attack could be established based on the limited number of attack sites in the PFSA membrane. Therefore, the properties of rapidly degraded films may be controlled to better represent long-time durability results.

Chain unzipping, chain scission, and radical side-group attack were all evaluated as possible pathways for free radical attack on Nafion® films. FTIR spectroscopy on degraded films and ion chromatography of the final supernatant solutions provided somewhat divergent results for the fluoride loss. Although fluoride was detected in all supernatants, there was no significant reduction in C-F vibrations relative to other vibrations in the polymer films. Fluoride loss was close to the detection limit of the FTIR, which could imply only partial chain unzipping and/or minimal chain scission. An

alternative explanation is that fluoride loss may have been accompanied by sulfonic acid leaching in the supernatant, but was overshadowed by SO_4^{2-} from the metal catalyst in ion chromatography. The changes in sulfonic acid and fluoride concentrations in the membrane would then go undetected by FTIR analysis if entire polymer chains were reduced to low molecular weight molecules that leached from membranes while the relative proportions of chemical bonds in the membranes were retained.

The unchanged proportionality of chemical bonds in degraded films also suggests that direct reactions with polymer side-chains were negligible compared to the other possible pathways. Complete chain unzipping of polymer structures does not exclude the possibility of chain scission reactions which may also produce undetected chemical losses in degraded membranes. It is therefore possible that the dominating pathway switches as a result of free radical availability from the hydrogen peroxide concentration. As an example, hydrogen peroxide radicals may preferentially cause chain scission at every active site on the polymer chain before switching to partial or complete chain unzipping if more radicals are available. The voids would then result from chain unzipping at higher hydrogen peroxide concentrations. If this were the case, then determining the total amount of hydrogen peroxide typically produced throughout fuel cell lifetimes would be essential for correlating real-time evaluations with accelerated Nafion® durability tests.

3.5. REFERENCES

1. Lemons, R.A., *Fuel cells for transportation.* Journal of Power Sources, 1990. **29**(1): p. 251-264.

2. Prater, K.B., *Polymer electrolyte fuel cells: a review of recent developments* Journal of Power Sources, 1994. **51**(1): p. 129-144.

3. Shah, R.K., et al. *Research Opportunities And Challenges In Fuel Cell Science And Engineering*. in *4 th Baltic Heat Transfer Conference*. 2003. Kaunas, Lithuania.

4. Tang, H., et al., *A degradation study of Nafion proton exchange membrane of PEM fuel cells.* Journal of Power Sources, 2007. **170**(1): p. 85-92.

5. Schiraldi, D.A., *Perfluorinated Polymer Electrolyte Membrane Durability*, in *Polymer Reviews*. 2006, Taylor & Francis Ltd. p. 315-327.

6. *Multi-Year Research, Development and Demonstration Plan: Planned program activities for 2005-2015*, US Department of Energy, Hydrogen, Fuel Cells & Infrastructure Technologies Program. p. 3.4-11.

7. Kinumoto, T., et al., *Durability of perfluorinated ionomer membrane against hydrogen peroxide.* Journal of Power Sources, 2006. **158**(2): p. 1222-1228.

8. Bosnjakovic, A. and S. Schlick, *Nafion Perfluorinated Membranes Treated in Fenton Media: Radical Species Detected by ESR Spectroscopy.* The Journal of Physical Chemistry B, 2004. **108**(14): p. 4332-4337.

9. Collier, A., et al., *Degradation of polymer electrolyte membranes.* International Journal of Hydrogen Energy, 2006. **31**(13): p. 1838-1854.

10. Wu, J., et al., *A review of PEM fuel cell durability: Degradation mechanisms and mitigation strategies.* Journal of Power Sources, 2008. **184**(1): p. 104-119.

11. Büchi, F.N., et al., *Study of radiation-grafted FEP-G-polystyrene membranes as polymer electrolytes in fuel cells.* Electrochimica Acta, 1995. **40**(3): p. 345-353.

12. Borup, R., et al., *Scientific Aspects of Polymer Electrolyte Fuel Cell Durability and Degradation.* Chemical Reviews, 2007. **107**(10): p. 3904-3951.

13. Kodama, K., et al., *Degradation of Nafion Membranes in Hydrogen Peroxide.* ECS Meeting Abstracts, 2006. **502**(33): p. 1185-1185.

14. Chen, C., et al., *XPS investigation of Nafion® membrane degradation.* Journal of Power Sources, 2007. **169**(2): p. 288-295.

15. Sormana, J.-L., S. Chattopadhyay, and J.C. Meredith, *High-throughput mechanical characterization of free-standing polymer films.* Review of Scientific Instruments, 2005. **76**(6): p. 062214-9.

16. Zapata, P., P. Basak, and J. Carson Meredith, *High-throughput screening of ionic conductivity in polymer membranes.* Electrochimica Acta, 2009. **54**(15): p. 3899-3909.

17. Liu, H., et al., *Chemical Degradation: Correlations Between Electrolyzer and Fuel Cell Findings*, in *Polymer Electrolyte Fuel Cell Durability*. 2009. p. 71-118.

18. Curtin, D.E., et al., *Advanced materials for improved PEMFC performance and life.* Journal of Power Sources, 2004. **131**(1-2): p. 41-48.

19. Kundu, S., L.C. Simon, and M.W. Fowler, *Comparison of two accelerated Nafion(TM) degradation experiments.* Polymer Degradation and Stability, 2008. **93**(1): p. 214-224.

20. Morgan, R.A. and W.H. Sloan. *Extrusion finishing of perfluorinated copolymers*. 1986. 4626587.

21. LaConti, A., M. Hamdan, and R. McDonald, *Mechanisms of membrane degradation*, in *Handbook of fuel cells : fundamentals, technology, and applications*, W. Vielstich, A. Lamm, and H.A. Gasteiger, Editors. 2003, Wiley: Hoboken, N.J. p. 647-662.

22. Merlo, L., et al., *Resistance to peroxide degradation of Hyflon® Ion membranes.* Journal of Power Sources, 2007. **171**(1): p. 140-147.

23. Tseng, J.M., et al., *Emergency response plan for boiler explosion with toxic chemical releases at Nan-Kung industrial park in central Taiwan.* Process Safety and Environmental Protection, 2008. **86**(6): p. 415-420.

24. Zhou, C., et al., *Chemical Durability Studies of Perfluorinated Sulfonic Acid Polymers and Model Compounds under Mimic Fuel Cell Conditions.* Macromolecules, 2007. **40**(24): p. 8695-8707.

Chapter 4
Sulfonation of Aromatic Polymers for Proton Exchange Membrane Fuel Cell Applications

The durability issues associated with perfluorosulfonic acid-based materials discussed in the previous chapter are a critical setback for the commercialization of proton exchange membrane fuel cells. The need for more robust materials has directed research towards the exploration of high-performance, hydrocarbon-based polymer systems that can be electrochemically modified to be used as low cost proton exchange membrane (PEM) alternatives. Aromatic sulfonation has become a popular method of converting electrically-insulating hydrocarbon materials into PEMs. However, depending on the polymer structure and the sulfonation procedure used, aromatic sulfonation can severely impact other key polymer properties, namely mechanical, chemical, and thermal stability. This chapter summarizes the current progress in alternative PEM development and also gives an overview of the more common sulfonation methods used for electrochemical enhancement. The state-of-the-art in hydrocarbon PEMs has motivated the preliminary investigation of two high-performance materials that have not yet been widely studied for possible fuel cell applications. These polymers have been modified according to previously-cited sulfonation procedures, and the effects of these procedures have been summarized.

4.1. INTRODUCTION

The proton exchange membrane fuel cell (PEMFC) is currently considered the most promising alternative power source for vehicle transportation and other applications requiring clean, quiet, and portable energy [1]. For this reason, much effort has gone into developing PEM materials, which have long been a critical setback for PEMFC commercialization. While the electrolyte material primarily serves as a highly proton conductive fuel and oxidant barrier, there are many other performance characteristics that are necessary for PEM functionality within a fuel cell system [2-4]. Membranes for PEMFC applications must be capable of fabrication into membrane electrode assemblies with high bonding strength for maximum catalytic and ion transport efficiency. The membrane's dielectric properties are essential for preventing short circuits during operation. Since proton transport is typically facilitated by membrane hydration, and since drying and flooding of the electrodes will significantly inhibit catalyst performance, strict membrane water management is vital for extended fuel cell efficiency. However, proper water management can limit fuel cell operating temperatures. Therefore, water permeation and diffusion through PEMs should be stable over a broad range of temperatures. In addition, PEMs must maintain high mechanical stability under repeated thermal and hydration cycling, which can lead to long-term durability issues. Due to the acidic nature of the PEMFC environment, as well as the possible formation of highly reactive free radicals during operation, chemical stability is also critical to long-term fuel cell durability. Such stability issues have typically been addressed by incorporating fluorinated carbons and/or aromatic rings into the polymer backbone and side groups. The use of such atoms and functional groups can require numerous processing steps, which in turn increases the cost of membrane fabrication. All of these specifications and constraints have made the search for the ideal PEM a

very challenging task. Within the past two decades, there has been incremental progress in the development of new PEMs, but there is still great potential for future advancement. This chapter highlights recent innovative strategies for developing PEMFC polymers and describes two approaches for developing new PEM materials based on the sulfonation of Ultem® polyetherimide (PEI) and Matrimid® polyimide.

4.2. BACKGROUND

The U.S. Department of Energy (DOE) has set target specifications for PEM performance during fuel cell operations. These targets can vary based on the specific application. PEMs for automotive applications are expected to sustain high power outputs (> 650 W/kg [2]) for at least 5,000 h at temperatures that range from 60 to 120 °C. Stationary applications require the same standard of performance for a much longer lifetime and higher temperature range (at least 40,000 h, up to 170 °C). In both cases, the cost of the PEM is intended to remain below \$20 /m^2 or \$5 /kW [3]. To meet these requirements, a number of polymer materials have been explored for commercial implementation.

4.2.1. Perfluorinated Sulfonic Acid Membranes (PFSAs)

The current state-of-the-art PEM for fuel cell applications is Nafion®, a commercial perfluorosulfonic acid polymer originally introduced by DuPont in the 1960's (see Figure 4-1a). Nafion displays superior proton conductivity when properly hydrated (~100 mS/cm), with high thermal and chemical stability afforded by its fluorinated backbone and side chains. The inertness of the polymer structure has proven to yield excellent lifetimes above 60,000 h when operated below 80 °C [2, 4]. Above 80 °C, the polymer's durability has been observed to drop below 1,000 h [4], and the reduction in membrane-water content drastically lowers ionic conductivity. The limited temperature range also prevents opportunities for improved electrode kinetics, possible heat recovery, and higher carbon monoxide tolerance, which is essential for reformed hydrogen fuel sources. These disadvantages as well as high manufacturing cost and high methanol permeability have motivated the search for alternatives [5]. Some alternatives have had moderate commercial success, including Aciplex® (Asahi Chemical Company), Flemion® (Asahi Glass Company), and a membrane from the Dow Chemical Company that is no longer available [6]. However all of these membranes are based on the Nafion® structure, sharing most of the disadvantages of the state-of-the-art membrane, namely limited performance at the higher end of the target operation temperature range.

Other perfluorosulfonic acid-based polymer alternatives have also been explored [7]. Researchers have tried replacing sulfonic acid with other ionic conducting groups such as sulfonyl imides and phosphonic acid to improve thermal stability [7, 8]. However, no significant improvements have resulted from this work. Nafion® has also been incorporated into composite membrane systems by impregnation into microporous poly(tetrafluoroethylene) (PTFE) matrices [8]. It was believed that the inert reinforcement would allow for thinner PEM at lower costs. When compared to pure Nafion®, these

authors found the composite membranes to display improved durability at lower thicknesses while maintaining comparable electrochemical characteristics. Although high temperature operation was still limited by membrane-water content, the Nafion®/PTFE composite membrane has been made commercially available by W.L. Gore & Associates (Gore-Select®) and is targeted for stationary applications [9].

Inorganic Nafion® composites have been evaluated for enhanced fuel cell performance with the incorporation of solid particles such as SiO_2, ZrP, and TiO_2. Researchers have found that these composite membranes display higher ion exchange capacity under low humidity conditions, allowing for a broader range of operation temperatures [2, 10-12]. However, the cost of these modified Nafion® membranes limits their use in the commercial fuel cell market. Therefore, much effort has been directed toward alternative hydrocarbon backbone polymers, which not only have the potential for higher-temperature performance under lower humidity conditions, but also promise cost advantages relative to commercially available PFSAs [1, 2].

4.2.2. Alternative PEMs

As mentioned previously, hydrocarbon PEMs are desirable for their potentially low manufacturing cost, since there are many high performance hydrocarbon polymers already available to be incorporated into PEMFCs. Such materials typically contain aromatic moieties which provide chemical and thermal stability. While still not as stable as conventional PFSAs, many of these hydrocarbon-based PEMs have been shown to be suitable for PEMFC applications when considering the possibility of significantly improved manufacturing costs. Since they are usually non-ionic, these hydrocarbon polymers also require chemical modification, typically through aromatic sulfonation, to induce the desired ionic transport characteristics. The sulfonation process itself adds multiple degrees of freedom to the PEM synthesis procedure, thus providing opportunities for further material optimization. There is a large amount of literature

investigating the optimized performance properties of sulfonated aromatic polymers as alternatives Nafion® in fuel cells. Those most commonly studied are described here.

4.2.2.1. Polystyrenes

Poly(styrene sulfonic acid) (PSSA, Figure 4-1b) is a basic PEM polymer from which many low-cost membranes have been derived. The styrene monomer is readily available, easily functionalized, and can be added to a broad range of commercially available polymers using graft radiation [10]. Researchers have investigated the properties of PSSA with non-fluorinated polymers (sulfonated poly(ethylene styrene) [11]), fluorinated polymers (PTFE-g-PSSA, [12]), and partially fluorinated polymers (PVDF-g-PSSA, [13-16]). Their results show that while sulfonated styrene-based membranes generally display electrochemical characteristics that are competitive with Nafion®, they are not mechanically compatible with other MEA components, and show weak barrier properties and low chemical resistance that ultimately lead to membrane lifetimes less than 200 h.

To improve the MEA compatibility of PSSA, it can be incorporated into more flexible polymer chains through copolymerization. Sulfonated poly(styrene-(ethylene-co-butylene)-styrene) (SEBS) is one example of a copolymer system that has been commercialized by Dais Analytics. It shows improved MEA compatibility and ionic conductivities comparable to Nafion®, but shares similar chemical instability characteristics as many other styrene-based PEMs [13]. For this reason, Dais membranes are targeted at portable fuel cell applications operating at 1 kW or less at temperatures less than 60 °C [6].

The stability of sulfonated styrene PEMs has been further enhanced in composites using a commercially available, low cost ion exchange resin from Scientific Polymer. The resin also consists of PSSA, which is cross-linked with divinylbenzene for mechanical reinforcement. The resin itself is nanoporous to permit water and cation

diffusion, but cannot be used directly in PEMFCs because its highly cross-linked structure severely limits flexibility. Combining the resin with flexible PSSA, which has good interfacial adhesion with resin, allows for easier MEA fabrication. Researchers found that this composite delivers a seven-fold increase in durability compared to the unreinforced polystyrene [14].

4.2.2.2. Polyphenylenes

Polyphenylenes provide the most basic aromatic back-bone structure from which an abundance of PEMs can be derived. A long chain of benzene rings alone offers excellent thermal and chemical stability, but is also very rigid in the range of temperatures used by PEMFCs [15]. To increase the materials flexibility, processability and further enhance its stability, functional groups are added to the polymer backbone. Two examples of the basic flexible polyphenylene polymer are poly(phenylene oxide) (PPO, Figure 4-1c), and poly(phenylene sulfide) (PPS), both of which are commercially available low-cost high performance polymers. They are also easily modified at the benzene rings with sulfonation to yield electrochemical properties. Sulfonated PPO has been shown to deliver good proton conductivity upon optimizing the degree of sulfonation, although the highest conductivity achieved is still lower than that Nafion® (84 mS/cm compared to 120 mS/cm), and mechanical properties are significantly reduced [16, 17]. The thermal properties of S-PPO are suitable for PEMFC applications, but its low oxidative stability at high operation temperatures leads to reactant gas crossover and shortened lifetimes [16]. Variations of PPO have been explored by Ballard Advanced Materials with methyl or benzyl groups substituted at the 2- and 6- carbons of the aromatic backbone. Although the oxidative stability was predicted to increase, membrane degradation remained an issue during fuel cell tests where the performance of the MEA lasted < 500 h. PPS also displays good proton conductivity when sulfonated, but is water soluble at degrees of sulfonation > 30 % [17].

Another common polyphenylene derivative is poly(4-phenoxybenzoyl-1,4-phenylene) (PPBP, Figure 4-1d), commercially available as a high-temperature engineering polymer (Poly-X 2000, Maxdem, Inc.). At high degrees of sulfonation (> 65%), these membranes display slightly lower conductivity characteristics than Nafion®, but remain thermally and electrochemically stable up to 140 °C due to their enhanced water uptake properties [18]. However, S-PPBP performance is strongly related to the fuel cells humidity conditions, making this material ideal for PEMFCs that are retrofitted with humidity control technology. Unfortunately, external humidification adds to the cost, volume and weight of the fuel cell.

4.2.2.3. Polyphenylquinoxaline

Polyphenylquinoxaline (PPQ, Figure 4-1e) is a more complex derivative of the polyphenylene family well-known for its processability, along with thermal and chemical stability characteristics similar to other polyphenylenes previously mentioned [19]. Ballard Advanced Materials investigated the use of sulfonated PPQ for fuel cell applications, designating it as their first generation PEM (BAM1G). The heterocyclic nature of the polymer provides good mechanical strength and the degree of sulfonation has previously been manipulated to provide electrochemical properties competitive with Nafion® [20]. Membrane durability during fuel cell operation, however, is a setback for this type of polymer, as its chemical instability can result in fuel/oxidant crossover within the first 350 h of fuel cell operation [20].

4.2.2.4. Poly(ether ketones)

Poly(ether ketones) are semicrystilline polymers that offer high thermal stability, chemical stability, and mechanical properties at a low cost. A large variety of these polymers based on the sequence of ether and ketone groups have been made commercially available. One of the most common examples is poly(ether ether ketone) (PEEK, Figure 4-1f), which has been manufactured under numerous trade names

including Victrex® (Victrex), Gatone® (Solvay), and Kadel® (Solvay), among others. Other polyether ketones are also widely available, such as poly(ether ketone) (PEK, from Victrex and Raychem), poly (ether ketone ketone) (PEKK, from CoorsTek), and poly (ether ether ketone ketone) (PEEKK, from Hoechst). Many more sequences have been developed in laboratories (i.e., PEEEK, PEEKEK, etc.) [21]. Although many of these poly(ether ketones) have been evaluated for fuel cell applications [17, 21-23], the PEEK derivative is most often studied for its availability, versatility, and low cost. Researchers have shown that once sulfonated under the appropriate conditions, S-PEEK membranes can display proton conductivities that are only slightly lower than Nafion® at 80 °C (134 mS/cm compared to 150 mS/cm, [24]). They also show lower methanol permeability than conventional PFSAs, making S-PEEK-based PEMFCs especially well-suited for direct methanol fuel cells. FuMA-Tech, a German company, has developed a S-PEEK membrane (Permasep® FKE) that shows better mechanical stability, efficiency, and power density than Nafion® membranes and is intended to operate in direct methanol fuel cells in the temperature range of 100 to 160 °C. One drawback to increasing the degree of sulfonation in PEEK membranes for improved electrochemical properties is the proportional increase in swelling capacity that leads to reduced mechanical stability. At 30 % sulfonation, S-PEEK is soluble only in strong acids. Above 30% sulfonation, the material is also soluble in several organic liquids. Above 70% sulfonation, S-PEEK becomes soluble in methanol, and at 100% sulfonation, membranes will dissolve in water [15]. Cross-linking can reduce S-PEEK swelling, but will also limit the material's proton conductivity [25, 26]. However, a study has shown that benzene dimethanol with a transition metal catalyst can be used as a S-PEEK cross-linking agent without sacrificing proton conductivity [27]. Other researchers have investigated the use of S-PEEK as composites membranes with metal oxides or complexes of metal oxides and heteropolyacids [15, 21, 28]. These composites, which do not require high levels of

sulfonation to be highly conductive, also show reduced swelling properties. Both methods will add to the costs of manufacturing S-PEEK membranes, so the balance between increased cost and improved performance will need to be evaluated.

4.2.2.5. Polysulfones

Like poly(ether ketones), there are a broad span of commercially available polysulfones (PSU) that display unique combinations of chemical and physical properties, along with high thermal stability and resistance to oxidation [21]. The most commercialized PSU is combination of diphenylsulfone and bisphenol A, currently manufactured by Solvay (Udel®, Figure 4-1g). Numerous performance studies have been conducted on sulfonated and phosphonated Udel®, as well as other modified PSU sequences [29-37]. Phosphonated PSU membranes have shown weak electrochemical properties, but S-PSU has potential for fuel cell applications. The ionic conductivity of S-PSU is significantly lower than Nafion®, but increases with operation temperature and the degree of sulfonation. Similar to S-PEEK, the upper limit of PSU sulfonation was constrained by high swelling and partial membrane dissolution. To overcome this limitation, researchers have explored S-PSU composites with components such as heteropolyacid acids [35, 38] and silica [39], which display markedly improved mechanical stability at higher degrees of sulfonation. The additional costs of producing a sulfonated PSU film with higher conductivities, which are still somewhat lower than conventional PFSAs, may prove to be a major setback to commercializing S-PSU films for fuel cell applications.

4.2.2.6. Polyimides

Sulfonated polyimides (S-PIs) were initially studied for electrodialysis applications, but the original five-member imide ring structure (phthalic S-PIs) proved to be very unstable in PEMFCs even under mild conditions [40]. The second generation of S-PIs based on six-member imide rings (naphthalenic S-PIs, Figure 4-1h) display more

promising performance properties, with reported fuel cell durability tests lasting up to 3,000 h at 60 °C [40, 41]. These membranes have been studied widely and continue to be improved by combining a variety of naphthalene-based dianhydrides with sulfonated diamines [41-49].

Most recent S-PI studies have shown that these materials can have significantly reduced gas and methanol permeabilities compared to Nafion®. As could be expected, the conductivity, swelling, chemical resistance and thermal stability of S-PI membranes all vary with degree of sulfonation. Proton conductivity can generally reach levels close to or even slightly above conventional PFSAs but is limited by extensive water swelling [17, 41, 44]. Fortunately, water stability can be improved by incorporating flexible, unsulfonated diamines into the S-PI backbone [42]. These unsulfonated diamines serve as spacers between rigid rod microstructures, thereby creating free volumes for water uptake. Still, most S-PIs and many of their monomer components are not commercially available, so the ultimate success of these materials in PEMFC applications will rely upon detailed cost assessments of laboratory scale-up.

4.2.2.7. Polybenzimidazole

Polybenzimidazoles (PBIs) are highly thermostable materials with glass temperatures around 420 °C and melting points > 600 °C. One of the more common forms of PBI is commercially available as Celazole® from Hoechst-Celanese, shown in Figure 4-1i. Even without modification, PBIs show some tendency for water uptake and proton conductivity, although it is very low [18]. Conductivity can be significantly enhanced through numerous methods. One method is PBI doping, which has been highly cited in literature [50-52]. Since the polymer has basic characteristics, it can form a complex with acids such as phosphoric acid while retaining its mechanical stability. The acid will hydrogen bond or allow proton transfer reactions with the polymer, providing a unique proton conduction mechanism that can be maintained under low

humidity conditions. Doping is typically accomplished by immersion in concentrated acid solutions with methanol, and can increase membrane conductivities up to that of free acid in its liquid state (70 mS/cm [53]). Acid-doped PBI membranes show 10 times less methanol crossover compared to Nafion®, but more importantly, these membranes have been shown to operate in fuel cells up to 200 °C and 0 % relative humidity [54]. One of the major limitations of acid-doped PBI is acid leaching during extended use, making MEA durability a serious concern. So far, there have been no reports on the long-term stability of this membrane [54].

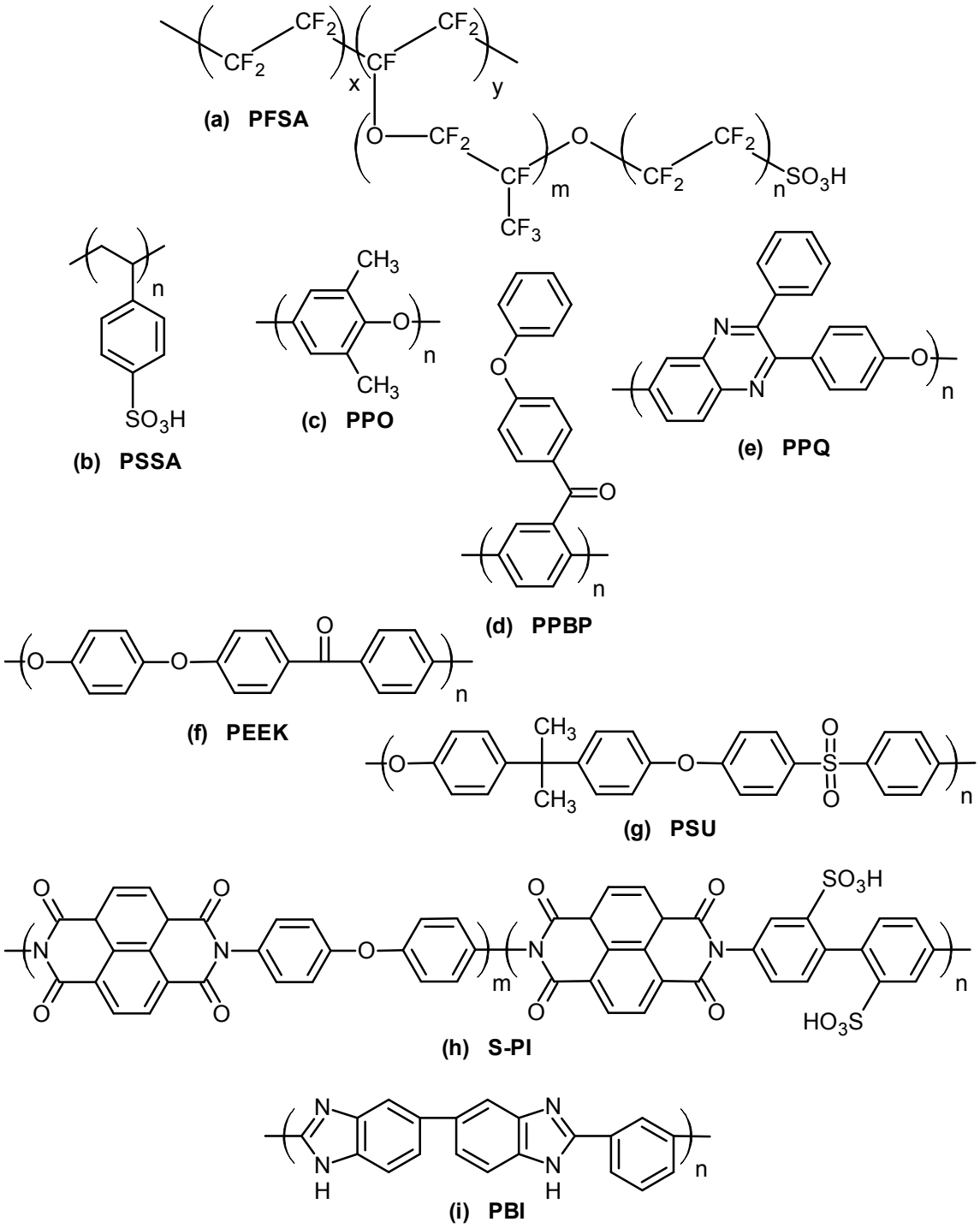

Figure 4-1: Common PEM base polymers. (a) perfluorinated sulfonic acid (Nafion®), (b) poly(styrene sulfonic acid), (c) poly(phenylene oxide), (d) poly(4-phenoxybenzoyl-1,4-phenylene), (e) poly(phenyl quinoxaline), (f) poly(ether ether ketone), (g) poly(ether sulfone), (h) sulfonated naphthalenic polyimide, and (i) polybenzimidazole.

4.2.2.8. Polymer Blends

Based on the previously mentioned polymers alone, there are substantial opportunities for engineering PEMs based on polymer blends that combine the high performance properties of individual components. The scope is even greater when considering the multitude of low-cost commercial polymers that have not typically been explored as PEMs but can still provide significant performance enhancements as polymer blend components. Unlike the development of complex copolymer systems, the blending process is relatively cheap and simple. However, phase separation can be an issue, possibly leading to heterogeneous membranes with poor performance. Blend miscibility can be improved with the proper selection of polymers that allow for favorable ionic interactions, hydrogen bonding, and/or ion-dipole interactions that can also act as cross-linkers for added mechanical stability [17]. The correct choice of a processing solvent is also essential for developing high performance polymer blends. One example of a promising polymer combination is cross-linked polyvinyl alcohol with polyethylene glycol and poly(acrylamide methyl propane sulfonic acid) [55]. The cross-linked blend, acting as a semi-interpenetrating network is cost-effective and has been optimized to display comparable conductivity and lower methanol permeability compared to Nafion®. However, the material's chemical and thermal stability under fuel cell operation temperatures above 80 °C have yet to be evaluated. Many other blends have been cited in literature [16, 17, 56-61]

4.2.3. Sulfonation Methods

Aromatic sulfonation is by far the most common method of enhancing the electrochemical properties of high performance polymers. Sulfonic acid addition is typically accomplished through electrophilic attack of a polymer's aromatic rings with a sulfonating agent containing SO_3 groups, as shown in the example in Figure 4-2.

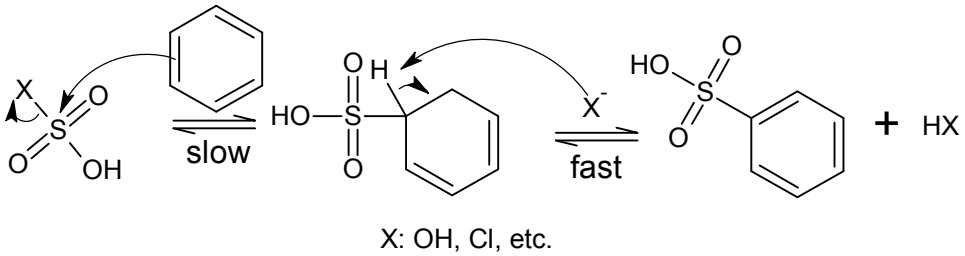

X: OH, Cl, etc.

Figure 4-2: Mechanism for electrophilic aromatic substitution.

The electrophilic attack site is preferential to electropositive carbons stabilized on aromatic rings. Therefore, sulfonation is often restricted to certain locations on the polymer chain. As an example, for bisphenol-based polymers such as PEEK and PSU, sulfonic acid groups will almost always be added at the activated positions ortho to the aromatic ether bond, since these bonds are furthest from the electron-withdrawing carbonyl and sulfonyl groups [62]. Most often, addition of one sulfonic acid group to the aromatic ring of a polymer repeat unit will deactivate the entire repeat unit and prevent its further sulfonation. In order to optimize sulfonated PEMs for commercial use, the degree of sulfonation must be well controlled. There are three keys aspects to controlling sulfonation, as described below.

4.2.3.1. Reaction Environment

Electrophilic aromatic sulfonation is strongly affected by the choice of reaction time and temperature, and detailed kinetic studies have been conducted for numerous sulfonation processes [22, 63-65]. Unlike other electrophilic aromatic substitutions such as nitration, the sulfonation reaction is reversible in the presence of water and at high temperatures. Therefore, water and excess heat must be removed from the reaction

environment to drive the forward reaction and achieve better control of the degree of sulfonation.

4.2.3.2. Direct vs. Post Sulfonation

There are two routes for introducing sulfonic acid groups onto a polymer chain. The direct sulfonation method involves the sulfonation of monomer units that are later polymerized with other monomer units to produce an organized, non-random copolymer system. Direct sulfonation allows for the addition of more than one sulfonic acid group per repeat unit since many aromatic monomers have more than one feasible sulfonation site [44, 46, 66]. Therefore, the degree of sulfonation for a directly sulfonated polymer can be higher than 100 %. Directly sulfonated polymers can also display optimal phase separation for better performance. By controlling sulfonated and unsulfonated block lengths, ionic segments can align into hydrophilic domains for proton transport while non-ionic segments serve to reduce swelling and maintain mechanical support. However, the direct sulfonation method can become complex and costly for commercial scaling when considering multi-process procedures and the current lack of commercially available sulfonated monomers.

Post sulfonation offers a simpler, more cost-effective alternative, since readily available high performance polymers can be used in the straightforward reactions with sulfonating agents. However, depending on the reaction conditions and the pairing of sulfonating agents and polymers, post sulfonation can produce serious defects in the polymer backbone through chain scissions. These defects significantly impact membrane mechanical properties and can not be completely avoided, even under relatively mild reaction conditions [67]. Post sulfonation can also cause cross-linking due to the formation of sulfonic acid bridges among polymer chains, but this can be avoided with appropriate choice of reaction conditions [68].

4.2.3.3. Sulfonating Agents

The traditional sulfonating agents for electrophilic aromatic substitution are sulfuric acid and fuming sulfuric acid (with sulfur trioxide). These reagents are inexpensive and due to their high reactivity can be used without heat in order to achieve desired degrees of sulfonation. Unfortunately the strength of these acids can also lead to significant chain cleavage and irreproducible sulfonation levels since polymer chains may phase separate from the reaction mixture [30, 69]. Also sulfuric acid produces water as a byproduct of sulfonation, which inhibits sulfonation, as mentioned previously. To avoid significant water accumulation during sulfuric acid sulfonations, high acid concentrations (i.e., 98 %wt) are typically used [70]. The use of chlorosulfonic acid is also an option, since it produces hydrochloric acid as a byproduct instead of water. However, chain cleavage, cross-linking, and phase separation remain issues [35, 71].

Although fuming sulfuric acid may be too strong of a sulfonating agent for many polymers, SO_3 can be used with triethyl phosphate (TEP) in solution to form a complex (SO_3•TEP) that provides a much milder sulfonation environement. SO_3•TEP has been shown to minimize cross-linking and cleavage, and the degree of sulfonation can be controlled by varying the ratio of SO_3 to TEP [30, 37, 72, 73]. However, the toxicity of SO_3 and the highly exothermic reaction that takes place with TEP could make industrial scaling very hazardous [70]. Some recent studies have shown that controlled aromatic sulfonation can be accomplished by metalation with n-butyllithium to produce a lithiated intermediate on aromatic rings that are more electron deficient than typical activated sites. The intermediate is converted to sulfonic acid by gassing with SO_2, and then oxidizing with an oxidant such as H_2O_2, as illustrated in Figure 4-3 [36]. While metalation is currently the most efficient mechanism for post sulfonating electron deficient rings, the procedure is complex, costly and therefore not ideal for industrial scale-up [35].

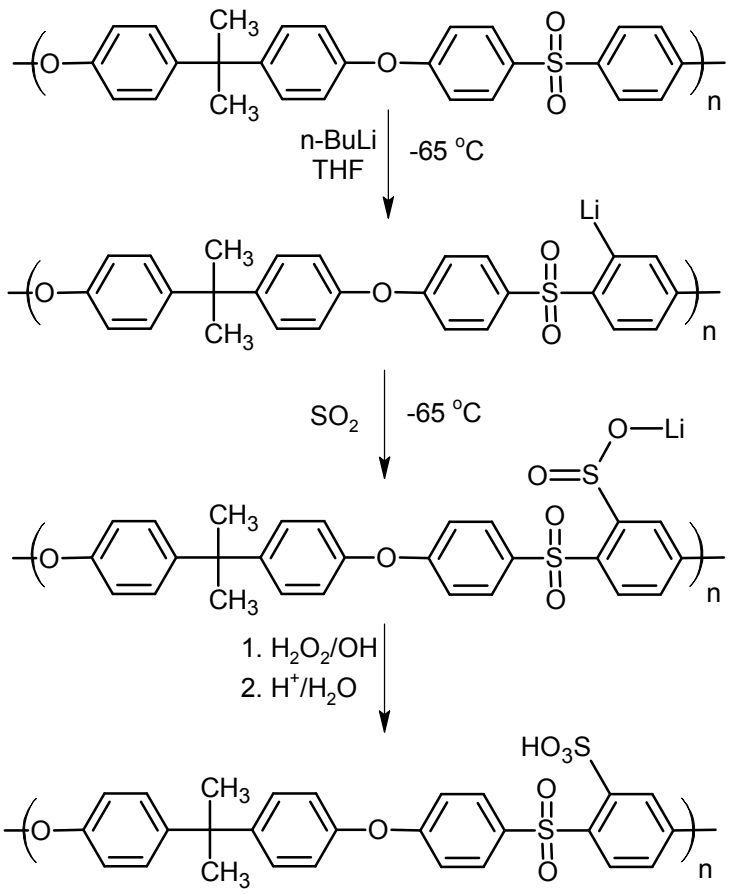

Figure 4-3: Metalation procedure for polysulfone.

Trimethylsilyl chlorosulfonate (TMSCS) has become the preferred sulfonating agent for electrophilic aromatic substitution [35]. Like SO_3•TEP, TMSCS provides a mild reaction environment, which significantly reduces or even eliminates chain cleavage and cross-linking [70, 74]. The trimethylsilyl sulfonated intermediate retains the hydrophobic characteristics of the original polymer and prevents precipitation that would typically occur with the use of strong concentrated acids. The intermediate can later be converted to its sulfonated salt or acid form by immersion in the necessary dilute ionic solution. The major drawback to using TMSCS is the cost of the sulfonating agent which is approximately 25 times higher than that of sulfuric acid. However, TMSCS does not need to be used in high molar excess to achieve high degrees of sulfonation since no water is produced during the reaction. Therefore, when considering the simplicity of this sulfonation procedure and possibility of using inexpensive solvents, industrial-scale TMSCS sulfonation of high performance polymers has the potential for being a cost-effective method for producing commercial PEMs.

4.2.4. Post Sulfonation of Matrimid® and Ultem®

Ultem® polyetherimide (PEI, Figure 4-4) is a low cost, high performance polymer that is electrically insulating, and shows high mechanical and chemical stability up to 170°C [75]. These features make Ultem® a good candidate for fuel cell applications, especially for high-temperature conditions. Some studies have demonstrated the performance of PEIs as stable host matrices for other sulfonated polymers and acid complexes [76-78], but very little has been reported on the use of sulfonated PEI [79]. Sulfonated PI is also a very good candidate material for fuel cell membranes, as mentioned previously. However, most studies on developing S-PI membranes use direct sulfonation, despite the complexities of scaling up the process [67]. It would therefore be more convenient to use a simple post sulfonation approach to modify currently available PIs. Matrimid® PI (Figure 4-4) is commonly used for gas separations and offers very

good thermal stability. Also, the chemical structure of this material is unique to the variety of PEMs previously discussed. The objective of this work was to explore the feasibility of sulfonating both Matrimid® and Ultem® using fuming sulfuric acid or TMSCS. Chemical properties, mechanical stabilities, and proton conductivities have been assessed in sulfonated films where possible.

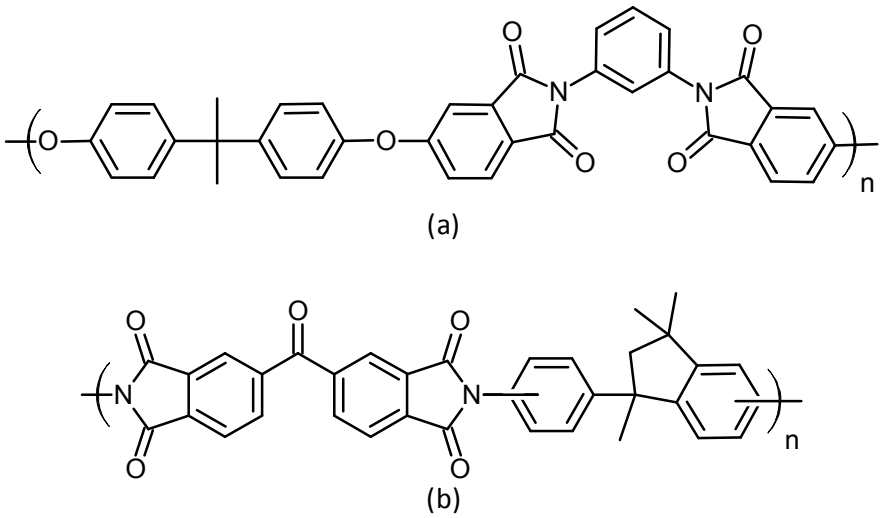

Figure 4-4: Polymer structures of (a) Ultem® PEI and (b) Matrimid® PI.

4.3. EXPERIMENTAL

4.3.1. Materials

Ultem®1000 PEI and Matrimid® 5218 PI were supplied by SABIC and Huntsman Advanced Materials, respectively. Both powders were dried overnight at 120 °C prior to sulfonation. TMSCS (99 %), dichloroethane (DCE, anhydrous and ACS reagent grade), sulfuric acid (puriss. p.a., 95-97 %), fuming sulfuric (ACS reagent grade, 20 % free SO_3,), and sodium methoxide (ACS reagent grade) were all supplied by Sigma-Aldrich. 1-Methyl-2-pyrrolidinone (NMP, production grade), phenolphthalein (1 %) and sodium hydroxide (ACS reagent grade) were obtained from VWR Scientific. Methanol (HPLC grade) was supplied by EMD Chemicals. Hydrochloric acid (ACS reagent grade) was obtained from Fischer Scientific. TMSCS and anhydrous dichloroethane were stored in a nitrogen glove box to prevent water contamination.

4.3.2. Sulfonation Reactions

4.3.2.1. Fuming Sulfuric Acid Sulfonation

Polymer solutions in concentrated sulfuric acid were made at 10 – 20 wt% by adding the acid dropwise to the initially dried polymer over an ice bath to remove ecess heat released during dissolution. The solutions were mixed for at least 30 mins or until the solids completely dissolved into the sulfuric acid. If solids were still present in the mixture after 1 h, mild heat (~50 °C) was used until the mixture was homogeneous. Fuming sulfuric acid was then added dropwise to the polymer solutions over an ice bath at a ratio of 1:2, fuming sulfuric acid to sulfuric acid. The solutions were allowed to mix for 30 mins over ice before slowly ramping the temperature to 55 °C, where the solutions were then mixed for an additional 2 h. After slowly cooling to room temperature, the modified polymers were precipitated over ice and recovered by filtration. The solid was rinsed thoroughly in large quantities of deionized water until a neutral pH was achieved.

4.3.2.2. TMSCS Sulfonation

A detailed procedure for TMSCS aromatic substitution has been previously reported for poly(ether ketone) and polysulfone derivatives [80], and has been adapted for use in this work. The polymer was dissolved in DCE at a concentration of 30 wt% under argon. A separate solution of 30 % TMSCS in anhydrous DCE was added to an addition funnel in the glove box and sealed under nitrogen before removing. Both solutions were made so that the mole ratio of TMSCS to polymer repeat unit was 1.1:1. The reaction vessel, which was continuously purged with argon, was charged with the polymer solution and fitted with the TMSCS addition funnel, a mechanical stirrer, and an acid trap containing an aqueous solution of sodium hydroxide with phenolphthalein. The TMSCS solution was added dropwise over period of 1h and the reaction was carried out for 72 h at room temperature. To complete the sulfonation reaction, a methanol solution with 30 wt% of sodium methoxide, in slight excess molar excess with respect to TMSCS, was added to the DCE solution. The sodium ion exchanges with trimethylsilyl groups on the sulfonated intermediate and neutralizes unreacted TMSCS. The solution was stirred for an addition 2 h before coagulating the mixture in an excess volume of methanol. The solid was filtered and rinsed thoroughly in methanol, and then deionized water until a neutral pH was achieved. The polymer salt was converted to its acidic form using a 1 M HCl at 60 °C, followed by thorough rinsing in deionized water until a neutral pH was achieved. The solids were then dried for at least 48 h at 60 °C under vacuum.

4.3.3. Membrane Characterization

4.3.3.1. Fourier Transform Infrared (FTIR) Analysis

Films were casted as 20 wt% solutions in NMP and dried at 60 °C under vacuum for 48 h. FTIR spectra were collected using a VERTEX 80v and a Hyperion 3000 Microscope with an attenuated total reflectance (ATR) attachment (Bruker Optics).

Spectra were collected at room temperature and pressure with 64 scans at a resolution of 4 cm^{-1}. An air background was subtracted from all measurements.

4.3.3.2. Conductivity

Films used for FTIR analysis were later analyzed for proton conductivity. These measurements were performed with electrochemical impedance spectroscopy (EIS) using a customized, fully automated, high-throughput conductivity (HTC) measurement device, described in detail elsewhere [81]. Swollen film samples were placed in a well-like, electrically insulating sample holder and held in place with a grid-like retention mechanism. The sample holder was filled with enough deionized water at room temperature to completely cover films and prevent dehydration. Before measuring conductivity, localized thickness measurements were taken using an Omega GP901-2 linear displacement digital gauging probe with a flat-tip, 0.12 μm resolution, and low spring constant to reduce sample compression (Omega Engineering, Inc.). To measure conductivity, the hydrated membrane was excited with an alternating current (AC) signal from the outer point-electrodes of a commercially available, tungsten carbide 4-point probe head (Jandel Engineering Ltd.). The response voltage from this AC excitation was measured with the inner point-electrodes, allowing for the calculation of complex impedance. Since electrodes are equally spaced apart, proton conductivity was estimated from complex impedance using the following simplified model:

$$\sigma \approx \frac{1}{Z}\frac{\ln(2)}{\pi h}$$

where σ is the membrane proton conductivity, Z is the membrane's complex impedance, and h is the membrane thickness. All proton conductivity measurements were averaged over a 10 sec stabilization period at room temperature with an excitation signal of 1 kHz.

4.4. RESULTS AND DISCUSSION

4.4.1.1. Fuming Sulfuric Acid Sulfonation

Upon precipitating modified Ultem® over ice, it was observed that the product was highly soluble in water. In order to recover the reacted solids, a sample of the aqueous polymer solution was separated for liquid-liquid extraction with chloroform. Although unmodified PEI is soluble in chloroform, the modified product remained in the aqueous phase. For this reason, rotovapping was used at 60 °C for 5 – 8 h, but the solution began to foam before separation could occur. Foaming is typical in surfactant solutions with short chain oligomers [82, 83], suggesting that a large amount of backbone cleavage took place during the Ultem® reaction in fuming sulfuric acid. The solid that was recovered formed a very brittle film upon casting, and was therefore blended with unmodified Ultem® at S-PEI to PEI ratio of 1:3 for characterization. The FTIR spectra for pure Ultem® and the polymer blend are shown in Figure 4-5.

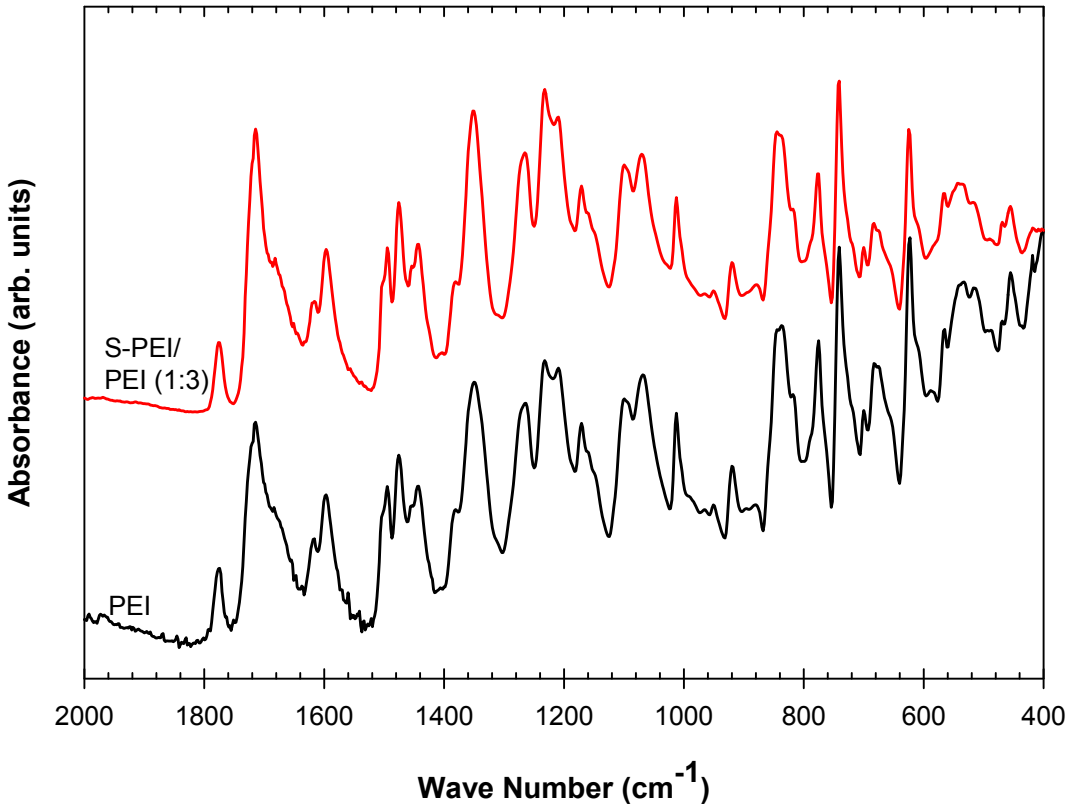

Figure 4-5: FTIR spectra of Ultem® PEI before and after reacting with fuming sulfuric acid.

The spectra suggest that the solid recovered from the reaction of Ultem® in fuming sulfuric acid was unsulfonated, despite its solubility in water. One possible explanation is that reaction conditions, i.e. temperature and time, were too mild for aromatic electrophilic attack. However, the evidence of chain cleavage suggests that these reaction conditions are too harsh. Therefore, fuming sulfuric acid may favor PEI cleavage before aromatic sulfonation, making this reaction method undesirable for Ultem® modifications. Another possibility is that the sulfonated product remained in the aqueous phase during rotovapping, so that only unreacted solid was recovered, which was still subjected to substantial chain cleavage based on mechanical stability. Although non-aqueous rinsing may have been beneficial for product recovery, the recovery of unreacted, mechanically unstable polymer would show that the fuming sulfuric acid reaction took place heterogeneously. Therefore, it would be difficult to control the degree of PEI sulfonation using fuming sulfuric acid.

The solids from the Matrimid® reaction in fuming sulfuric acid were also soluble in water, but could be easily recovered using liquid-liquid extraction with chloroform. The product formed a rigid solid at the water-chloroform interface that was filtered, rinsed with chloroform, and dried. The modified Matrimid® films were extremely brittle, even for thicknesses > 300 μm. A film was made by blending the original polymer with the reacted polymer at 25 wt% of the latter. The FTIR spectra for pure Matrimid® and the polymer blend are shown in Figure 4-6.

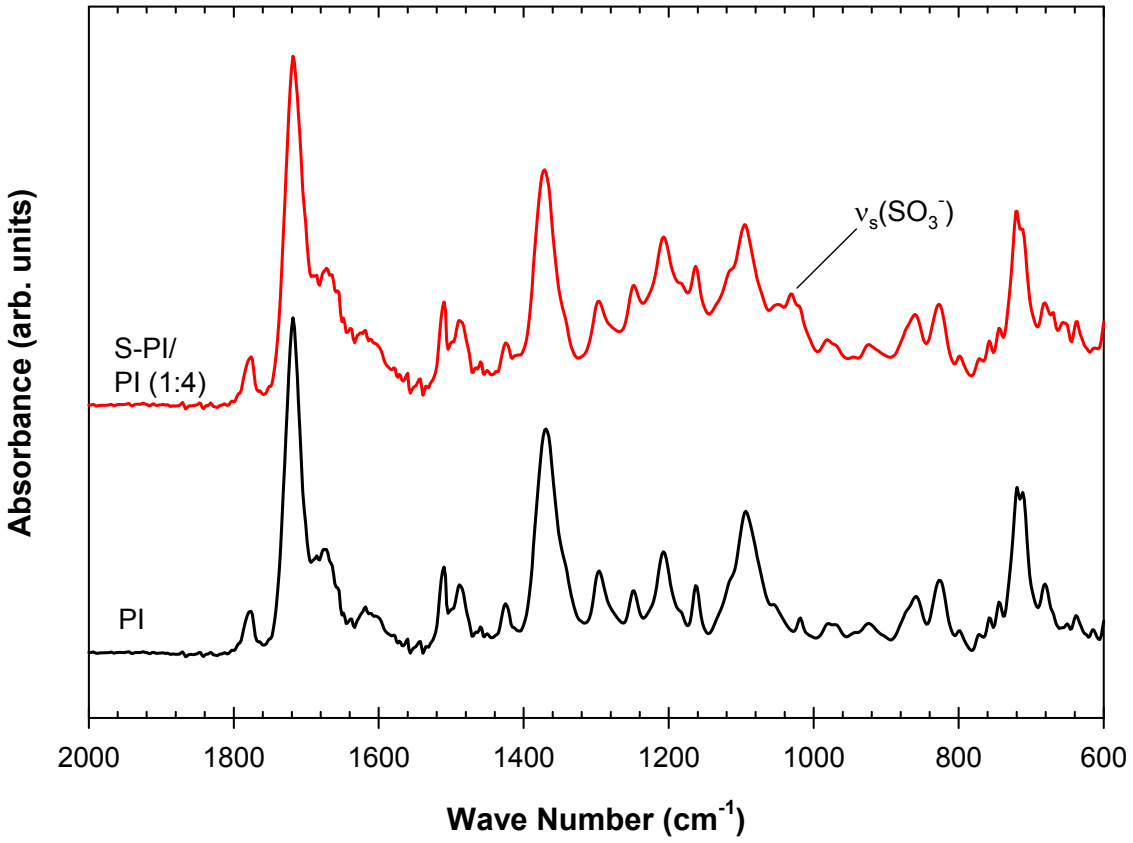

Figure 4-6: FTIR spectra of Matrimid® PI before and after reacting with fuming sulfuric acid.

As a result of the sulfuric acid treatment, a peak appears at 1030 cm^{-1}, which has been assigned to the symmetric stretching of the sulfonate group [84]. Therefore, fuming sulfuric acid treatment is an effective method of adding sulfonic acid groups to Matrimid®. As mentioned previously, typical sulfonation sites on a polymer are electron rich and stabilized through aromatic resonance. Based on the structure of the polymer repeat unit, the sulfonation site is mostly likely located on either of the two aromatic rings not associated with the diamine. Solid state NMR should be used to verify the site of aromatic sulfonation.

In both cases, the mechanical instability of the reacted polymers after solvent casting was an issue. For modified Ultem®, where no sulfonation could be detected with FTIR, the instability of the film was most likely due to excessive chain cleavage. For Matrimid®, chain cleavage was also likely, but studies have shown that increased sulfonation generally weakens a polymer's mechanical properties even when cleavage is minimized [14, 35, 85]. It is also possible that cross-linking occurred during the sulfonation reactions. These phenomena should be further investigated with gel permeation chromatography to evaluate possible cleavage, and differential scanning calorimetry to evaluate possible cross-linking.

For both modified products, the ionic conductivities of the polymer blends were less than < 1 mS/cm. This was expected for modified Ultem®, due the lack of sulfonic acid moieties shown by FTIR. For sulfonated Matrimid® the lack of ionic conductivity could possibly be explained by extensive phase separation between the sulfonated and unsulfoned PI components which was visible to the eye. This phase separation can lead to anisotropic water uptake, which has been previously suggested to reduce ionic transport [86]. To determine if increasing the concentration of S-PI would affect conductivity, a moderately stable polymer blend was made with 40 wt% of the modified component, but this film showed no improvements in ionic conductivity. Another possible

explanation for lack of conductive properties is that the sulfonated polymer phase leaches from the film during swelling due to its water solubility. While no optical changes were observed in the aqueous swelling solution, further chemical analysis, such as pH or ion chromatography, should be investigated for future experiments.

4.4.1.2. TMSCS Sulfonation

Ultem® PEI was selected for sulfonation with TMSCS since fuming sulfuric acid proved to be ineffective. The reacted solid was immiscible in methanol and water even after protonation. Films casted from the TMSCS product (~40 μm thick) were more mechanically stable than those films from fuming sulfuric but were still too fragile for handling. FTIR spectra were collected on a film made with pure S-PEI as well as a film made with 1:3 ratio of S-PEI to PEI (see Figure 4-7). The pure S-PEI product shows evidence of sulfonation with the appearance of bands at 1090 and 1160 cm^{-1}, and the broadening of the peak at 1025 cm^{-1}. These bands have been previously assigned to the asymmetric and symmetric stretching of the sulfonate group [79, 87]. The blended sample, however, shows no evidence of aromatic sulfonation, possibly due to phase separation between the sulfonated and unsulfonated polymers. The degree of phase separation needs to be evaluated with scanning electron microscopy to see if sulfonic acid aggregation appears beneath the surface of the film beyond the penetration depth of the ATR (on the order of 10^2 nm). Still, based on the ease of recovery of the reacted solid, it is believed that TMSCS is a good sulfonating agent for Ultem®, causing less chain cleavage and cross-linking than other post sulfonation methods.

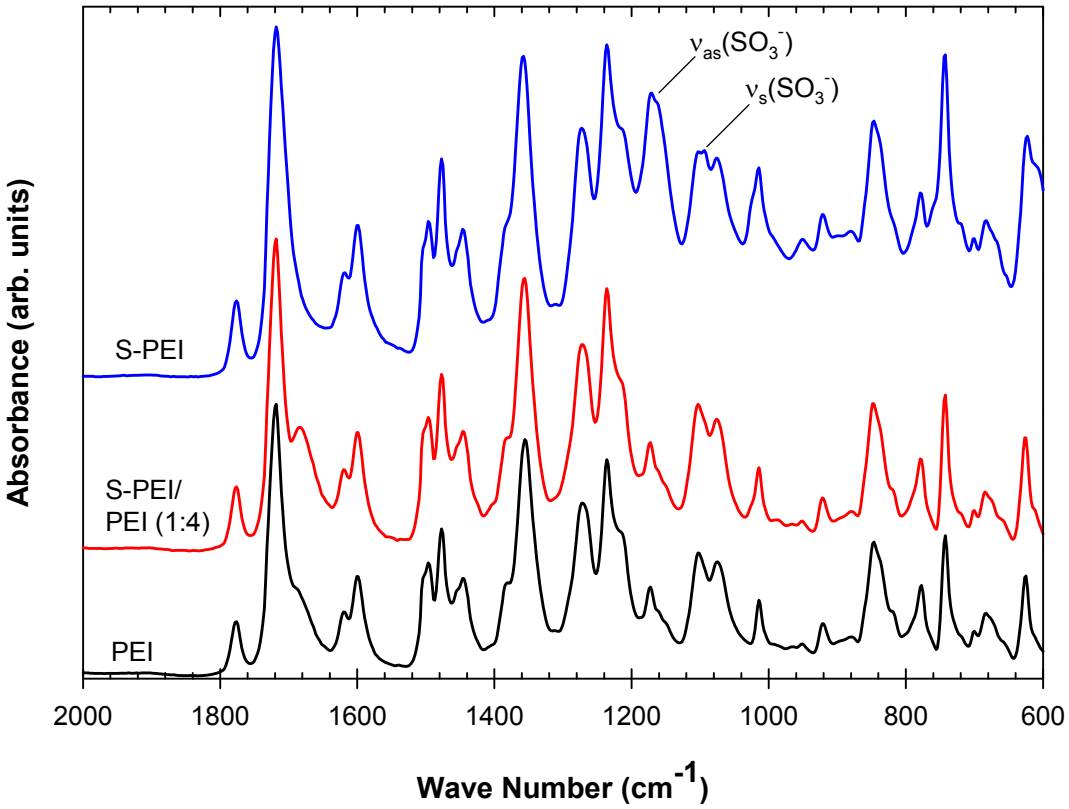

Figure 4-7: FTIR spectra of Ultem® PI before and after reacting with TMSCS.

The polymer blend and pure modified polymer films both displayed poor conductivity < 1 mS/cm. Low proton conductivity can be explained by possibility of insufficient protonation of the sulfonic acid groups during ion exchange with 1 M HCl. Since the reacted solids did not dissolve or swell in the aqueous acidic solution, it is possible that the heterogeneous mixture provided limited ion exchange between phases. To quantify the effectiveness of the protonation step in the future, the protonated solid should be converted back into a sodium salt in a concentrated solution of sodium chloride, which could then be titrated with base to determine the moles of neutralized protons. Other solvents can also be used for ionic exchange, such as NMP and dimethylacetamide, which both dissolve S-PEI. However the solvent interactions with proton-donating acids need to be evaluated. Poor ionic transport through the sulfonated films could also be explained by poor phase separation between hydrophobic and hydrophilic chain segments, which might prevent water uptake. Swelling experiments will need to be conducted to determine if these sulfonated or partially sulfonated films have an affinity for water. Finally, low conductivities for sulfonated amine-based polymers may be attributed to a strong interaction between protons and nitrogen atoms, which could significantly reduce proton mobility. This phenomenon has been suggested by other researchers who found that the conductivity of some S-PBI membranes were very low on the order of 10^{-1} mS/cm up to 66 % sulfonation [88]. Other researchers have also observed very low conductivity values for S-PBI membranes [89] at high sulfonation levels.

4.5. CONCLUSIONS

Electrophilic aromatic sulfonation provides a potentially cost-effective approach to converting low-cost, high performance polymers into PEMs to replace conventional PFSAs in fuel cells. A variety of sulfonated aromatic-based polymers and numerous sulfonation methods have been reviewed here. Two sulfonation procedures were used to evaluate the feasibility of electrochemically enhancing a commercially available PI and PEI. The fuming sulfuric acid method was effective in sulfonating Matrimid® PI, but the reacted polymer formed brittle films that were too fragile for further handling. Although many polymers have been observed to show reduced mechanical strength with an increase in the degree of sulfonation, degraded mechanical properties could be the result of a combination chain cleavage and sulfonate cross-linking. Ultem® PEI also showed poor mechanical stability after being reacted in fuming sulfuric acid, but this change was attributed to significant chain cleavage since the modified polymer dissolved easily in water and FTIR spectra showed no evidence of sulfonation in blended films. The results from Ultem® sulfonation with TMSCS were significantly better, with much improved mechanical stability and sulfonic acid addition as determined by FTIR. Due to the mild conditions of the reaction, TMSCS is the preferred sulfonation method for PEI. Still the proton conductivity of this polymer and all others were < 1 mS/cm. The low conductivity may be due to poor phase separation limiting the sulfonic acid pathways through films, or limited proton mobility due to possible sulfonic acid interactions with nitrogen groups. Although the work presented here is only a brief assessment of sulfonation strategies and potential PEMs, future detailed studies should include additional characterization methods to better understand the effects of the sulfonation on PEM performance.

4.6. REFERENCES

1. Rikukawa, M. and K. Sanui, *Proton-conducting polymer electrolyte membranes based on hydrocarbon polymers.* Progress in Polymer Science, 2000. **25**(10): p. 1463-1502.

2. *Encyclopedia of energy engineering and technology*, ed. B.L. Capehart. 2007, Boca Raton, FL: CRC Press.

3. Ahluwalia, R.K. and X. Wang, *Fuel cell systems for transportation: Status and trends.* Journal of Power Sources, 2008. **177**(1): p. 167-176.

4. Tang, H., et al., *A degradation study of Nafion proton exchange membrane of PEM fuel cells.* Journal of Power Sources, 2007. **170**(1): p. 85-92.

5. Gao, Y., et al., *Sulfonation of poly(phthalazinones) with fuming sulfuric acid mixtures for proton exchange membrane materials.* Journal of Membrane Science, 2003. **227**(1-2): p. 39-50.

6. Hickner, M.A., et al., *Alternative Polymer Systems for Proton Exchange Membranes (PEMs).* Chemical Reviews, 2004. **104**(10): p. 4587-4612.

7. Thampan, T.M., et al., *Systematic Approach to Design Higher Temperature Composite PEMs.* Journal of The Electrochemical Society, 2005. **152**(2): p. A316-A325.

8. Nouel, K.M. and P.S. Fedkiw, *Nafion®-based composite polymer electrolyte membranes.* Electrochimica Acta, 1998. **43**(16-17): p. 2381-2387.

9. Liu, W., K. Ruth, and G. Rusch, *Membrane durability in PEM fuel cells.* Journal of New Materials for Materials for Electrochemical Systems 2001. **4**: p. 227-231.

10. Rajendran, R.G., *Polymer electrolyte membrane technology for fuel cells.* MRS Bulletin, 2005. **30**: p. 587–590.

11. Wnek, G.E. and S.G. Ehrenberg. *Water- and ion-conducting membranes and uses thereof*. 2002. USPTO# 6413298.

12. Gupta, B., et al., *Materials research aspects of organic solid proton conductors.* Solid State Ionics, 1993. **61**(1-3): p. 213-218.

13. Weiss, R.A., et al., *Block copolymer ionomers: 1. Synthesis and physical properties of sulphonated poly(styrene-ethylene/butylene-styrene).* Polymer, 1991. **32**(10): p. 1867-1874.

14. Chen, S.-L., et al., *Ion exchange resin/polystyrene sulfonate composite membranes for PEM fuel cells.* Journal of Membrane Science, 2004. **243**(1-2): p. 327-333.

15. Li, Q., et al., *Approaches and Recent Development of Polymer Electrolyte Membranes for Fuel Cells Operating above 100 ^{o}C.* Chemistry of Materials, 2003. **15**(26): p. 4896-4915.

16. Xu, T., D. Wu, and L. Wu, *Poly(2,6-dimethyl-1,4-phenylene oxide) (PPO)--A versatile starting polymer for proton conductive membranes (PCMs).* Progress in Polymer Science, 2008. **33**(9): p. 894-915.

17. Rozière, J. and D.J. Jones, *NON-FLUORINATED POLYMER MATERIALS FOR PROTON EXCHANGE MEMBRANE FUEL CELLS.* Annual Review of Materials Research, 2003. **33**(1): p. 503-555.

18. Bae, J.M., et al., *Properties of selected sulfonated polymers as proton-conducting electrolytes for polymer electrolyte fuel cells.* Solid State Ionics, 2002. **147**(1-2): p. 189-194.

19. Rusanov, A.L., et al., *Preparation and Characterization of Sulfonated Polyphenylquinoxalines.* High Performance Polymers, 2008. **20**(6): p. 627-641.

20. Kopitzke, R.W., et al., *Conductivity and Water Uptake of Aromatic-Based Proton Exchange Membrane Electrolytes.* Journal of the Electrochemical Society, 2000. **147**(5): p. 1677-1681.

21. Maier, G. and J. Meier-Haack, *Sulfonated Aromatic Polymers for Fuel Cell Membranes*, in *Fuel Cells II*. 2008. p. 1-62.

22. Huang, R.Y.M., et al., *Sulfonation of poly(ether ether ketone)(PEEK): Kinetic study and characterization.* Journal of Applied Polymer Science, 2001. **82**(11): p. 2651-2660.

23. Zhang, L. and S. Mukerjee, *Investigation of Durability Issues of Selected Nonfluorinated Proton Exchange Membranes for Fuel Cell Application.* Journal of The Electrochemical Society, 2006. **153**(6): p. A1062-A1072.

24. Gil, M., et al., *Direct synthesis of sulfonated aromatic poly(ether ether ketone) proton exchange membranes for fuel cell applications.* Journal of Membrane Science, 2004. **234**(1-2): p. 75-81.

25. Ye, Y.-S., et al., *Sulfonated poly(ether ether ketone) membranes crosslinked with sulfonic acid containing benzoxazine monomer as proton exchange membranes.* Polymer, 2009. **50**(14): p. 3196-3203.

26. Zhong, S., et al., *Crosslinked sulfonated poly(ether ether ketone) proton exchange membranes for direct methanol fuel cell applications.* Journal of Power Sources, 2007. **164**(1): p. 65-72.

27. Linkous, C.A., et al. *Water Uptake and Conductivity of Cross-linked SPEEK Membranes*. in *214th ECS Meeting*. 2008. Honolulu, HI: The Electrochemical Society.

28. Colicchio, I., et al., *Development of Hybrid Polymer Electrolyte Membranes Based on the Semi-Interpenetrating Network Concept.* Fuel Cells, 2006. **6**(3-4): p. 225-236.

29. Wang, F., et al., *Direct polymerization of sulfonated poly(arylene ether sulfone) random (statistical) copolymers: candidates for new proton exchange membranes.* Journal of Membrane Science, 2002. **197**(1-2): p. 231-242.

30. Dyck, A., D. Fritsch, and S.P. Nunes, *Proton-conductive membranes of sulfonated polyphenylsulfone.* Journal of Applied Polymer Science, 2002. **86**(11): p. 2820-2827.

31. Lufrano, F., et al., *Sulfonated polysulfone ionomer membranes for fuel cells.* Solid State Ionics, 2001. **145**(1-4): p. 47-51.

32. Lufrano, F., et al., *Sulfonated polysulfone as promising membranes for polymer electrolyte fuel cells.* Journal of Applied Polymer Science, 2000. **77**(6): p. 1250-1256.

33. Lafitte, B. and P. Jannasch, *Phosphonation of polysulfones via lithiation and reaction with chlorophosphonic acid esters.* Journal of Polymer Science Part A: Polymer Chemistry, 2005. **43**(2): p. 273-286.

34. Naim, R., et al. *Development of sulfonated polysulfone membranes as a material for Proton Exchange Membrane (PEM)*. in *Proceedings of Regional Symposium on Membrane Science and Technology 2004, 21-25 April 2004, Puteri Pan Pacific Hotel, Johor Bharu, Malaysia*. 2004. Johor Bharu, Malaysia.

35. Genova-Dimitrova, P., et al., *Ionomeric membranes for proton exchange membrane fuel cell (PEMFC): sulfonated polysulfone associated with phosphatoantimonic acid.* Journal of Membrane Science, 2001. **185**(1): p. 59-71.

36. Kerres, J., W. Cui, and S. Reichle, *New sulfonated engineering polymers via the metalation route. I. Sulfonated poly(ethersulfone) PSU Udel® via metalation-sulfination-oxidation.* Journal of Polymer Science Part A: Polymer Chemistry, 1996. **34**(12): p. 2421-2438.

37. Matsumoto, Y., M. Sudoh, and Y. Suzuki, *Preparation of composite UF membranes of sulfonated polysulfone coated on ceramics.* Journal of Membrane Science, 1999. **158**(1-2): p. 55-62.

38. Kim, Y.S., et al., *Fabrication and characterization of heteropolyacid (H3PW12O40)/directly polymerized sulfonated poly(arylene ether sulfone) copolymer composite membranes for higher temperature fuel cell applications.* Journal of Membrane Science, 2003. **212**(1-2): p. 263-282.

39. Shahi, V.K., *Highly charged proton-exchange membrane: Sulfonated poly(ether sulfone)-silica polyelectrolyte composite membranes for fuel cells.* Solid State Ionics, 2007. **177**(39-40): p. 3395-3404.

40. Faure, S., et al. *Sulfonated polyimides as novel proton exchange membranes for H2/O2 fuel cells*. in *Proceedings of Second International Symposium on New Materials for Fuel Cell and Modern Battery Systems*. 1997. Montreal, Canada.

41. Meyer, G., et al., *Degradation of sulfonated polyimide membranes in fuel cell conditions* Journal of Power Sources, 2006. **157**(1): p. 293-301

42. Watari, T., et al., *Synthesis, water stability and proton conductivity of novel sulfonated polyimides from 4,4'-bis(4-aminophenoxy)biphenyl-3,3'-disulfonic acid.* Journal of Membrane Science, 2004. **230**(1-2): p. 111-120.

43. Jeon, J.-Y. and B.-S. Shim, *Preparation of sulfonated novel poly(bis[4-(3-aminophenoxy) phenyl]sulfone pyromellite)imide derivatives by heterogeneous sulfonation.* Journal of Applied Polymer Science, 2002. **85**(9): p. 1881-1887.

44. Guo, X., et al., *Novel Sulfonated Polyimides as Polyelectrolytes for Fuel Cell Application. 2. Synthesis and Proton Conductivity of Polyimides from 9,9-Bis(4-aminophenyl)fluorene-2,7-disulfonic Acid.* Macromolecules, 2002. **35**(17): p. 6707-6713.

45. Genies, C., et al., *Soluble sulfonated naphthalenic polyimides as materials for proton exchange membranes.* Polymer, 2001. **42**(2): p. 359-373.

46. Fang, J., et al., *Novel Sulfonated Polyimides as Polyelectrolytes for Fuel Cell Application. 1. Synthesis, Proton Conductivity, and Water Stability of Polyimides from 4,4-Diaminodiphenyl Ether-2,2-disulfonic Acid.* Macromolecules, 2002. **35**(24): p. 9022-9028.

47. Okamoto, K.-i., *Sulfonated Polyimides for Polymer Electrolyte Membrane Fuel Cell.* Journal of Photopolymer Science and Technology, 2003. **16**(2): p. 247-254.

48. Einsla, B.R., et al., *Sulfonated naphthalene dianhydride based polyimide copolymers for proton-exchange-membrane fuel cells: II. Membrane properties and fuel cell performance.* Journal of Membrane Science, 2005. **255**(1-2): p. 141-148.

49. Essafi, W., G. Gebel, and R. Mercier, *Sulfonated Polyimide Ionomers: A Structural Study.* Macromolecules, 2003. **37**(4): p. 1431-1440.

50. Zhang, J., et al., *Polybenzimidazole-membrane-based PEM fuel cell in the temperature range of 120-200 °C.* Journal of Power Sources, 2007. **172**(1): p. 163-171.

51. Asensio, J.A., S. Borrós, and P. Gómez-Romero, *Enhanced conductivity in polyanion-containing polybenzimidazoles. Improved materials for proton-exchange membranes and PEM fuel cells.* Electrochemistry Communications, 2003. **5**(11): p. 967-972.

52. Ma, Y.L., et al., *Conductivity of PBI Membranes for High-Temperature Polymer Electrolyte Fuel Cells.* Journal of The Electrochemical Society, 2004. **151**(1): p. A8-A16.

53. Seland, F., et al., *Improving the performance of high-temperature PEM fuel cells based on PBI electrolyte.* Journal of Power Sources, 2006. **160**(1): p. 27-36.

54. Kerres, J., et al., *Preparation, characterization, and fuel cell application of new acid-base blend membranes.* Journal of New Materials for Electrochemical Systems, 2000. **3**(3): p. 229-240.

55. Hamaya, T., et al., *Novel proton-conducting polymer electrolyte membranes based on PVA/PAMPS/PEG400 blend* Journal of Power Sources, 2006. **156**(2): p. 311-314.

56. Lipatov, Y. and T. Alekseeva, *Phase-Separated Interpenetrating Polymer Networks*, in *Phase-Separated Interpenetrating Polymer Networks*. 2007. p. 1-227.

57. Neburchilov, V., et al., *A review of polymer electrolyte membranes for direct methanol fuel cells.* Journal of Power Sources, 2007. **169**(2): p. 221-238.

58. Hwang, G.-J., H. Ohya, and T. Nagai, *Ion exchange membrane based on block copolymers. Part III: preparation of cation exchange membrane.* Journal of Membrane Science, 1999. **156**(1): p. 61-65.

59. Saimani, S. and A. Kumar, *Semi-IPN asymmetric membranes based on polyether imide (ULTEM) and polyethylene glycol diacrylate for gaseous separation.* Journal of Applied Polymer Science, 2008. **110**(6): p. 3606-3615.

60. Kreuer, K.D., *On the development of proton conducting polymer membranes for hydrogen and methanol fuel cells.* Journal of Membrane Science, 2001. **185**(1): p. 29-39.

61. Manea, C. and M. Mulder, *Characterization of polymer blends of polyethersulfone/sulfonated polysulfone and polyethersulfone/sulfonated polyetheretherketone for direct methanol fuel cell applications.* Journal of Membrane Science, 2002. **206**(1-2): p. 443-453.

62. McGrath, J.E., et al. *Ion-conducting sulfonated polymeric materials invention*. 2008. USPTO# 20080275146.

63. Shibuya, N. and R.S. Porter, *Kinetics of PEEK sulfonation in concentrated sulfuric acid.* Macromolecules, 2002. **25**(24): p. 6495-6499.

64. Cerfontain, H., *Mechanistic aspects in aromatic sulfonation and desulfonation*. Interscience monographs on organic chemistry., New York, Interscience Publishers [1968].

65. Daoust, D., J. Devaux, and P. Godard, *Mechanism and kinetics of poly(ether ether ketone) (PEEK) sulfonation in concentrated sulfuric acid at room temperature Part 1. Qualitative comparison between polymer and monomer model compound sulfonation.* Polymer International, 2001. **50**(8): p. 917-924.

66. Wang, F., T. Chen, and J. Xu, *Sodium sulfonate-functionalized poly(ether ether ketone)s.* Macromolecular Chemistry and Physics, 1998. **199**(7): p. 1421-1426.

67. Marestin, C., et al., *Sulfonated Polyimides*, in *Fuel Cells II*. 2008. p. 185-258.

68. Trotta, F., et al., *Sulfonation of polyetheretherketone by chlorosulfuric acid.* Journal of Applied Polymer Science, 1998. **70**(3): p. 477-482.

69. Linkous, C.A., et al., *Development of new proton exchange membrane electrolytes for water electrolysis at higher temperatures.* International Journal of Hydrogen Energy, 1998. **23**(7): p. 525-529.

70. Iojoiu, C., et al., *Mastering Sulfonation of Aromatic Polysulfones: Crucial for Membranes for Fuel Cell Application.* Fuel Cells, 2005. **5**(3): p. 344-354.

71. Bailly, C., et al., *The sodium salts of sulphonated poly(aryl-ether-ether-ketone) (PEEK): Preparation and characterization.* Polymer, 1987. **28**(6): p. 1009-1016.

72. Noshay, A. and L.M. Robeson, *Sulfonated polysulfone.* Journal of Applied Polymer Science, 1976. **20**(7): p. 1885-1903.

73. Johnson, B.C., et al., *Synthesis and characterization of sulfonated poly(acrylene ether sulfones).* Journal of Polymer Science: Polymer Chemistry Edition, 1984. **22**(3): p. 721-737.

74. Aparicio, M., et al., *Synthesis and characterization of proton-conducting sol-gel membranes produced from 1,4-bis(triethoxysilyl)benzene and (3-glycidoxypropyl)trimethoxysilane.* Journal of Power Sources, 2005. **151**: p. 57-62.

75. Holmberg, B.A. and Y. Yan, *An Apparatus for Direct Proton Conductivity Measurement of Powdered Materials.* Journal of The Electrochemical Society, 2006. **153**(1): p. A146-A149.

76. Mikhailenko, S.D., S.M.J. Zaidi, and S. Kaliaguine, *Electrical properties of sulfonated polyether ether ketone/polyetherimide blend membranes doped with inorganic acids.* Journal of Polymer Science Part B: Polymer Physics, 2000. **38**(10): p. 1386-1395.

77. Liang, Y.F., et al., *Studies on synthesis and property of novel acid-base proton exchange membranes.* Chinese Chemical Letters, 2007. **18**(5): p. 609-612.

78. Zhu, X., et al., *Synthesis and properties of novel H-bonded composite membranes from sulfonated poly(phthalazinone ether)s for PEMFC.* Journal of Membrane Science, 2008. **312**(1-2): p. 59-65.

79. Guhathakurta, S. and K. Min, *Influence of crystal morphology of 1H-1,2,4-triazole on anhydrous state proton conductivity of sulfonated bisphenol A polyetherimide based polyelectrolytes.* Polymer, 2009. **50**(4): p. 1034-1045.

80. Chao, H.S. and D.R. Kelsey. *Poly(aryl ether) resins having repeat units of the structure*. 1986. USPTO# 4625000.

81. Zapata, P., P. Basak, and J. Carson Meredith, *High-throughput screening of ionic conductivity in polymer membranes.* Electrochimica Acta, 2009. **54**(15): p. 3899-3909.

82. Straus, A.E., et al. *Foam well cleanout using oligomeric sulfonates*. 1976. USPTO#

83. Porter, M.R., *Handbook of surfactants*. 1994, Glasgow; New York: Blackie ; Chapman and Hall.

84. Lee, W.-J., Y.-J. Kim, and S. Kaang, *Electrical properties of polyaniline/sulfonated polycarbonate blends.* Synthetic Metals, 2000. **113**(3): p. 237-243.

85. Guan, R., et al., *Development and characterization of homogeneous membranes prepared from sulfonated poly(phenylene oxide).* Journal of Applied Polymer Science, 2005. **98**(3): p. 1244-1250.

86. Santiago, E.I., et al., *Nafion-TiO2 hybrid electrolytes for stable operation of PEM fuel cells at high temperature.* Electrochimica Acta, 2009. **54**(16): p. 4111-4117.

87. Guhathakurta, S. and K. Min. *Post Sulfonation of Bisphenol A Polyetherimide*. in *Proceedings of the ACS Division of Polymeric Materials: Science & Engineering*. 2008. New Orleans, LA: American Chemical Society.

88. Staiti, P., et al., *Sulfonated polybenzimidazole membranes -- preparation and physico-chemical characterization.* Journal of Membrane Science, 2001. **188**(1): p. 71-78.

89. Ariza, M.J., D.J. Jones, and J. Rozière, *Role of post-sulfonation thermal treatment in conducting and thermal properties of sulfuric acid sulfonated poly(benzimidazole) membranes.* Desalination, 2002. **147**(1-3): p. 183-189.

Chapter 5
Synthesis and Characterization of Polymer Blends from Poly(ether imide) and Sulfonated Poly(ether imide)

Reproduced with permission from Keith Reed, JH Lee, and J.C. Meredith
Unpublished work (*to be submitted for publication*)

The increasing focus on proton exchange membrane fuel cells (PEMFCs) for potential automotive applications has brought about a significant research effort for developing highly functional but low cost polymeric materials to replace the state-of-the-art perfluorosulfonic acid (PFSA) membranes currently used in PEMFCs. One approach to achieving this goal is to modify commercially available, high-performance, hydrocarbon polymers using a simple post sulfonation reaction to add proton-conducting groups to the activated aromatic rings of the polymer backbone. This study investigates the use of trimethylsilyl chlorosulfonate (TMSCS) as a sulfonating agent to functionalize a commercially-available polyetherimide (PEI), an amorphous thermoplastic currently used in a broad range of high temperature applications. We have attempted to achieve balanced electrochemical and mechanical properties by optimizing polymer blends of PEI with highly sulfonated PEI (S-PEI). Films were characterized for blend compatibility, annealing effects, and performance properties using a combination of characterization techniques including scanning electron microscopy, water uptake, and high-throughput mechanical and conductivity testing. While the overall performance properties were less

than those of comparable PFSAs, the PEI/S-PEI combination did display optimal mechanical and electrochemical characteristics between 20 and 30 % S-PEI, thus demonstrating the potential for using post-sulfonation and polymer blending with lower-cost, high-performance polymers to develop novel membrane systems.

5.1. INTRODUCTION

If PEMFCs are to be commercially successful as automotive power sources in the near future, they will need to demonstrate high performance over a broad range of operating temperatures. Unfortunately, the conventional PFSA polymers currently used as PEMs are severely limited in performance at operating temperatures above 80 °C. These limitations have stimulated a variety of approaches in developing alternative PEM materials. One strategy that many researchers are currently investigating is the use of aromatic electrophilic substitution to add proton conducting sulfonic acid groups to low cost, high-performance polymers. This method has been used to produce a number of materials that show promising performance characteristics over conventional PFSAs [1-10]. While a higher degree of sulfonation offers improved ionic conductivity, it also deteriorates mechanical properties with excess water, which results in poor long-term performance. To balance and optimize electrochemical properties and mechanical stability, one can vary the degree of sulfonation by tuning sulfonation reaction variables such as the choice of sulfonating agent, the reaction temperature, and the reaction time. Unfortunately, identifying the relationships among these variables can be a difficult task, further complicated by the need to minimize sulfonation side reactions such as polymer chain cleavage and cross-linking [1].

As an alternative to managing sulfonation reactions directly, highly sulfonated ion conductive polymers can be incorporated into polymer blends with unmodified high-

performance polymers for improved mechanical stability. Polymer blending is an economical approach to combining the favorable properties of multiple polymers into a single system. By adjusting relative compositions, blended materials can be optimized for fuel cell performance without extensive synthetic procedures. Numerous studies have reported the use of polymer blending with sulfonated components to produce new PEMs. These blends include the combination of sulfonated polymers such as sulfonated poly(ether ether ketone) (S-PEEK), sulfonated polysulfone (S-PSU), and sulfonated poly(phenylene oxide) (S-PPO) with materials such as poly(ether sulfone) (PES), polysulfone (PSU), poly(ether imide) (PEI), polyamine (PA) and polybenzimidazole (PBI) [2-8]. Although, many promising polymer combinations have been derived for fuel cell applications, none have surpassed the performance of conventional PFSAs. However, there are still an enormous variety of polymer blend combinations that have yet to be explored.

One critical aspect to polymer blending is the compatibility of each component. Solubility of polymer components in the solution phase is critical and can be adjusted with the proper choice of solvent. In the solid state, achieving a precise degree of nanoscale phase separation (<100 nm) is especially important so that sulfonated groups are able to organize into ion conducting domains for proton transport [9]. However, microphase separation (>500 nm) can lead to anisotropic swelling, poor mechanical properties, and poor electrochemical performance [10]. To control and limit phase separation in polymer blends and maintain solution miscibility, we have investigated the compatibility and functionality of chemically similar polymer blends consisting of PEI and S-PEI. The sulfonating agent used to functionalize PEI was trimethylsilyl chlorosulfonate (TMSCS), which provides a mild reaction environment with minimal side-reactions [11]. The TMSCS sulfonation reaction also produces a trimethylsilyl-capped intermediate, which keeps the functionalized polymer in the reaction phase and may improve blend

miscibility and interfacial interaction with the non-functionalized component. We have also explored the use of thermal annealing above the glass transition temperature (T_g) of PEI, which is approximately 215 °C [2], in order to adjust the degree of phase separation and resulting morphology of the cast blends [12, 13]. Annealing is often important in solvent-cast PEIs to improve chemical, thermal, and mechanical stability via densification of the polymer chains and relaxation of non-equilibrium structures [14].

5.2. EXPERIMENTAL

5.2.1. Materials

Ultem®1000 PEI was supplied by SABIC. TMSCS (99 % purity), dichloroethane (DCE, anhydrous and ACS reagent grade), and sulfuric acid (puriss. p.a., 95-97 %) were all supplied by Sigma-Aldrich. N-methyl-2-pyrrolidinone (NMP, production grade), phenolphthalein (1 %) and sodium hydroxide (ACS reagent grade) were obtained from VWR Scientific. TMSCS and anhydrous dichloroethane were stored in a nitrogen glove box to prevent water contamination.

5.2.2. Sulfonation Reactions

A detailed procedure for TMSCS aromatic substitution has been previously reported for poly(ether ketone) and polysulfone derivatives [15], and has been adapted for use in this work. PEI granules were dried overnight at 120 °C, after which they were dissolved in DCE at a concentration of 30 wt% under argon. A separate solution of 30 wt% TMSCS in anhydrous DCE was added to an addition funnel in the glove box and sealed under nitrogen before removing. Both solutions were made according to a mole ratio of 1.1:1, TMSCS to the PEI repeat unit. The reaction vessel, continuously purged with argon, was charged with the PEI solution and fitted with the TMSCS addition funnel, a mechanical stirrer, and an acid trap containing 1 M aqueous sodium hydroxide. The

TMSCS solution was added dropwise over a period of 1 h and the reaction was carried out for 5 days at room temperature. The product mixture was coagulated in excess deionized water, and allowed to soak in deionized water for 48 hrs before filtering. The trimethylsilyl substituted PEI was dried under vacuum at 50 °C for 3 days to remove water from the modified polymer.

5.2.3. Membrane Fabrication

5.2.3.1. Film Casting, Protonation, and Thermal Annealing

All pure and polymer blend solutions were made with 20 wt% solids in NMP and S-PEI dry weight fractions ranging from 10 to 60 %. Solutions were mixed for 2 days at room temperature, followed by sonication for 3 hrs at 50 °C, then additional mixing for 24 h. Films were casted on untreated glass plates at room temperature using a bird-type film applicator. Since water absorbs quickly into the solvent under atmospheric conditions and can lead to heterogeneous membrane morphologies, casted films were immediately dried under vacuum at 60 °C for 48 h to remove solvent. Films detached naturally from their glass substrates under ambient conditions. The free standing polymer samples were soaked in deionized water at 60 °C for 2 h to remove any residual solvent. In order replace trimethylsilyl groups with protons, films were immersed in 0.5 M H_2SO_4 for 2 h at 60 °C. Samples were rinsed thoroughly with deioniized water until a neutral pH was achieved, then stored in deionized water for characterization. A sample from each protonated film was thermally annealed for 3 days at 230 °C under vacuum, and then allowed to cool to room temperature overnight under vacuum.

As references for imaging purposes, two additional films were casted with S-PEI that was protonated prior to being dissolved in NMP solutions. The S-PEI solid was converted to its acid form using the same protonation procedure described above; with additional deionized water rinsing and vacuum drying at 40 °C to remove water. The film casting and drying procedures were also the same for these blends.

5.2.4. Membrane Characterization

5.2.4.1. Ion Exchange Capcaity and Degree of Sulfonation

The degree of sulfonation was determined by titration. A sample of the protonated film with 100 wt% S-PEI was dried overnight under vacuum at 50 °C to remove all water before weighing. The sample was deprotonated in an aqueous solution of concentrated NaCl with phenolphthalein at 60 °C for 2 h. The solution was then titrated with an aqueous solution of 0.0635 M NaOH until equilibrated. The ion exchange capacity (IEC) is expressed as milliequivalents of sulfonic groups per gram of dry polymer. The degree of sulfonation is expressed as the moles of sulfonic acid groups per moles of polymer repeat units using a 100 % sulfonated mass basis.

5.2.4.2. Fourier Transform Infrared (FTIR) Analysis

FTIR spectra were collected using a VERTEX 80v and a Hyperion 3000 Microscope with an attenuated total reflectance (ATR) attachment (Bruker Optics). Spectra were take at room temperature and pressure with 64 scans at a resolution of 4 cm^{-1}. An air background was subtracted from all measurements.

5.2.4.3. Scanning Electron Microscopy (SEM)

High resolution images of blended films were obtained using a LEO 1530 thermally-assisted field emission scanning electron microscope (SEM), operated at 10keV. Samples were cryogenically broken in liquid nitrogen and metalized using gold or copper sputtering prior to imaging.

5.2.4.4. Conductivity

Proton conductivity measurements were performed with electrochemical impedance spectroscopy (EIS) using a customized, fully automated, high-throughput conductivity (HTC) measurement device, described in detail elsewhere [16]. Swollen film samples were placed in a well-like, electrically insulating sample holder and held in place with a grid-like retention mechanism. The sample holder was filled with enough

deionized water at room temperature to completely cover films and prevent dehydration. Before measuring conductivity, localized thickness measurements were taken using an Omega GP901-2 linear displacement digital gauging probe with a flat-tip, 0.12 μm resolution, and low spring constant to reduce sample compression (Omega Engineering, Inc.). To measure conductivity, the hydrated membrane was excited with an alternating current (AC) signal from the outer point-electrodes of a commercially available, tungsten carbide 4-point probe head (Jandel Engineering Ltd.). The response voltage from this AC excitation was measured with the inner point-electrodes, allowing for the calculation of complex impedance. Since electrodes are equally spaced apart, proton conductivity was estimated from complex impedance using the following simplified model:

$$\sigma \approx \frac{1}{Z}\frac{\ln(2)}{\pi h} \qquad \textbf{Equation 5-1}$$

where σ is the membrane proton conductivity, Z is the membrane's complex impedance, and h is the membrane thickness. All proton conductivity measurements were determined at room temperature with an excitation signal of 1 kHz and averaged over a 15 s stabilization time period.

5.2.4.5. High-Throughput Mechanical Tests

Polymer blends were characterized for mechanical strength in the wet and dry state using a custom, fully automated, high-throughput mechanical testing apparatus (HTMECH). A detailed description of HTMECH is described elsewhere [17] and a basic overview of the instrument is given here. Samples were mounted between two steel plates perforated with a 10 x 10 grid of holes that are 3.00 mm in diameter. The sample holder is affixed to a linear motor that moves along the z-axis. At the base of the instrument is a hemispherical-tip needle (1.00 mm in diameter) connected to a force-sensitive load cell that moves along the x and y-axis. After the needle was positioned below the desired sample location on the grid, the holder was brought down to the

needle at a velocity of 10 mm/s. Sample indentation generates a force vs. time profile that describes the evolution of axisymmetric biaxial deformation and failure. Analysis of this profile was performed using a customized algorithm that allows for the assessment of properties such as tensile strength, ultimate elongation, and toughness. All mechanical characterization tests were performed under ambient conditions.

5.2.4.6. Water Uptake

Dried samples were weighed prior to being immersed in deionized water overnight at 60 °C. After cooling to room temperature, swollen films were lightly blotted with to remove excess water before quickly measuring mass again. Fractional water uptake was calculated using the wet and dry masses, according to the following equation:

$$q_m = \frac{m_{wet} - m_{dry}}{m_{dry}} \qquad \textbf{Equation 5-2}$$

where q_m is fractional water uptake, and m is the film mass.

5.3. RESULTS AND DISCUSSION

5.3.1. PEI Sulfonation and Membrane Fabrication

The PEI product formed a continuous, stable solid once coagulated in deionized water. It also displayed a noticeable affinity to water as observed by the transition from flexible polymer to a brittle powder after drying. The dried product was added to numerous solvents to test for solubility changes as a result of the TMSCS reaction. It was observed that the modified polymer was no longer soluble in chloroform, but dissolved easily in tetrahydrofuran (THF), which is not a good solvent for PEI. The modified polymer's miscibility in THF increased with the addition of small amounts of water, which was evident by the change in the solution's optical properties from hazy

and white to clear. The changes in solvent miscibility and the enhancement of solid's solubility in THF with water addition suggest that PEI was successfully functionalized with TMSCS. Titration of the sulfonated solid provided an IEC of 1.43 meq/g and a degree of sulfonation equal to 96 %.

The modified polymer was casted from a solution with NMP to form a mechanically unstable film with a thickness over 1 mm. The FTIR spectrum for the sulfonated PEI capped with trimethylsilyl groups is shown in Figure 5-1, along with the original, unmodified polymer. New absorbance peaks appeared at 1090 and 1020 cm^{-1}, indicating the addition of sulfonate groups to the polymer backbone [7, 18-20]. Another new group of bands appeared in the wavelength range of 1630 to 1690 cm^{-1}. These bands may be related to the trimethylsilyl capping group since they disappear after protonation, as discussed later. Since TMSCS does not show any vibrational bands in the range 1630 to 1690 cm^{-1}, the peaks may have been the result of trimethylsilyl interactions with other groups on the PEI backbone such as amines or carbonyls.

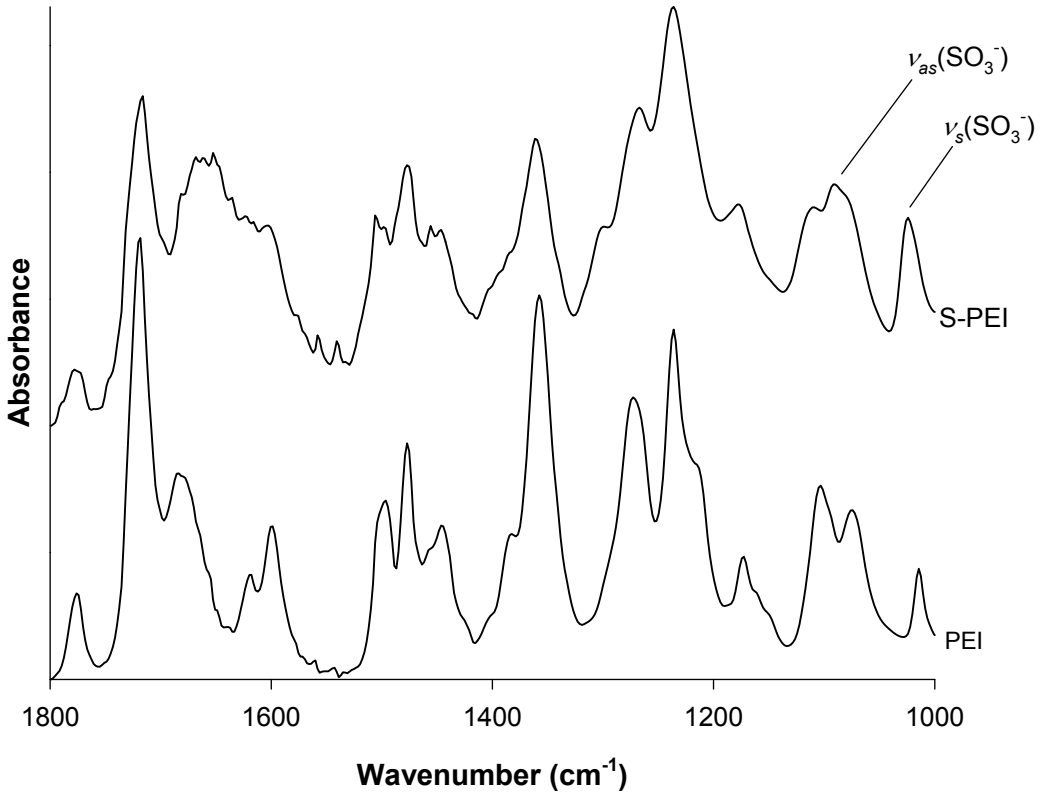

Figure 5-1: FTIR spectra of PEI and the modified PEI product from the sulfonation reaction with TMSCS.

Polymer solutions containing both PEI and trimethylsilyl-capped S-PEI in NMP were homogenous and clear only up to 30 % S-PEI by dry mass. Beyond that composition, the solutions separated into two visibly distinct liquid phases, an S-PEI-rich phase and a more viscous PEI-rich phase. The heterogeneous solutions were heated to 60 °C and sonicated for an extra 24 h, but settled into their original state after 1 h at room temperature. Additional solutions were made with solid mass fractions 30 and 50 % S-PEI using S-PEI solids that were protonated with dilute sulfuric acid prior to mixing. The solution with the solid composition of 30 % S-PEI was clear, but the solution with 50 % S-PEI contained a noticeable amount of solids that would not dissolve after extended sonication for 48 h. Therefore, the trimethylsilyl group did enhance the solubility of S-PEI in NMP in the blend solution.

It was also observed that a solution of 20 wt% pure S-PEI in NMP was less viscous than a solution of PEI with the same concentration, suggesting a possible loss in molecular weight from of chain scissions during the TMSCS sulfonation reaction [21, 22]. However, the change in viscosity may be directly related to the presence of functional groups on the S-PEI backbone. While numerous studies have shown that the viscosity of directly sulfonated polymers increases with the degree of sulfonation and IEC [22-24], another study has shown that viscosity of directly sulfonated polymers can be lower than their unsulfonated counterparts if completely saturated with sulfonic acid groups [25]. Furthermore, it is well known that the hydrodynamic behavior of polyelectrolytes are completely different from that of non-ionic polymers since chain conformations vary based on intramolecular interactions and chain-to-chain interactions [21]. Therefore, gel permeation chromatography (GPC) may be a more suitable approach for determining the extent of chain cleavage in completely sulfonated polymers. However, this characterization technique is limited by the solubility of both the sulfonated and unsulfonated polymers in a common GPC eluent.

Solvent-cast blend films were visibly homogeneous but opaque at 10 and 20 % S-PEI, despite the clarity of the individual pure films. The film consisting of 30 % S-PEI was translucent but not uniform in optical clarity. Films made with 40 and 50 % S-PEI displayed obvious macro-phase separation like their original solutions. One phase remained strongly adhered to the glass substrate and the other phase was easily lifted. At 60 %wt, the PEI-rich phase formed disconnected islands on the glass substrate, so neither phase could be recovered or characterized. All free standing films up to 30 % S-PEI had average thicknesses ranging from 38 to 71 μm with standard deviations up to 5 μm. The free standing films at 40 % and 50 % S-PEI were much thicker on average at 89 and 101 μm, respectively, but also had very high thickness variability with standard deviations around 25 μm.

5.3.2. FTIR Analysis of Polymer Blends

FTIR measurements were taken at multiple locations on each sample. Despite the lack of optical uniformity in some films, all spectra for each sample were identical. The absorbance data for membranes with varying S-PEI concentrations before and after film protonation are shown in Figure 5-2. As could be expected, the peaks representing sulfonate and possible trimethylsilyl groups increase with S-PEI concentration. Although the films with higher S-PEI content were heterogeneous, the PEI-rich phases did contain significant quantities of the sulfonated polymer, showing that a miscibility limit exists for S-PEI / PEI blends.

With exception to the 50 % S-PEI film, sulfonate peaks are unaffected by protonation. In all cases, protonation did remove those bands between 1630 and 1690 cm^{-1} thought to be associated with interactions between trimethylsilyl groups and other components on the polymer backbone. Therefore, the protonation procedure was effective in converting S-PEI to its acid form. For the 50 % S-PEI film, protonation caused the loss of sulfonic acid functionality, which could be explained by the instability

or poor interfacial interaction of the saturated S-PEI phase in the free standing polymer. It is therefore possible that the extent of S-PEI aggregation was so high that the agglomerates easily separated from the more stable PEI phase in the mildly acidic protonation solution.

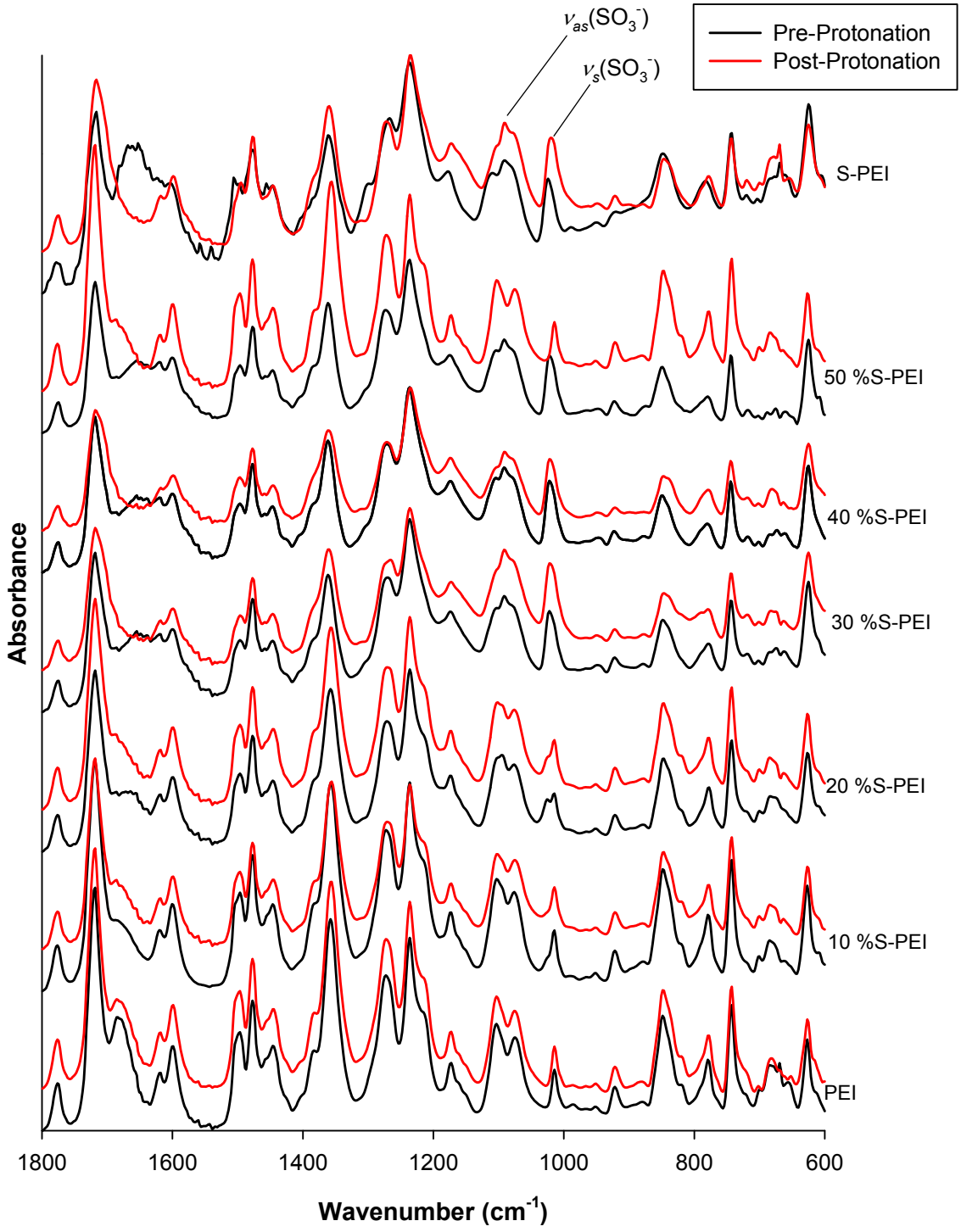

Figure 5-2: FTIR spectra of PEI/S-PEI polymer blend films before (black) and after (red) protonation.

Thermal annealing experiments resulted in dark, transparent membranes at 10 – 30 % S-PEI. The films made with 40 and 50 % S-PEI were more rigid and had increased surface roughness that indicated the formation of gas during annealing. These features all suggest thermal-induced desulfonation. The removal of sulfonic acid groups was confirmed with FTIR (see Figure 5-3) showing that the chemistry of each blended film was identical to the original PEI as a result of the annealing process. Desulfonation has been observed in previous studies that evaluated the thermal properties of sulfonated polymers such as S-PSU [20, 26], S-PI [27], S-PEEK [28], and others [29-31]. These studies reported desulfonation temperatures as low as 200 °C, where the lower temperatures were attributed to the instability of sulfonic acid attachment to activated phenyl rings, as opposed to deactivated phenyl ring attachment which has been shown to be more thermally stable [32-34]. Therefore, S-PEI desulfonation limits the use of high thermal annealing to improve phase interaction between the blend components. To improve the thermal stability of the sulfonate groups on the S-PEI polymer structure, alternative post-sulfonation methods should be investigated that allow for substitution on deactivated aromatic rings.

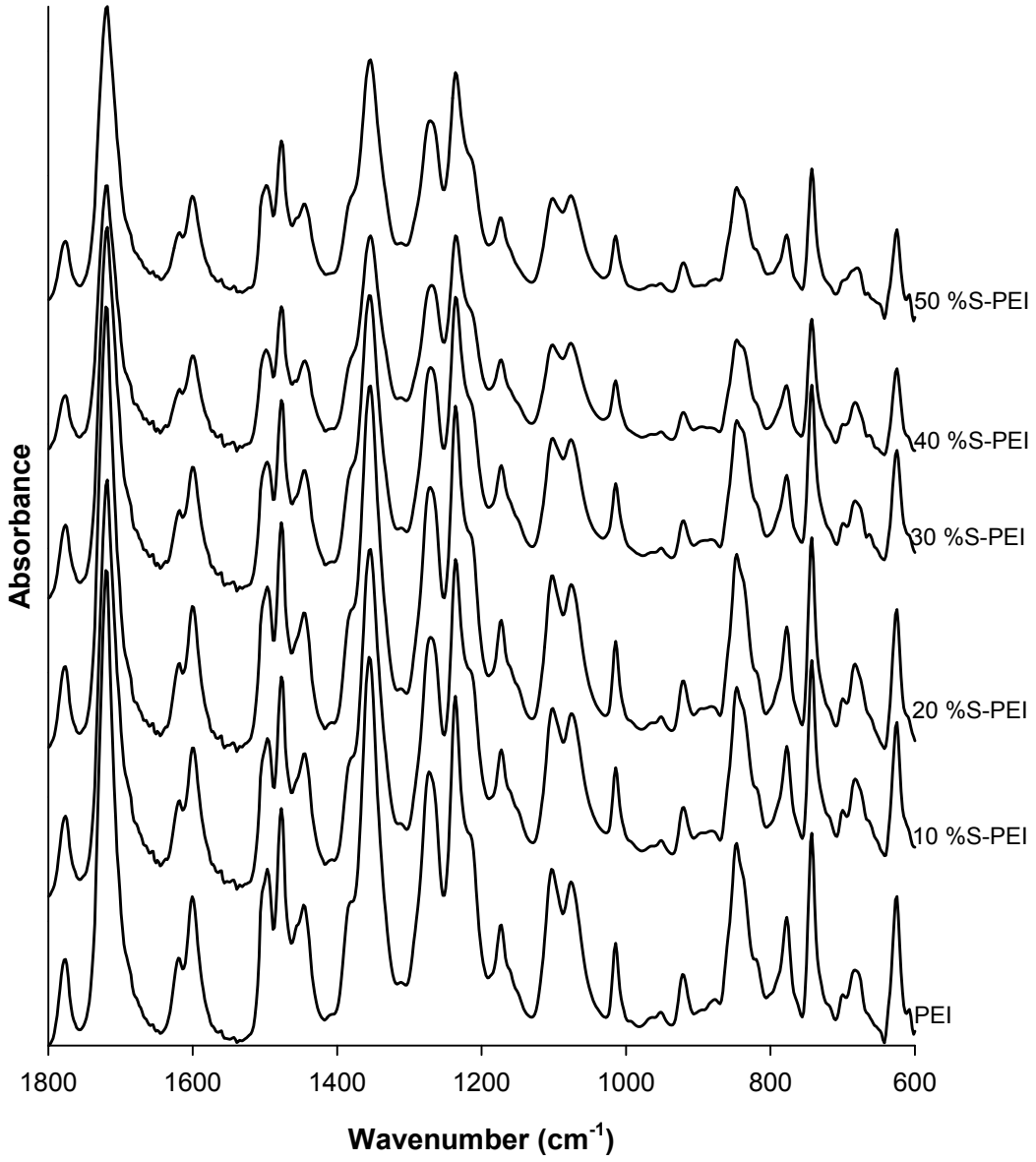

Figure 5-3: FTIR spectra of PEI/S-PEI polymer blend films after thermal annealing at 230 °C for 3 days.

5.3.3. SEM Analysis of Blend Morphologies

Representative cross-sectional SEM images of protonated blends before and after annealing are shown in Figure 5-4 through Figure 5-8. Phase separation was observed even at the lowest concentration of S-PEI, which displayed a composite-like morphology. The average cross-sectional diameter of S-PEI aggregates were 2 – 3 μm for the 10 % S-PEI film and grew progressively larger and more disperse in size with increasing S-PEI concentration. The unannealed films all displayed poor adhesion at the PEI/S-PEI interfaces, indicated by the void space separating the two phases. These morphologies were almost identical to the two films made with protonated S-PEI solids prior to film casting (see Figure 5-9 and Figure 5-10), although for the films made with 50 % S-PEI, the protonated film showed more uniformity than that made with pre-protonated solid. Therefore, the use of trimethylsilyl groups to cover sulfonated functionalities was ineffective in improving interfacial contact and may have been mildly effective in improving film uniformity at higher S-PEI concentrations.

Annealing proved to significantly enhance all polymer blend morphologies, as shown by the improved interfacial contact between sulfonated and unsulfonated domains. However, the improvement was a combined result of desulfonation, which converted S-PEI back to PEI, and polymer chain reorganization made possible by annealing close to the T_g of PEI. In all cases the void spaces were significantly reduced or completely removed after annealing. The gas released from desulfonation only created large pores (> 20 μm in diameter) in the annealed films made at 40 and 50 % S-PEI, which are not displayed in SEM micrographs. It is likely that smaller voids developed initially at the onset of desulfonation, but were able to aggregate over the 3-day period.

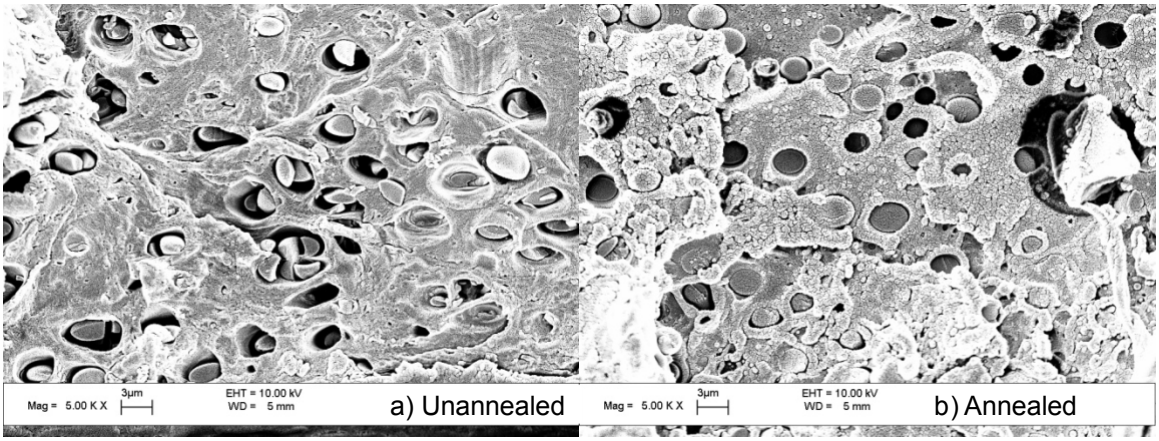

Figure 5-4: Cross-sectional SEM images of PEI/S-PEI blend films with 10 % S-PEI. The film was protonated after casting.

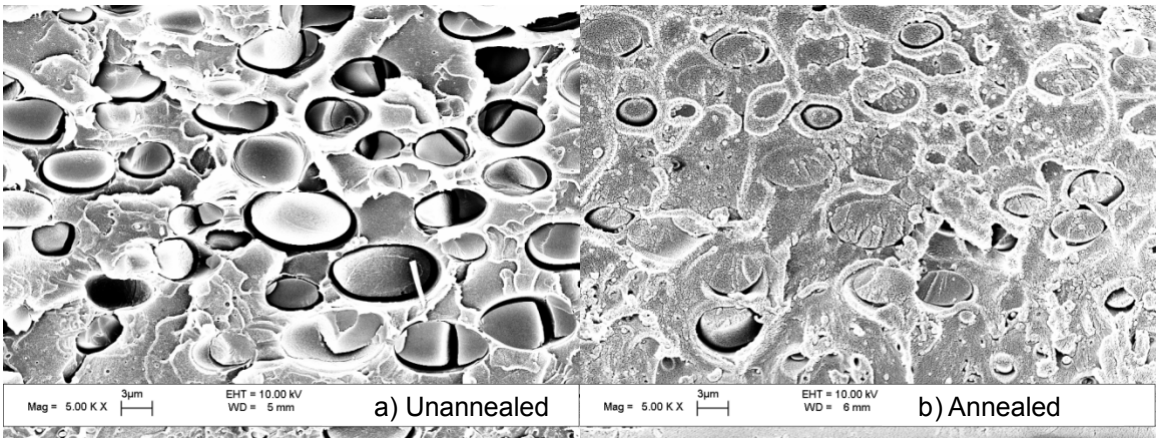

Figure 5-5: Cross-sectional SEM images of PEI/S-PEI blend films with 20 % S-PEI. The film was protonated after casting.

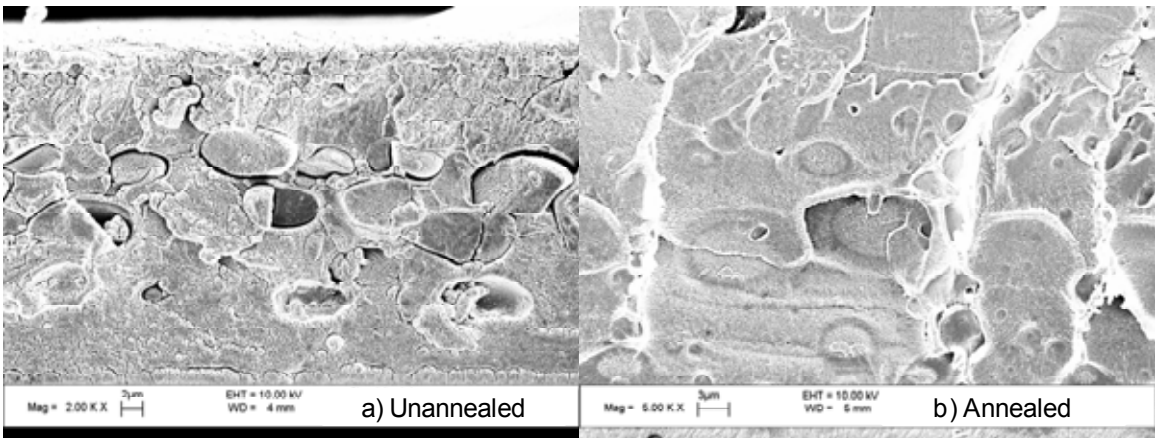

Figure 5-6: Cross-sectional SEM images of PEI/S-PEI blend films with 30 % S-PEI. The film was protonated after casting.

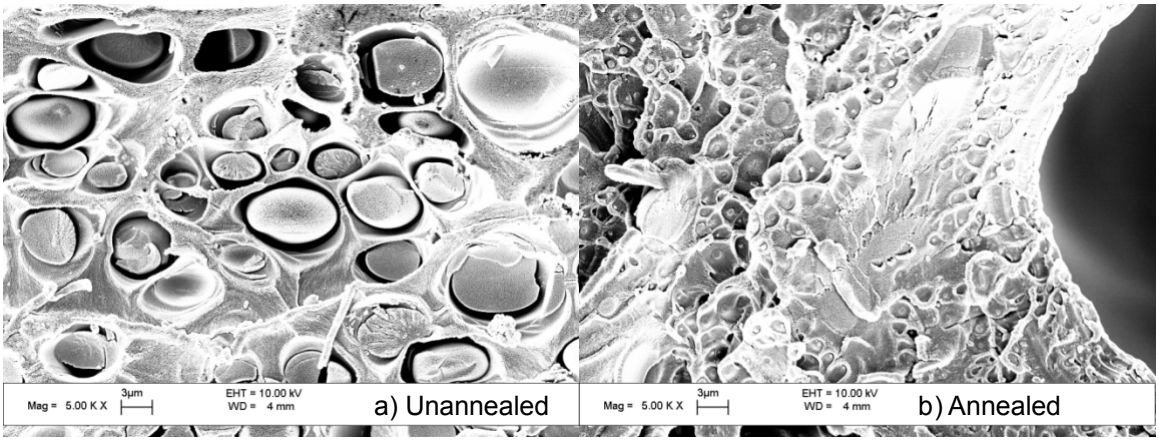

Figure 5-7: Cross-sectional SEM images of PEI/S-PEI blend films with 40 % S-PEI. The film was protonated after casting.

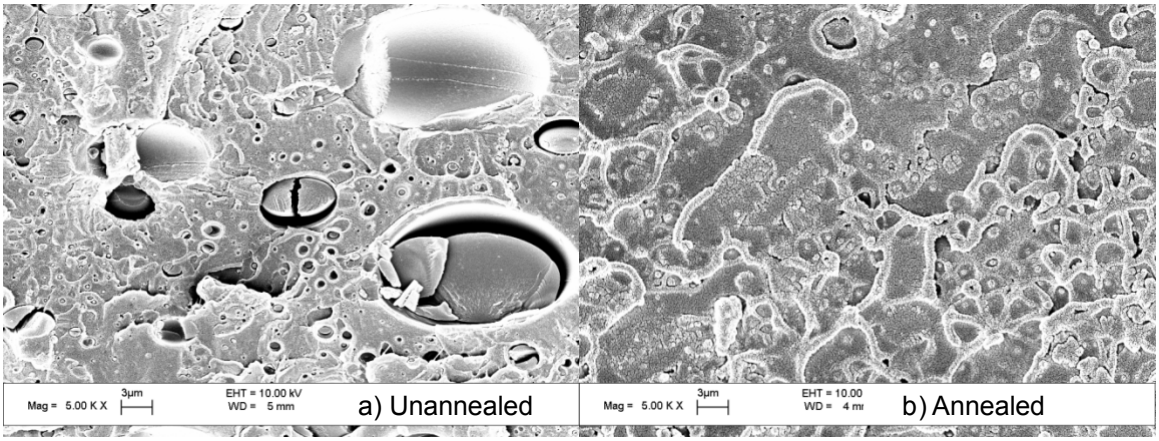

Figure 5-8: Cross-sectional SEM images of PEI/S-PEI blend films with 50 % S-PEI. The film was protonated after casting.

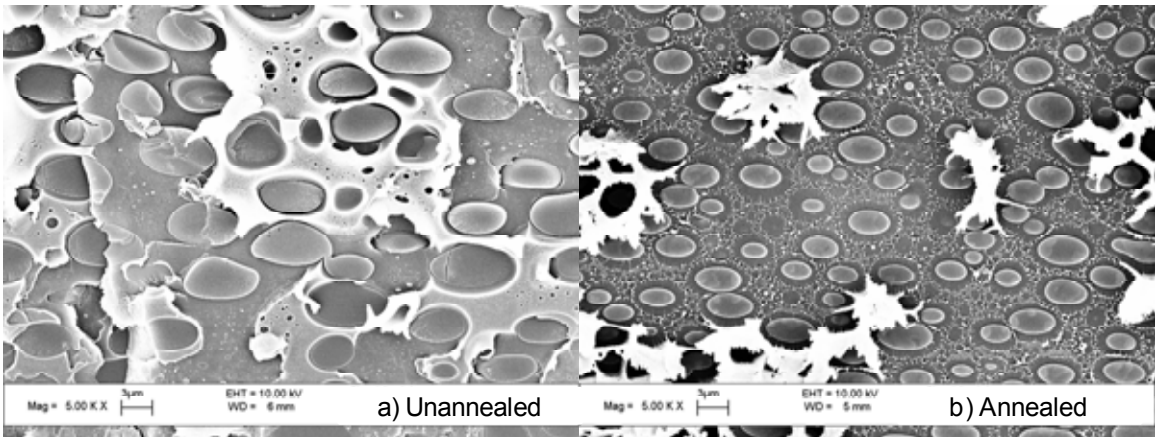

Figure 5-9: Cross-sectional SEM images of PEI/S-PEI blend films with 30 % S-PEI. The S-PEI solid was protonated before making solutions for film casting.

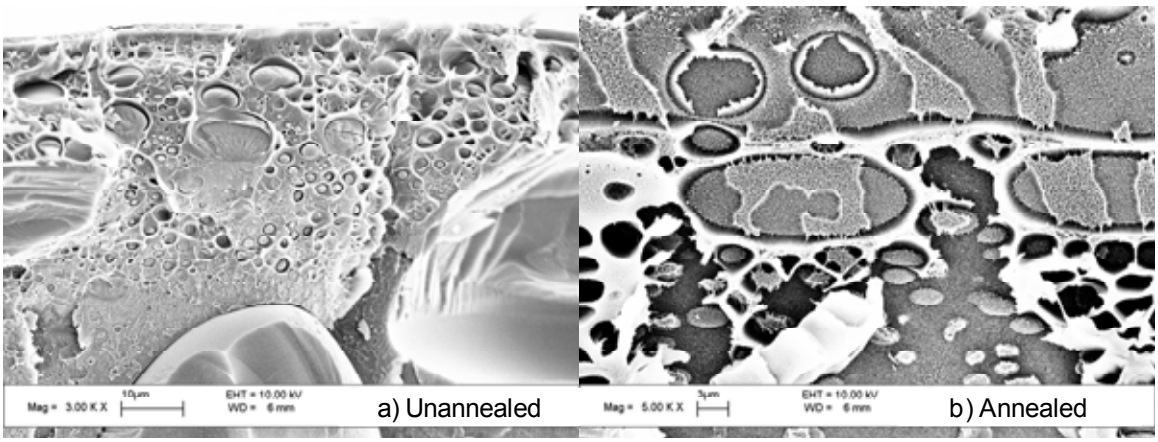

Figure 5-10: Cross-sectional SEM images of PEI/S-PEI blend films with 50 % S-PEI. The S-PEI solid was protonated before making solutions for film casting.

5.3.4. Water Uptake

Swelling experiments were used to determine the effect of sulfonation on water uptake in blended films, and the results are shown in Figure 5-11. Before annealing protonated films, water uptake remained low overall (< 20 wt% water in the dry polymer) but did show a proportional trend with S-PEI content up to 30 % S-PEI. Since water uptake should scale with sulfonic acid concentration up to complete sulfonation [35], the restriction of water uptake in the heterogeneous films with 40 and 50 % S-PEI is further evidence of a miscibility limit for S-PEI in PEI. Water uptake in the annealed blends overall remained low due to desulfonation from high-temperature annealing.

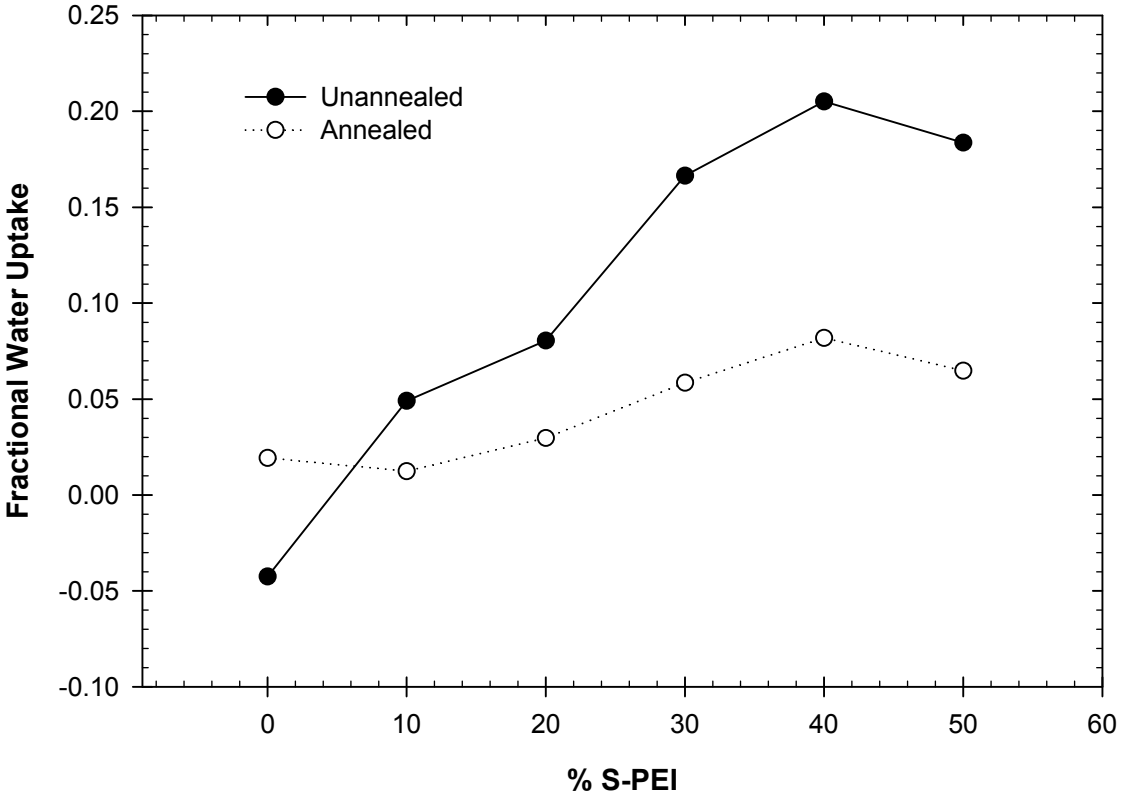

Figure 5-11: Water uptake from swelling experiments in PEI/S-PEI polymer blends before and after thermal annealing at 230 °C for 3 days.

5.3.5. Mechanical Properties

The indentation force data for annealed blends were all beyond the measurement limits of the HTMECH instrument (~ 35 N), showing that thermal annealing above the T_g of PEI was effective in increasing the mechanical strength of the polymer blends. The mechanical properties of the pure PEI film also improved somewhat after annealing, but the force data for this film was well within the measurement range of HTMECH. The considerable change in mechanical properties from the annealed PEI to the annealed blends with low S-PEI content indicates that presence of S-PEI during the annealing process had a significant effect on chain reorganization, which may have been induced by desulfonation. It should also be noted that although mechanical data could not be obtained for the annealed blends, the elastic properties of those films did not seem to be significantly different from that of the annealed PEI film.

The films made with 40 and 50 % S-PEI became more brittle after annealing as a result of large pore structures throughout the film thickness. The mechanical properties of unannealed, protonated polymer blends in the wet and dry states are shown in Figure 5-12 through Figure 5-15 for S-PEI concentrations varying from 0 to 50 %. The trends for normalized maximum force, ultimate tensile strength, and toughness show that increasing S-PEI content decreases the mechanical stability of the PEI/S-PEI blends, as expected. This destabilization was due to the weak mechanical properties of the pure S-PEI film. However, the strength and toughness of the wet and dry films only decreased until 30 % S-PEI and remained relatively stable thereafter. This plateau in mechanical strength at higher S-PEI concentrations is further evidence of the limited blend miscibility and S-PEI saturation in the PEI-rich phase. The ultimate elongation of the polymer also decreased with S-PEI concentration, but unlike other mechanical properties mentioned previously, the film ductility was minimized at 30 % SPEI and increased slightly at the higher concentrations. This effect may be a result of immiscible S-PEI-rich phase

entrapped in the film, which could introduce voids to the membrane structure due to poor interfacial adhesion with the PEI-rich phase. As shown in previous work with poly(methyl methacrylate) films, the presence of voids in polymer structures may improve the ductility of some materials [36, 37].

Absorbed water is well-known to act as a plasticizer in polymers, resulting in deteriorated mechanical strength [38-40]. The mechanical data from this study is consistent with the plasticization effect of water. However, as shown by the lower ultimate elongations of swollen samples, water does not seem to increase the overall mobility of the polymer chains. Instead, the observed loss of mechanical strength with water sorption may be the combined result of plasticization and high interfacial tension between both polymer phases created by swelling of S-PEI regions. Water uptake also restricted the ultimate elongation in the pure PEI film, showing that absorbed water could inhibit film ductility by limiting polymer chain mobility. This would be possible if water molecules formed ionic bridges between polymer chains through hydrogen bonding with the amine and carbonyl groups on the backbone structure.

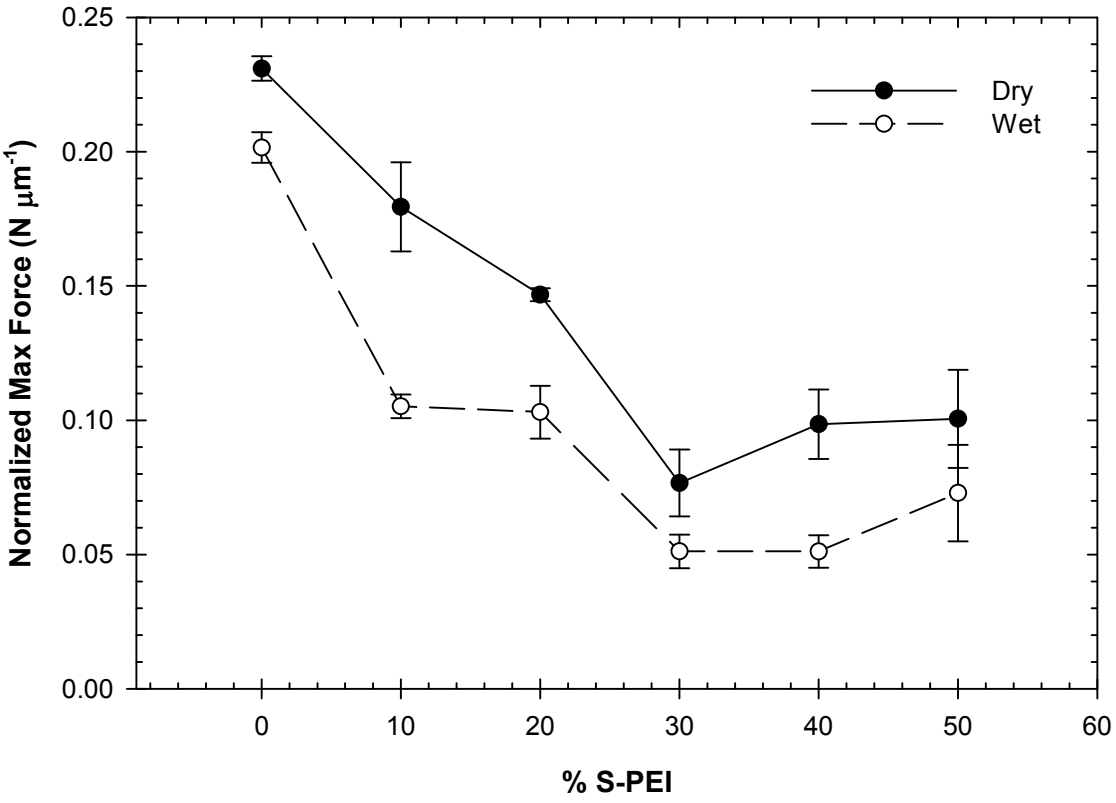

Figure 5-12: Normalized maximum force of protonated PEI/S-PEI blends before annealing. Error bars represent 95 % confidence intervals.

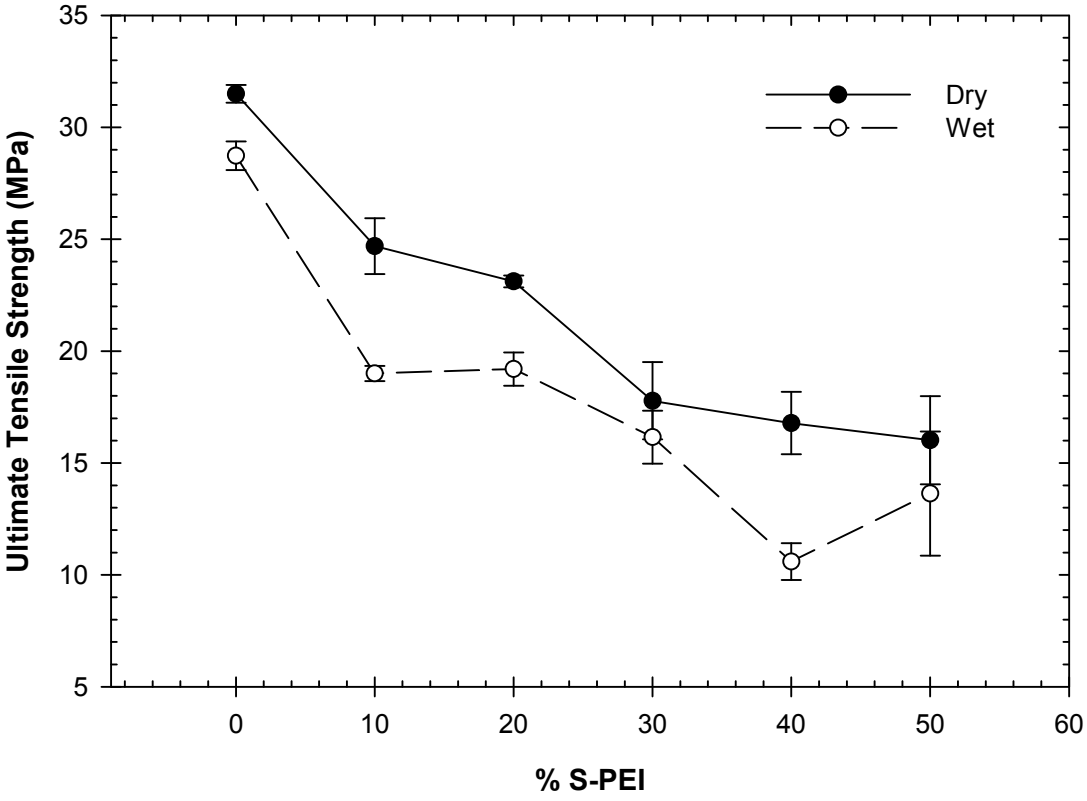

Figure 5-13: Ultimate tensile strenght of protonated PEI/S-PEI blends before annealing. Error bars represent 95 % confidence intervals.

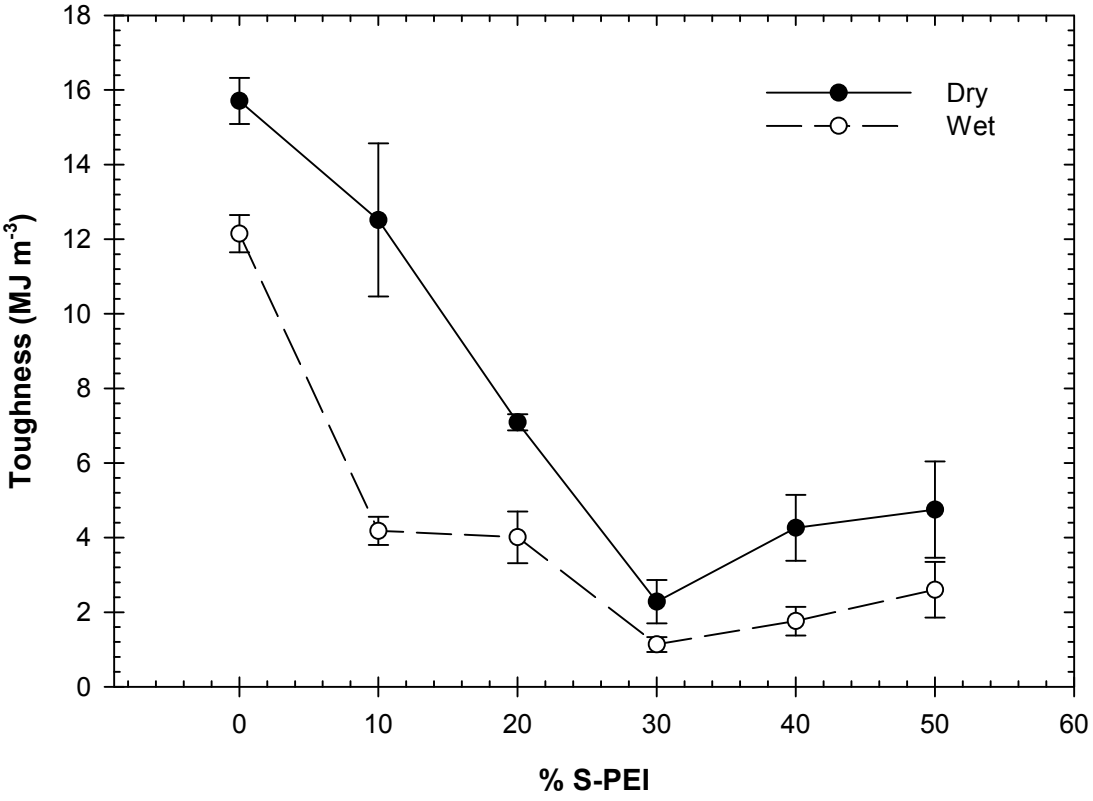

Figure 5-14: Toughness of protonated PEI/S-PEI blends before annealing. Error bars represent 95 % confidence intervals.

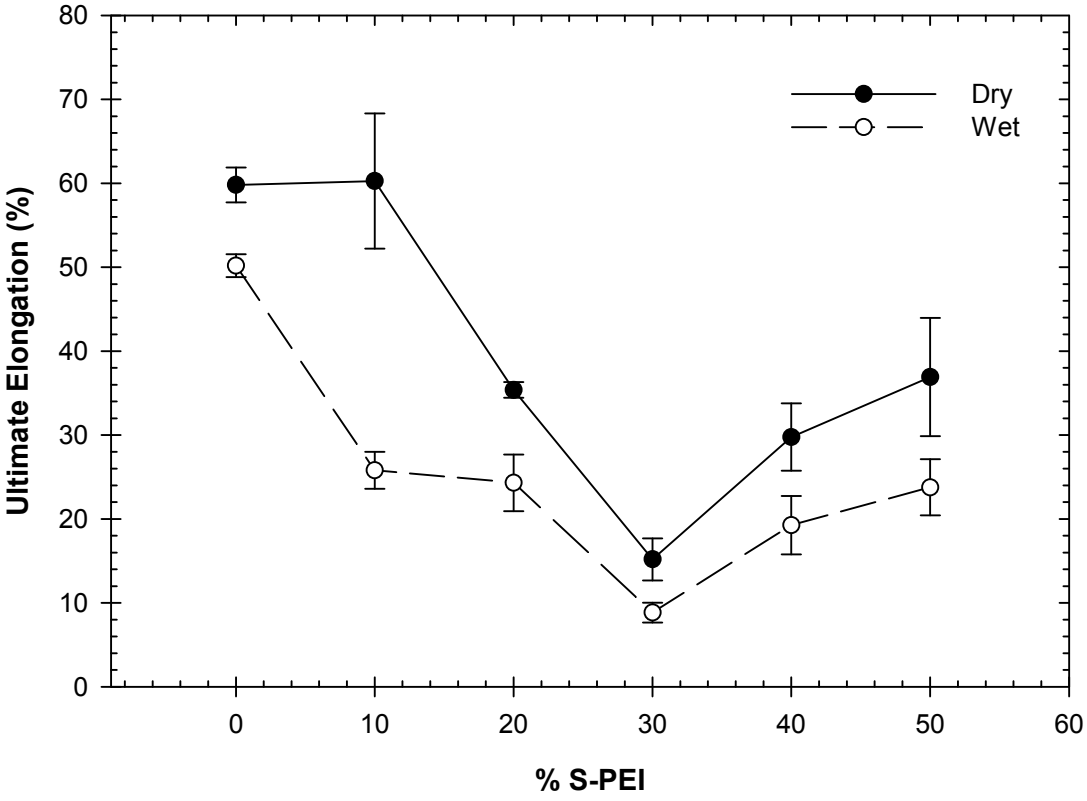

Figure 5-15: Ultimate elongation of protonated PEI/S-PEI blends before annealing. Error bars represent 95 % confidence intervals.

5.3.6. Conductive Properties

Ionic conductivities for the PEI/S-PEI blends are shown in Figure 5-16. Although pure PEI is hydrophobic, the film displayed conductivity values close to 1 mS/cm in liquid water at room temperature. The mild conductive properties of PEI is are most likely due to trace amounts of NMP that remained in the polymer after exposure to the mildly acidic ion-exchange solution and rinsing. The conductivity of PEI was also measured in the dry state under ambient conditions and was an order of magnitude lower than the swollen film (0.16 ± 0.01 mS/cm), which could suggest that water binds to electron-rich groups on polymer backbone to provide mild proton transporting characteristics. The conductivities of swollen blends with 10 and 20 % S-PEI did not deviate significantly from the pure swollen PEI film, which may be due to the high degree of phase separation between PEI and S-PEI. It is likely that microphase separation at low S-PEI concentrations is not suitable for ionic channel formation through the film, since phase continuity could not be achieved through the thickness of the film.

A significant increase in conductivity at 30 % S-PEI was observed. Although still almost two orders of magnitude lower than the conductivities of some commercially available PFSAs, the trend in conductivity up to 30 % S-PEI is consistent with trends in mechanical properties, observed blend miscibilities, and water uptake properties. The ionic conductivities after 30 % S-PEI drop back to that of the non-functionalized polymer or lower, most likely due to high degrees of phase separation leading to poor proton transport, and the effects of increased film thickness, which can also limit proton transport with respect to the formation of ionic channels [41]. These trends suggest that the PEI/S-PEI blend can be optimized for maximum performance between 20 and 40 % S-PEI. Although percolated networks for proton transport began to form with increasing S-PEI, the increasing degree of phase separation limits the use of PEI/S-PEI blends as PEMs.

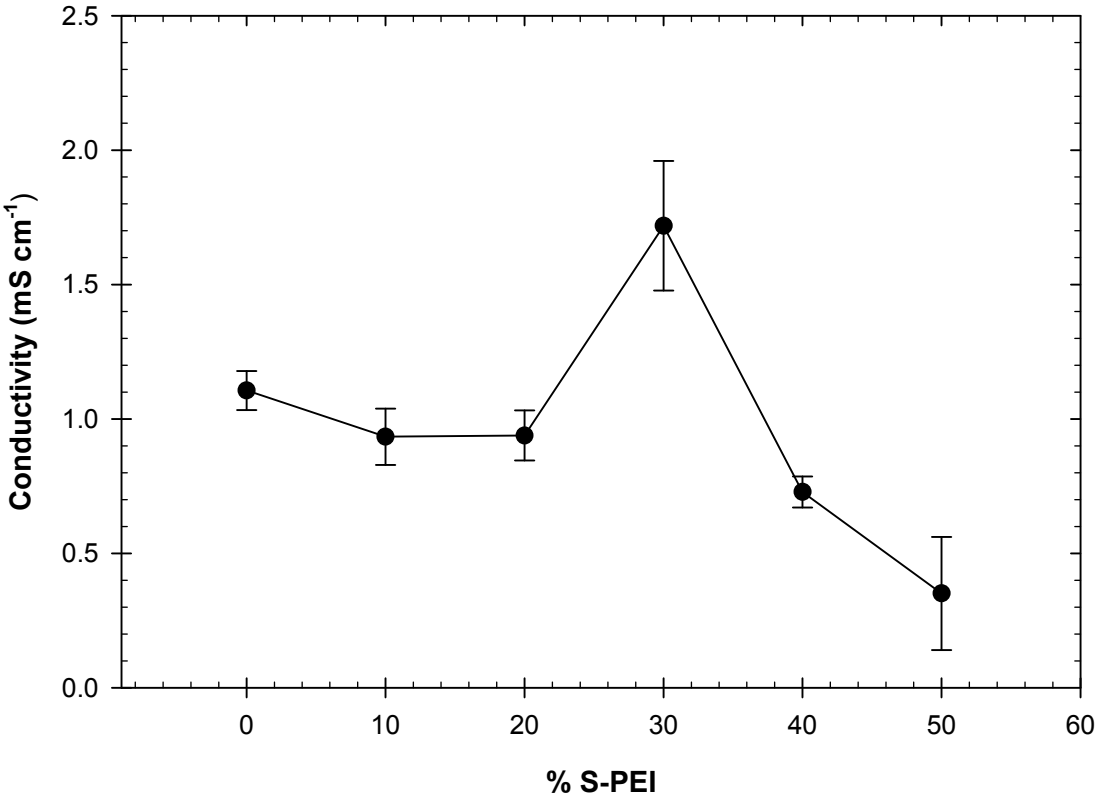

Figure 5-16: Ionic conductivities of PEI/S-PEI polymer blends in deionized water at room temperature.

5.4. CONCLUSIONS

Polymer blends of PEI and S-PEI were made in order to develop an optimized membrane with combined electrochemical and mechanical properties. Titration showed that the S-PEI, made by exposing PEI to TMSCS, had a degree of sulfonation of 96%, but the solid and film casted from NMP had very poor mechanical stability, thus requiring the addition of a more stable component. The use of trimethylsilyl intermediate improved the solubility of S-PEI in NMP in the blended solutions, but had little to no effect on membrane morphologies compared with membranes made from protonated S-PEI solids. As expected, the mechanical properties of the blends decreased and water uptake increased with S-PEI content. However, these properties all stabilized at 30 % S-PEI, indicating saturation of the S-PEI phase in PEI. Most likely, the S-PEI aggregate regions, which were observed even at 10 % S-PEI using SEM, grew large enough to form macrophase structures, which were obvious to the eye in blend solutions and membranes made with 40 and 50 % S-PEI. Phase aggregation also limited water uptake and proton transport since a continuous, percolated network of sulfonic acid groups could not be established at higher concentrations before macro-phase separation occurred. Conductivity values were much lower than commercial PFSAs overall but showed some improvement at 30 % SPEI. Therefore, although the performance characteristics are not suitable for fuel cell applications, a blend concentration between 20 and 30 % S-PEI seems to show the best combination of electrochemical and mechanical properties.

Annealing the polymer blends around the T_g of PEI caused desulfonation of S-PEI. Since the functional groups were removed and chains were able to reorganize into more ordered structures, the initial void spaces between phases in the unannealed films were significantly reduced or completely removed. It was also observed that the

nonporous annealed blends had much better mechanical strengths than the pure annealed PEI film.

5.5. REFERENCES

1. McGrath, J.E., et al. *Ion-conducting sulfonated polymeric materials invention*. 2008. USPTO# 20080275146.

2. Cui, W., J. Kerres, and G. Eigenberger, *Development and characterization of ion-exchange polymer blend membranes.* Separation and Purification Technology, 1998. **14**(1-3): p. 145-154.

3. Manea, C. and M. Mulder, *Characterization of polymer blends of polyethersulfone/sulfonated polysulfone and polyethersulfone/sulfonated polyetheretherketone for direct methanol fuel cell applications.* Journal of Membrane Science, 2002. **206**(1-2): p. 443-453.

4. Kreuer, K.D., *On the development of proton conducting polymer membranes for hydrogen and methanol fuel cells.* Journal of Membrane Science, 2001. **185**(1): p. 29-39.

5. Mikhailenko, S.D., S.M.J. Zaidi, and S. Kaliaguine, *Electrical properties of sulfonated polyether ether ketone/polyetherimide blend membranes doped with inorganic acids.* Journal of Polymer Science Part B: Polymer Physics, 2000. **38**(10): p. 1386-1395.

6. Wilhelm, F.G., et al., *Cation permeable membranes from blends of sulfonated poly(ether ether ketone) and poly(ether sulfone).* Journal of Membrane Science, 2002. **199**(1-2): p. 167-176.

7. Xing, P., et al., *Synthesis and characterization of sulfonated poly(ether ether ketone) for proton exchange membranes.* Journal of Membrane Science, 2004. **229**(1-2): p. 95-106.

8. Deimede, V., et al., *Miscibility Behavior of Polybenzimidazole/Sulfonated Polysulfone Blends for Use in Fuel Cell Applications.* Macromolecules, 2000. **33**(20): p. 7609-7617.

9. Steele, B.C.H. and A. Heinzel, *Materials for fuel-cell technologies.* Nature, 2001. **414**(6861): p. 345-352.

10. Eikerling, M., et al., *Mechanisms of Proton Conductance in Polymer Electrolyte Membranes.* The Journal of Physical Chemistry B, 2001. **105**(17): p. 3646-3662.

11. Iojoiu, C., et al., *Mastering Sulfonation of Aromatic Polysulfones: Crucial for Membranes for Fuel Cell Application.* Fuel Cells, 2005. **5**(3): p. 344-354.

12. Nguyen, T.-Q., et al., *Controlling Interchain Interactions in Conjugated Polymers: The Effects of Chain Morphology on Excitonâ^'Exciton Annihilation and Aggregation in MEHâ^'PPV Films.* The Journal of Physical Chemistry B, 1999. **104**(2): p. 237-255.

13. Liu, J., T.-F. Guo, and Y. Yang, *Effects of thermal annealing on the performance of polymer light emitting diodes*, in *Journal of Applied Physics*. 2002, American Institute of Physics. p. 1595.

14. Park, H.B., et al., *Annealing effect of sulfonated polysulfone ionomer membranes on proton conductivity and methanol transport.* Journal of Membrane Science, 2005. **247**(1-2): p. 103-110.

15. Chao, H.S. and D.R. Kelsey. *Poly(aryl ether) resins having repeat units of the structure*. 1986. USPTO# 4625000.

16. Zapata, P., P. Basak, and J. Carson Meredith, *High-throughput screening of ionic conductivity in polymer membranes.* Electrochimica Acta, 2009. **54**(15): p. 3899-3909.

17. Sormana, J.-L., S. Chattopadhyay, and J.C. Meredith, *High-throughput mechanical characterization of free-standing polymer films.* Review of Scientific Instruments, 2005. **76**(6): p. 062214-9.

18. Guhathakurta, S. and K. Min, *Influence of crystal morphology of 1H-1,2,4-triazole on anhydrous state proton conductivity of sulfonated bisphenol A polyetherimide based polyelectrolytes.* Polymer, 2009. **50**(4): p. 1034-1045.

19. Guhathakurta, S. and K. Min. *Post Sulfonation of Bisphenol A Polyetherimide*. in *Proceedings of the ACS Division of Polymeric Materials: Science & Engineering*. 2008. New Orleans, LA: American Chemical Society.

20. Naim, R., et al. *Development of sulfonated polysulfone membranes as a material for Proton Exchange Membrane (PEM)*. in *Proceedings of Regional Symposium on Membrane Science and Technology 2004, 21-25 April 2004, Puteri Pan Pacific Hotel, Johor Bharu, Malaysia*. 2004. Johor Bharu, Malaysia.

21. Genova-Dimitrova, P., et al., *Ionomeric membranes for proton exchange membrane fuel cell (PEMFC): sulfonated polysulfone associated with phosphatoantimonic acid.* Journal of Membrane Science, 2001. **185**(1): p. 59-71.

22. Wang, F., et al., *Direct polymerization of sulfonated poly(arylene ether sulfone) random (statistical) copolymers: candidates for new proton exchange membranes.* Journal of Membrane Science, 2002. **197**(1-2): p. 231-242.

23. Harrison, W.L., et al., *Influence of the bisphenol structure on the direct synthesis of sulfonated poly(arylene ether) copolymers. I.* Journal of Polymer Science Part A: Polymer Chemistry, 2003. **41**(14): p. 2264-2276.

24. Xiao, G., et al., *Synthesis of sulfonated poly(phthalazinone ether sulfone)s by direct polymerization.* Polymer, 2002. **43**(19): p. 5335-5339.

25. Liu, S., F. Wang, and T. Chen, *Synthesis of Poly(ether ether ketone)s with High Content of Sodium Sulfonate Groups as Gas Dehumidification Membrane Materials.* Macromolecular Rapid Communications, 2001. **22**(8): p. 579-582.

26. Lufrano, F., et al., *Sulfonated polysulfone as promising membranes for polymer electrolyte fuel cells.* Journal of Applied Polymer Science, 2000. **77**(6): p. 1250-1256.

27. Woo, Y., et al., *Synthesis and characterization of sulfonated polyimide membranes for direct methanol fuel cell.* Journal of Membrane Science, 2003. **220**(1-2): p. 31-45.

28. Mikhailenko, S.D., et al., *Proton conducting membranes based on cross-linked sulfonated poly(ether ether ketone) (SPEEK).* Journal of Membrane Science, 2004. **233**(1-2): p. 93-99.

29. Zhai, M., et al., *Synthesis of fluorinated polymer electrolyte membranes by radiation grafting and atom transfer radical polymerization techniques.* Polymer, 2009. **50**(5): p. 1159-1165.

30. Hietala, S., et al., *Thermal stability of styrene grafted and sulfonated proton conducting membranes based on poly(vinylidene fluoride).* Journal of Materials Chemistry, 1998. **8**(5): p. 1127–1132.

31. Chen, H.G., et al., *Novel sulfonated poly(phthalazinone ether ketone) ionomers containing benzonitrile moiety for PEM fuel cell applications.* Journal of Power Sources, 2007. **165**(1): p. 16-23.

32. Meier-Haack, J., et al., *Membranes from sulfonated block copolymers for use in fuel cells.* Separation and Purification Technology, 2005. **41**(3): p. 207-220.

33. McGrath, J.E., D.G. Baird, and M.v. Spakovsky, *Advanced Materials for PEM-Based Fuel Cell Systems*. 2005.

34. Wiles, K.B., F. Wang, and J.E. McGrath, *Directly copolymerized poly(arylene sulfide sulfone) disulfonated copolymers for PEM-based fuel cell systems. I. Synthesis and characterization.* Journal of Polymer Science Part A: Polymer Chemistry, 2005. **43**(14): p. 2964-2976.

35. Peinemann, K.V. and S.P. Nunes, *Membranes for energy conversion*. Membrane technology, v. 2. 2008, Weinheim; Chichester: Wiley-VCH.

36. Sternstein, S.S., in *Polymeric materials : relationships between structure and mechanical behavior*, Baer and Radcliffe, Editors. 1973, American Society for Metals: Metals Park, Ohio. p. 369–410.

37. Ash, B.J., et al., *Mechanical properties of Al_2O_3/polymethylmethacrylate nanocomposites.* Polymer Composites, 2002. **23**(6): p. 1014-1025.

38. Solasi, R., et al., *On mechanical behavior and in-plane modeling of constrained PEM fuel cell membranes subjected to hydration and temperature cycles.* Journal of Power Sources, 2007. **167**(2): p. 366-377.

39. Shang, X.Y., et al., *Fluorene-containing sulfonated poly(arylene ether 1,3,4-oxadiazole) as proton-exchange membrane for PEM fuel cell application.* Journal of Membrane Science, 2007. **291**(1-2): p. 140-147.

40. Lee, H.C., et al., *Preparation and evaluation of sulfonated-fluorinated poly(arylene ether)s membranes for a proton exchange membrane fuel cell (PEMFC).* Electrochimica Acta, 2004. **49**(14): p. 2315-2323.

41. Dimitrova, P., et al., *Transport properties of ionomer composite membranes for direct methanol fuel cells.* Journal of Electroanalytical Chemistry, 2002. **532**(1-2): p. 75-83.

Chapter 6
Conclusions and Recommendations for Future Work

The need for low-cost, high-performance polymers in proton exchange membrane fuel cells (PEMFCs) has motivated the use of combinatorial synthesis and high-throughput screening for efficiently discovering structure-property relationships while developing novel membrane materials. To meet the growing need for high-throughput polymer characterization techniques, a high-throughput mass transport assay (HT-MTA) has been developed that is capable of measuring the flux and permeability of fluids at multiple sample locations using a low-cost design with rapid pseudo steady-state results compared to conventional mass transport analysis methods. The functionality of HT-MTA has been demonstrated with water pervaporation through a number of proton exchange materials, and was also used in conjunction with other polymer characterization tools to investigate rapid degradation mechanisms in Nafion®, the current state-of-the-art perfluorinated sulfonic acid (PFSA) fuel cell polymer. To extend this research further for novel proton exchange membrane development, the polymer characterization toolset was used to optimize mechanical and electrochemical properties of a polymer blend consisting of polyetherimide (PEI) and sulfonated polyetherimide (S-PEI) that was functionalized using a simple, cost-effective post sulfonation method.

6.1. CONCLUSIONS

6.1.1. High-Throughput Mass Transport

HT-MTA was developed based on the variable pressure method for simultaneously measuring permeate accumulation in multiple downstream chambers. The instrument has been used to determine pseudo steady-state flux and permeability values for water pervaporation through standard and modified Nafion® membranes at various temperatures, as well as model polymer blends of PVDF and an acrylic, proton-conducting polyelectrolyte. For standard Nafion® films, the pervaporation flux and permeability values were approximately one to two orders of magnitude lower than some previously reported values. The reduced transport properties are the result of the stagnant downstream conditions in HT-MTA, which differ from standard pervaporation techniques that use convective sweep gas or evacuation with liquid nitrogen trapping. Still, Arrhenius trends for flux and permeability were observed with respect to pervaporation temperature and the respective activation energies were obtained for water transport through Nafion®. Based on the activation energy for permeability, which was positive, unlike some reported pervaporation values, the HT-MTA provides results that may be more comparable to standard liquid permeation experiments which also show a positive correlation between temperature and permeability due to downstream permeate accumulation.

HT-MTA was used to determine the water transport effects of cationic substitution and rapid degradation of Nafion® membranes. Cationic substitution with hydrocarbon-based salts caused an expected reduction in water transport properties due to the blockage of sulfonic acid groups with hydrophobic groups. Flux and permeability increased slightly as result of rapid free radical Nafion® degradation, most likely due polymer chain scissions and chain unzipping that can remove repeat units, decrease

chain entanglements, and increase chain mobility. The HT-MTA also detected changes in transport properties due to increasing the polyelectrolyte (PE) content in semi-interpenetrating networks based on commercially available polyvinylidene fluoride resins. Both water flux and permeability were maximized in the range of 40 – 55 wt% PE, consistent with a previous study showing optimal proton conductivities for the same polymer system over the same concentration range.

6.1.2. High-Throughput Characterization of Nafion® Degradation

HT-MTA was incorporated into the PEM characterization toolset used to investigate the rapid free radical degradation of Nafion® membranes with aqueous solutions of hydrogen peroxide and iron(II) sulfate at various concentrations. In general, the higher hydrogen peroxide concentration resulted in degraded samples with higher fluoride loss, lower ionic conductivity, and lower mechanical stability than the original polymer due to severe morphological changes. For films exposed to the more dilute hydrogen peroxide concentration, proton conductivities increased, and for some concentrations of Fe^{2+}, mechanical properties were higher than the original polymer. These improvements have been attributed to increased polymer chain mobility under mild chain degradation where membrane integrity was preserved. Water transport characteristics of degraded films, among other properties, showed that the negative effects of free radical degradation were maximized at a Fe^{2+} concentration of 50 ppm, most likely due to a balance between the rate of free radical generation and neutralization.

Chain unzipping, chain scission, and side-group attack were all evaluated as possible pathways for free radical degradation in Nafion® films. Both the chemical and performance properties of aged films suggest that the dominating pathway is initially polymer chain scission, but changes to complete chain unzipping at later times as a result of the availability of free radicals from hydrogen peroxide. Therefore, future

correlations of rapid *ex-situ* PEM degradation experiments with real-time *in-situ* lifetime tests may rely on mainly on tuning *ex-situ* hydrogen peroxide concentrations to control membrane degradation mechanisms that are consistent with long-term *in situ* experiements.

6.1.3. Optimization the Functionality of Sulfonated Polymer Blends

To work toward developing novel PEM materials while using our polymer characterization toolset to efficiently screen for optimal performance properties, a range of blended membranes of PEI and S-PEI with various composition ratios were prepared. S-PEI was created using a simple post sulfonation reaction where the base polymer was exposed to trimethylsilyl chlorosulfonate (TMSCS) under mild conditions to obtain a degree of sulfonation of 96% with minimal side reactions. As expected, the mechanical properties of the blends decreased and water uptake increased with S-PEI content. However, these properties all stabilized at an S-PEI/PEI ratio of 3:7, indicating the existence of a saturation limit for the two polymers despite structural similarities. Scanning electron microscopy identified micron-sized phase separation with poor interfacial adhesion even at an S-PEI/PEI ratio of 1:9. Due to the lack of S-PEI phase continuity, water uptake was limited overall and proton transport in all blends was two orders of magnitude lower than Nafion® films. Despite the poor performance properties of the S-PEI/PEI blends, the polymer characterization toolset was used to find optimal performance properties between 20 and 30 % S-PEI by dry mass. Annealing of the polymer blends resulted in significantly improved interfacial adhesion between the polymer phases, and for films with low S-PEI contents, also resulted in mechanical properties that surpassed those of pure annealed PEI films. However, due to the high annealing temperature needed for polymer chain reorganization, desulfonation took place and reversed any electrochemical improvements that were observed in unannealed blends.

6.2. RECOMMENDATIONS FOR FUTURE STUDY

6.2.1. HT-MTA Functionality

Although HT-MTA has demonstrated the capability of screening multiple membrane samples for mass transport characteristics, there are numerous opportunities for improving the functionality of this instrument. A major addition that should be considered for future implementation is an array of well-sealed downstream pneumatic valves to control permeate accumulation during pervaporation experiments. When the valves are open to oven conditions, evacuation could be used to establish zero downstream partial permeate pressure at the start of experiments, thereby allowing for rapid steady-state flux and permeability calculations since the equilibrium pressure driving force could be approximated as the permeate saturation pressure. A valve system would also allow for quick experimental repetition and easy temperature ramping experiments since the retention mechanism could then be left in place while removing accumulated permeate from downstream chambers. The use of pneumatic valves (LFVA Series from The LEE Company) was initially investigated for the HT-MTA. However, based on the dimensions of the downstream chambers and the sensitivity of the pressure transducers, the rate of downstream gas leakage became significant compared to the flux rates of water through Nafion® films over the experimental timeframe. Therefore, alternative valve devices should be considered or the dimensions of HT-MTA, i.e., exposed transport surface areas and permeate chamber volumes, will need to be increased to reduce the sensitivity of the system to the small pressure changes caused by valve leakage.

Another improvement to HT-MTA that should be considered is the relocation of system electronics, i.e. pressure transducers and wiring, outside of the vacuum oven.

This would to allow for a broader temperature range for mass transport experiments and also for faster post-drying to remove permeate from the system. The current configuration with electronics in the oven allows for temperatures up to ~60 °C. If temperature sensitive components could be placed in a well insulated compartment outside of the oven, then the experimental temperature range could be expanded beyond 80 °C, which would be highly relevant to fuel cell operating conditions.

6.2.2. Future HT-MTA Experiments

Future testing with HT-MTA should include methanol pervaporation as well O_2 permeation to better assess the fuel cell performance capabilities of PEM materials. Methanol fuel crossover is major concern for Nafion® membranes [1], and while accelerated degradation testing may not lead to liquid breakthrough, as shown in this work, gas crossover could be significantly affected by chain scissions and chain unzipping that affect membrane morphologies [2, 3]. In addition, water vapor permeation and the effect of water on the mass transport of other permeates through PEMs are also important to characterizing fuel cell performance [4-6]. Therefore, the system's compatibility with humidified and possibly pressurized upstream gases should be considered.

6.2.3. Detailed Free-Radical Degradation Characterization

The characterization toolset provided an efficient strategy for screening the performance properties of rapidly aged Nafion®, but could only be used to infer possible free radical degradation pathways. For this reason, other characterization methods should be incorporated into the toolset for conducting detailed analyses of free radical degradation in PEMs. Residual gas mass spectroscopy or gas chromatography would allow for the determination of CO_2 released from samples during the decomposition process [7]. In addition to ion chromatography, nuclear magnetic resonance (NMR) could be used to identify organic fragments in reactant solutions. This analysis method

has proven to be highly effective in previous PFSA degradation studies [8, 9]. For a better direct analysis of rapidly aged films, solid state NMR and X-ray photoelectron spectroscopy (XPS) could provide more sensitive alternatives to FTIR in determining chemical changes [9-11]. Sold state NMR could also prove to be useful in characterizing changes in polymer chain mobility since individual relaxation times obtained from resolved carbon resonances can provide information on the local mobility [12].

6.2.4. TMSCS Sulfonation

Using TMSCS for electrophilic aromatic substitution provided a simple post-sulfonation strategy for modifying PEI resin. Although the reaction conditions were mild and numerous studies have shown this reaction to minimize side reactions [13], the resulting mechanical stability of pure S-PEI films suggests that significant chain cleavage may have occurred during sulfonation process. Since PEI is not soluble in most common gel permeation chromatography eluents, and different chain conformations of PEI and S-PEI may produce misleading viscosity measurements, alternative methods for assessing sulfonation chain cleavage are needed. One approach would be to use solid state NMR, which was previously suggested for free radical PEM degradation analysis. Another approach would be to anneal samples above the desulfonation temperature to remove functional groups and then conduct viscosity measurements with a solvent such as n-methylpyrrolidone. If sulfonation side reactions prove to be significant for polymers such as PEI, then a detailed kinetic study of reaction temperature, time, and reactant mole ratio should be conducted to optimize the degree of sulfonation with respect to chain-cleavage.

6.2.5. Combinatorial Polymer Blend Optimization

The development of polymer blends using high-throughput characterization tools allows for the use of combinatorial techniques to quickly determine the effects of certain processing variables. Future work in screening novel polymer blends should focus on

developing and using those process gradient techniques that have been shown to significantly alter PEM performance, namely, composition, thermal annealing, and possibly chemical cross-linking. Composition gradients would allow for efficient screening of blend components and determination of blend saturation limits. This gradient technique is currently being developed in our lab. Annealing temperature gradients would allow for possible improvements in blend compatibility and ionic channel arrangement while also providing an efficient method for discovering desulfonation temperatures in sulfonated components. This technique has already been developed in our lab and has used for screening cell interactions with polymer surfaces [14]. Chemical cross-linking can reduce swelling for better PEM water management and enhance the mechanical strength of hydrophilic polymers under hydration. However, the reduction of water content in PEMs can severely impact the proton conduction capacity of the material. Therefore, it is necessary to balance the extent of cross-linking so that water stability can be achieved without sacrificing the electrochemical chemical properties of the polymer. Since the method used for cross-linking depends on a polymer's chemistry, numerous methods could be developed based on simple low cost designs for controlled exposure to cross-linking solutions and UV irradiation with photoinitiator incorporated into the polymer blend. Cross-linking gradient techniques such as these have been incorporated into numerous combinatorial studies [15-17].

6.2.6. Enhancement of PEI Mechanical Properties with Annealing

The study of annealed PEI/S-PEI blends showed very interesting effects on the membranes mechanical properties. At low S-PEI concentrations, the force data for annealed films went beyond the detection limit of HTMECH, such that the normalized maximum force of these films were at least double that of the pure PEI film before and after annealing. The sulfonated membrane also seemed to maintain its flexibility and transparency after the annealing process, despite desulfonation as result of the high

temperature annealing. These results suggest that commercially available high-performance resins may be further improved by using post sulfonated resin as an additive and inducing desulfonation to obtain the chemical properties of the original material with superior performance. Although these materials would not be functional as PEMs, they could be significantly expanded into a number of applications requiring low-cast, highly stabile polymers. Thermal gravimetric analysis and differential scanning calorimetry are needed to determine if thermal properties were also enhanced as a result of desulfonation. Also the relationship between desulfonation and polymer chain reorganization should be further investigated. To date, no other studies have explored this phenomenon.

6.3. REFERENCES

1. Heinzel, A. and V.M. Barragán, *A review of the state-of-the-art of the methanol crossover in direct methanol fuel cells.* Journal of Power Sources, 1999. **84**(1): p. 70-74.

2. Tang, H., et al., *A degradation study of Nafion proton exchange membrane of PEM fuel cells.* Journal of Power Sources, 2007. **170**(1): p. 85-92.

3. Kundu, S., L.C. Simon, and M.W. Fowler, *Comparison of two accelerated Nafion(TM) degradation experiments.* Polymer Degradation and Stability, 2008. **93**(1): p. 214-224.

4. Rivin, D., et al., *Solubility and transport behavior of water and alcohols in Nafion(TM).* Polymer, 2001. **42**(2): p. 623-635.

5. Rivin, D., et al., *Simultaneous Transport of Water and Organic Molecules through Polyelectrolyte Membranes.* The Journal of Physical Chemistry B, 2004. **108**(26): p. 8900-8909.

6. Reucroft, P.J., D. Rivin, and N.S. Schneider, *Thermodynamics of Nafion(TM)-vapor interactions. I. Water vapor.* Polymer, 2002. **43**(19): p. 5157-5161.

7. Prosser, S.J., et al., *Rapid, automated analysis of ^{13}C and ^{18}O of CO_2 in gas samples by continuous-flow, isotope ratio mass spectrometry.* Biological Mass Spectrometry, 1991. **20**(11): p. 724-730.

8. Healy, J., et al., *Aspects of the Chemical Degradation of PFSA Ionomers used in PEM Fuel Cells.* Fuel Cells, 2005. **5**(2): p. 302-308.

9. Chen, C., et al., *XPS investigation of Nafion® membrane degradation.* Journal of Power Sources, 2007. **169**(2): p. 288-295.

10. Ghassemzadeh, L., et al., *Chemical degradation of proton conducting perflurosulfonic acid ionomer membranes studied by solid-state nuclear magnetic resonance spectroscopy.* Journal of Power Sources, 2009. **186**(2): p. 334-338.

11. Schulze, M., et al., *XPS analysis of the degradation of Nafion.* Fresenius' Journal of Analytical Chemistry, 1999. **365**(1): p. 106-113.

12. Schantz, S., *Structure and Mobility in Poly(ethylene oxide)/Poly(methyl methacrylate) Blends Investigated by 13C Solid-State NMR.* Macromolecules, 1997. **30**(5): p. 1419-1425.

13. Iojoiu, C., et al., *Mastering Sulfonation of Aromatic Polysulfones: Crucial for Membranes for Fuel Cell Application.* Fuel Cells, 2005. **5**(3): p. 344-354.

14. Meredith, J.C., et al., *Combinatorial characterization of cell interactions with polymer surfaces.* Journal of Biomedical Materials Research Part A, 2003. **66A**(3): p. 483-490.

15. Yeom, C.K. and K.-H. Lee, *A study on permeation behavior of a liquid mixture through PVA membranes having a crosslinking gradient structure in pervaporation.* Journal of Applied Polymer Science, 1996. **59**(8): p. 1271-1279.

16. Yeom, C.K. and K.H. Lee, *Vapor permeation of ethanol-water mixtures using sodium alginate membranes with crosslinking gradient structure.* Journal of Membrane Science, 1997. **135**(2): p. 225-235.

17. Broer, D.J., et al., *Photo-Induced Diffusion in Polymerizing Chiral-Nematic Media.* Advanced Materials, 1999. **11**(7): p. 573-578.

Vita

Keith Gregory Reed was born to Wanda and Gregory K. Reed on August 9, 1982, in Washington, D.C. While, attending Gaithersburg High School from 1996 to 2000, he played JV and Varsity football, threw shot put and discus for the indoor and outdoor track teams, served on the National Honor Society, the Spanish Honor Society, and was President of the NAACP youth council. In the summer prior to his senior year, Keith participated in the NASA Summer High School Research Apprenticeship Program at the Georgia Institute Technology, which inspired his pursuit of career in Chemical Engineering. Keith began his undergraduate career at the Massachusetts Institute of Technology in 2000, where he joined the Delta Kappa Epsilon Fraternity and continued playing Varsity football while majoring in Chemical Engineering. During his time at MIT, Keith did summer internships with 3M Company and Cummins, Inc., and worked as an undergraduate researcher for Dr. Karen Gleason and Dr. Paula Hammond. Keith decided to return to Georgia Tech to pursue an advanced degree under the guidance of Dr. J. Carson Meredith. As a graduate student, he was awarded fellowships from FACES and Applied Materials, and was awarded the Teamwork Award from the School of Chemical and Biomolecular Engineering. While attending graduate school, Keith served as a member of Georgia Tech Advisory Board, and has held executive officer positions with the Black Graduate Student Association and Association for ChemE Graduate Students. Keith also served as an ExxonMobil Tutor and Mentor and received a Certificate of Public Policy from the Ivan Allen Collage of Liberal Arts. After graduating with PhD in Chemical Engineering in December 2009, Keith hopes to pursue energy-related polymer research at a research institution or in industry, with goals of later teaching and possibly serving as a scientific advisor to the US Congress.